Exact Solutions of the Field Equations in the Quasi-Steady State Cosmological Model and Relation to Observations

Diploma Thesis

by

Rainer Sachs

Inter-University Centre for Astronomy and Astrophysics
Ganeshkhind, Pune 411 007, India

and

Technische Universität München
Physik-Department T30
85747 Garching, Germany

September 1995

Contents

1 Introduction 4

2 Standard Relativistic Cosmology 7
- 2.1 Field Equations . . . 7
- 2.2 Friedmann-Robertson-Walker Model . . . 9
- 2.3 Inflation . . . 13

3 Motivations for Alternative Cosmologies 17
- 3.1 The Cosmological Constant . . . 17
- 3.2 The Age Problem . . . 19

4 Quasi-Steady State Cosmology 23
- 4.1 The Steady State Theory . . . 23
- 4.2 Field Equations . . . 24
- 4.3 The Cosmological Constant Revisited . . . 28
- 4.4 Creation of Matter . . . 29

5 The Dynamics of QSSC 32
- 5.1 The Field Equations in Robertson-Walker Metrics . . . 32
- 5.2 The Creative Mode . . . 33
- 5.3 The Non-Creative Mode . . . 34
  - 5.3.1 Phase Space Analysis . . . 35
  - 5.3.2 Exact Solution . . . 40
- 5.4 The Composite Solution . . . 45

6 Observational Tests 49
- 6.1 Parameters of QSSC . . . 49
- 6.2 Counts of Radio Sources . . . 52
  - 6.2.1 Principles . . . 52
  - 6.2.2 Source Counts in QSSC . . . 56
- 6.3 Magnitude-Redshift Relation . . . 65
- 6.4 Iron Whiskers . . . 66

7 Conclusion **73**
7.1 Summary 73
7.2 Ideas for Future Investigations 75

A Conventions and Notation **76**

B Source Counts Codes **77**

Preface

This thesis is part of the degree "Diplom-Physiker", which corresponds to a M.Sc., at the Technische Universität München, Germany. The work was done under guidance of Professor J. V. Narlikar at the Inter-University Centre for Astronomy and Astrophysics at Pune, India.

I thank the Inter-University Centre for a fellowship that made my stay here possible.

Many people helped me to do this work and made my visit at IUCAA a pleasure. I am grateful to all members of IUCAA for their cooperation and help in all, even trivial problems I encountered. Special thanks to Jasjeet S. Bagla and L. Sriramkumar for their numerous advices and productive comments.

Last, but not least, I am indebted to Professor J. V. Narlikar. I thank him for countless critical reflections on my results and the many helpful discussions and answers to all my questions.

Pune, September 1995 Rainer Sachs

Chapter 1

Introduction

"But whoever loves the truth
must give special consideration to what
is right or wrong in this matter."
(Tobias Adami)

Cosmology may be considered as one of the most natural areas of man's interest. Since the early days of history curious scientists were concerned with the nature of the world they inhabited. Cosmology deals with the basic questions, physical as well as philosophical, like the origin of the world, its outer part, if there is any, the formation of observable structures and as a last consequence the reason for our existence.

During the centuries the scientists' horizon went from different continents, over the entire earth, the solar system to finally the universe as a whole, hand in hand with the availability of more and better observational data. The latest crucial step was Einstein's development of a theory of gravitation in the beginning of this century, the General Theory of Relativity (GR). It is a theory for large scales, for the macroscopic features of our world. So far no attempt to disprove GR has been successful.

Besides providing solutions for local gravitational fields like the Schwarzschild solution, GR can also yield a description of the whole universe. According to his philosophical view Einstein proposed a static universe which had been disproved subsequently by Eddington. Nowadays the most successful cosmological model is based on the solution of the field equations found by the Russian mathematician A. Friedmann. It contains a beginning of the universe in a singularity, for which Fred Hoyle coined the name "Big Bang", and an expansion afterwards. The vast majority of the cosmological community supports this so-called standard model.

Nevertheless scientists suggested alternative theories, but the more and more severe constraints put by better observations left them abandoned finally, with big bang cosmology, including inflation, remaining a promising idea on the way to a final theory.

However, there are some problems still to be solved, enough justification for the quest for another model. Recent observations of the cosmic microwave background radiation and the Hubble constant led to a new discussion about the validity of the standard model.

The purpose of this work is to take a closer look at an alternative model, the quasi-steady state cosmology, henceforward QSSC in brief, as suggested by F. Hoyle, G. Burbidge and J. V. Narlikar in the early nineties. The main difference to the standard model is the absence of a singular beginning of the universe. Instead, there is an endless series of oscillations of the scale factor.

In Chapter 2 we give an introduction to the standard model. We start with the derivation of Einstein's field equations and demonstrate their solution by means of the Friedmann-Robertson-Walker model, the basis of standard relativistic cosmology. It is a very simple and therefore elegant and preferred picture of the universe. It predicted for example the presence of the CMB as a relic of the big bang and provides explanations for a range of observational data like the abundance of the light elements. Some of its problems can be solved by introducing an inflationary phase, done in 1981 by A. Guth. Nevertheless we are yet not able to explain the singularity itself, leaving the problem of the initial conditions and the breakdown of physical laws unresolved. New contributions are expected from high energy physics and quantum theory.

Chapter 3 contains some motivations and reasons for looking for alternative cosmologies. The cosmological constant problem is present since the foundation of GR, and still after 70 years there is no satisfying solution available. The latest measurements of Hubble's constant lead to the dilemma of the universe being younger than its oldest structures. Obviously, this is a serious contradiction.

Quasi-steady state cosmology, outlined in Chapter 4, provides solutions for these challenges. As a historically interesting remark we first give a brief description of the famous steady state theory that sponsored the development of QSSC. Like in Chapter 2 we derive the field equations which become modified under the more general assumptions in this theory. Nonetheless they can be reduced to their well known form, so that the standard model is contained in this framework. We are also able to derive the cosmological constant instead of introducing it by hand like big bang cosmologists do up to now. Steady state as well as QSSC requires the creation of matter, a process which can be described by means of a negative energy field. This C-field was introduced in the 60's and widely used by F. Hoyle and J. V. Narlikar. We will demonstrate the underlying basic principles of this creation mechanism.

The behaviour of the scale factor in QSSC will be calculated and analysed in Chapter 5. We will obtain the equations of motion in a Robertson-Walker metric and we will see that there is no singularity, therefore no origin of the universe in this model. The scale factor is a superposition of an overall steady state-like exponential expansion and a series of short term oscillations. We investigate the creative and non-creative modes separately, depending on whether the condition

of creation of matter is satisfied or not. We will illustrate the qualitative behaviour in a phase space analysis. After that we will calculate the exact solution. It turns out that there are some deviations from the solution used by Hoyle, Burbidge and Narlikar.

We use the exact solution to calculate data which can be related to observations in the next Chapter 6. First we will fix the set of parameters of QSSC by assuming a reasonable value for the Hubble constant and the maximum redshift for sources at the last minimum of the scale factor. It is shown that the results do not vary much when we change the parameters' values. Next we will look into counts of radio sources. Whereas big bang needs to assume evolution of sources, QSSC can match the observational data under much simpler conditions. For the first scenario we will assume that the sources do not evolve with time. It will lead to some problem with blueshifted sources, that will be solved by introducing periodic evolution. Another test involving blueshifts is an extension of Hubble's diagram, the magnitude-redshift relation. We will calculate and discuss its form. The last point will be iron whiskers, the thermalizing agent to produce the CMB in QSSC. We will calculate the optical depth arising from these structures and their influence on high redshift objects especially in the infrared.

In Chapter 7 we will summarize and compare to the results obtained with the approximate solution. We will give suggestions for future investigations.

Chapter 2

Standard Relativistic Cosmology

2.1 Field Equations

There are many conventions used in GR. The differences are only formal but may cause a lot of unnecessary confusion. In this thesis we will follow the notation of Narlikar [38]. Appendix A contains a summary and a list of all abbreviations we used.

As it is true with all physical laws, we can derive the field equations from an action using the variational principle. In GR we usually start with an action that consists of two parts, one for the gravitational field, the other for the physical properties, i.e., the matter content, of our system.

$$A = A_{\mathbf{grav}} + A_{\mathbf{matter}}$$

Let us consider $A_{\mathbf{grav}}$ first. Following the general principle of GR, we have to choose a quantity that is covariant under coordinate transformations. Regard

$$A = \int_V L\sqrt{-g}\, d^4x \tag{2.1}$$

The factor $\sqrt{-g}$ is needed to get a covariant volume element, as follows from the transformation rules for the metric tensor g_{ik}. The quantity L has to be a scalar, also due to the principle of covariance. It turns out, that a suitable scalar in gravitational theory is the curvature R. This is the ***only*** scalar, that contains the second derivatives of g_{ik} in linear order, the first derivatives in second order. We can not use any scalar containing only first derivatives of the metric, as these can always be made to zero by transforming to a local inertial frame. A suitable choice is therefore

$$A_{\mathbf{grav}} = \frac{c^3}{16\pi G}\int_V (R - 2\lambda)\sqrt{-g}\, d^4x, \tag{2.2}$$

where the factor is introduced for future convenience. Note, that we can include an arbitrary constant λ without destroying the covariance. We will postpone the discussion of this constant to a later chapter.

The field equations can be obtained by varying the above action with respect to g_{ik}

$$g_{ik} \mapsto g_{ik} + \delta g_{ik}$$

and setting $\delta A = 0$. The result of this calculation, found by Hilbert [22] shortly after Einstein [15] published his equations, is

$$G_{ik} + \lambda g_{ik} = -\kappa T_{ik}. \tag{2.3}$$

The Einstein tensor G_{ik} is given by

$$G_{ik} = R_{ik} - \frac{1}{2} g_{ik} R \tag{2.4}$$

The numerical value for κ in conventional units is

$$\kappa = \frac{8\pi G}{c^4} = 2.07 \cdot 10^{-48} \mathrm{cm}^{-1}\mathrm{g}^{-1}\mathrm{s}^2 \tag{2.5}$$

and T_{ik} is *defined* such that

$$\delta A_{\mathrm{matter}} = \frac{1}{2} \int_V T_{ik} \delta g_{ik} \sqrt{-g}\, d^4x. \tag{2.6}$$

The usual form of A_{matter} for a special relativistic particle moving in flat spacetime is given by

$$A_{\mathrm{matter}} = -mc \int ds, \qquad ds = \sqrt{\eta_{ik} dx^i dx^k} \tag{2.7}$$

This can be seen if we start with the well known form of the action for a freely moving particle in classical mechanics

$$A = \int \frac{m}{2} v^2 \, dt \tag{2.8}$$

and regard the form of the line element in special relativity

$$\begin{aligned} ds &= \sqrt{c^2 dt^2 - dx^2 - dy^2 - dz^2} \\ &= c\sqrt{1 - \left(\frac{v}{c}\right)^2}\, dt \\ &\approx cdt - \frac{1}{2}\left(\frac{v}{c}\right)^2 cdt. \end{aligned} \tag{2.9}$$

With this approximation we may write

$$\int mc\, ds = \int mc^2\, dt - \int \frac{m}{2} v^2\, dt. \tag{2.10}$$

The first term on the right hand side of (2.10) drops out under variation, so we see that (2.7) follows from (2.8) and (2.10). For the GR case we have to replace η_{ik} by g_{ik} in (2.7).

The task of finding a solution of the field equations (2.3) is not done by simply assuming a certain matter contribution in spacetime and solving the differential equations. There are constraints given by the *Bianchi identities* for the curvature tensor. It can be shown, that only for

$$G^{ik}{}_{;k} = 0 \tag{2.11}$$

it is possible to find a metric. From (2.3) we see, if we neglect λ for the moment, that the energy-momentum tensor has to fulfill the conservation law

$$T^{ik}{}_{;k} = 0. \tag{2.12}$$

It so happens, that only for this particular matter distribution a solution for the metric can be found. But unfortunately, we have to calculate the covariant derivative in (2.12) with respect to exactly this metric. So, generally spoken, it is impossible to solve the field equations for a given matter distribution in a straightforward manner. The geometry of spacetime influences the distribution of matter and vice versa.

2.2 Friedmann-Robertson-Walker Model

As we have already seen, the solution of Einstein's field equations is everything else but easy. So we have to make some assumptions to simplify this problem. This is done by two postulates, both of which the solution should obey.

The first is called *Weyl's postulate* [57] and states that world lines of fundamental observers, e.g., galaxies, do not intersect and are orthogonal to a set of spacelike hypersurfaces. Our coordinate system does therefore not break down in the sense that we have two different coordinates for a single point in spacetime.

More popular is the second postulate, the *cosmological principle*. We assume the universe to be *homogeneous* and *isotropic*, provided we average over a sufficient large region of spacetime.

The most general line element satisfying these principles was found independently by Robertson [45] and Walker [55]. It has the well known form

$$ds^2 = c^2dt^2 - S^2(t)\left(\frac{dr^2}{1-kr^2} + r^2\left(d\theta^2 + \sin^2\theta d\phi^2\right)\right). \tag{2.13}$$

Here $S(t)$ is called the scale factor and k specifies the curvature with the usual values $k = 0, \pm 1$.

Using this metric we get from the field equations (2.3) with $\lambda = 0$ two differential equations

$$3\frac{\dot{S}^2 + kc^2}{S^2} = \frac{8\pi G}{c^2}T^0_0 \tag{2.14}$$

$$2\frac{\ddot{S}}{S} + \frac{\dot{S}^2 + kc^2}{S^2} = \frac{8\pi G}{c^2}T^\alpha_\alpha \tag{2.15}$$

Because of symmetries of the metric (2.13) we were able to reduce the number of unknown quantities to two as compared to the 10 components of g_{ik} in the general case.

The symmetry furthermore demands the energy-momentum tensor to take the form of an ideal liquid.

$$T_{ik} = (p + \rho c^2) u_i u_k - p g_{ik}, \tag{2.16}$$

where p denotes the pressure and ρ the matter density. Both are only functions of time, which reflects the homogeneity and isotropy. u_i is the i-th component of the 4-velocity

$$u^i = \frac{dx^i}{d\tau}, \quad u^i u_i = c^2. \tag{2.17}$$

Here τ is the proper time and is defined by

$$ds^2 = c^2 d\tau^2. \tag{2.18}$$

Therefore we get from (2.14) and (2.15), when we make use of this form of the energy-momentum tensor

$$3\frac{\dot{S}^2 + kc^2}{S^2} = 8\pi G\rho \tag{2.19}$$

$$2\frac{\ddot{S}}{S} + \frac{\dot{S}^2 + kc^2}{S^2} = -\frac{8\pi G}{c^2} p \tag{2.20}$$

The conservation law $T^{ik}{}_{;k} = 0$ reads in the context of the RW-metric like

$$\frac{d}{dS}\left(\rho c^2 S^3\right) + 3pS^2 = 0, \tag{2.21}$$

which can also be arrived at by taking the time derivative of (2.19) and making use of (2.20).

As we have only two equations for three variables S, p and ρ, we have the freedom to choose one more relation between p and ρ. This *equation of state* specifies the properties of our model. There are basically two epochs in the FRW model, one being dominated by matter, the other by radiation.

Let us consider the matter-dominated epoch first. If we neglect the pressure, we get from (2.21)

$$\rho \sim S^{-3}. \tag{2.22}$$

The simplest case is the *euclidean* or flat universe with $k = 0$. In the literature it is also commonly referred to as *Einstein-de Sitter* universe. Equation (2.19) yields

$$\dot{S}^2 = \frac{8\pi G\rho_0}{3}\frac{S_0^3}{S}, \tag{2.23}$$

k	q_0	Ω_0	ρ_0	topology
+1	$> \frac{1}{2}$	> 1	$> \rho_c$	spherical, closed
0	$\frac{1}{2}$	1	ρ_c	euclidean, open
-1	$\lesssim \frac{1}{2}$	< 1	$< \rho_c$	hyperbolical, open

Table 2.1: Characteristics of FRW models

which can be easily solved by

$$S(t) = S_0 \left(\frac{t}{t_0}\right)^{2/3}. \tag{2.24}$$

The ***Hubble parameter*** is defined as

$$H_0 = \left.\frac{\dot{S}}{S}\right|_{t_0}. \tag{2.25}$$

Usually it is written as

$$H_0 = 100\, h_0 \,\mathrm{km\ s^{-1}Mpc^{-1}}, \quad 0 \leq h_0 \leq 1. \tag{2.26}$$

The second parameter connected with the dynamics of spacetime in the ***deceleration parameter***, defined as

$$q_0 = -\left.\frac{\ddot{S}S}{\dot{S}^2}\right|_{t_0}. \tag{2.27}$$

With use of (2.25) we can write (2.23) as

$$H_0^2 = \frac{8\pi G}{3}\rho_0 \tag{2.28}$$

or

$$\rho_c \equiv \rho_0 = \frac{3H_0^2}{8\pi G} = 2 \cdot 10^{-29}\, h_0^2\, \mathrm{g\,cm^{-3}}, \tag{2.29}$$

where ρ_c is called the ***critical*** or ***closure density***. For $\rho > \rho_c$ the universe is closed, whereas for $\rho < \rho_c$ it is open. Finally we define the ***density parameter*** Ω as

$$\rho = \Omega \rho_c \tag{2.30}$$

Making use of these quantities we can simply characterize the three possibilities $k = 0, \pm 1$ as shown in Table 2.1. Common to all these models is that they

imply a scale factor of zero at a certain epoch back in time, a singularity which is known as big bang. The universe according to FRW models had a beginning.

The epoch prior to the one described above is dominated by radiation, as the energy density of radiation goes like

$$\rho \sim S^{-4} \tag{2.31}$$

and $S(t) \sim t^{1/2}$. Consequently we can deduce the behaviour of temperature as $T \sim t^{-1/2}$. However, at some time both matter and radiation were equally important. This time can be specified by the redshift z, with

$$1 + z = \frac{S_0}{S}. \tag{2.32}$$

It turns out that $z_{eq} \approx 1000$, so the universe is matter dominated for $z < 1000$ and radiation dominated for $z > 1000$.

On our way further back we may encounter several other significant epochs. The time of recombination is the first at a temperature of about 3000–4000 K. Electrons and protons, being free up to now, form H-atoms, so that the universe becomes transparent for photons. Matter and radiation decouple.

During the second epoch neutrons and protons form stable light nuclei at temperatures of about $10^8 - 10^9$ K.

The transition to the third epoch marks the breakdown of the GUT's, electroweak and strong interaction separate. This happens at energies of $\approx 10^{14}$ GeV, or 10^{-35} s after the big bang.

Prior to this epoch is the domain of quantum cosmology. We can trace back to $\approx 10^{-43}$ s after the big bang, the Planck time. The physics we know so far does not allow us to step any further. A quantum theory of gravity is required to tell us what happened prior to the Planck time.

This model is very well developed and provided predictions and explanations for a lot of observable features of the universe. We would like to stress the point, that confirmed predictions are always a sign of a good theory. In the case of big bang there is first the nature of expansion, predicted by Friedmann's solution and observed by Hubble. Second, the cosmic microwave background radiation (CMB) was expected by Gamow in the 1940's and finally detected by Penzias and Wilson in 1965 [44]. A third prediction were the abundances of light nuclei, especially ^{4}He and ^{2}H, calculated by Gamow [19], Alpher and Herman [4], which can be interpreted as relics from the second epoch. Furthermore the application of particle physics during the GUT epoch predicted that there should be only threee species of neutrinos. This was verified by accelerator experiments, particularly the Z° boson decay observed at CERN. Finally we should not forget that the underlying theory, general relativity, is widely tested and could not be disproved until today.

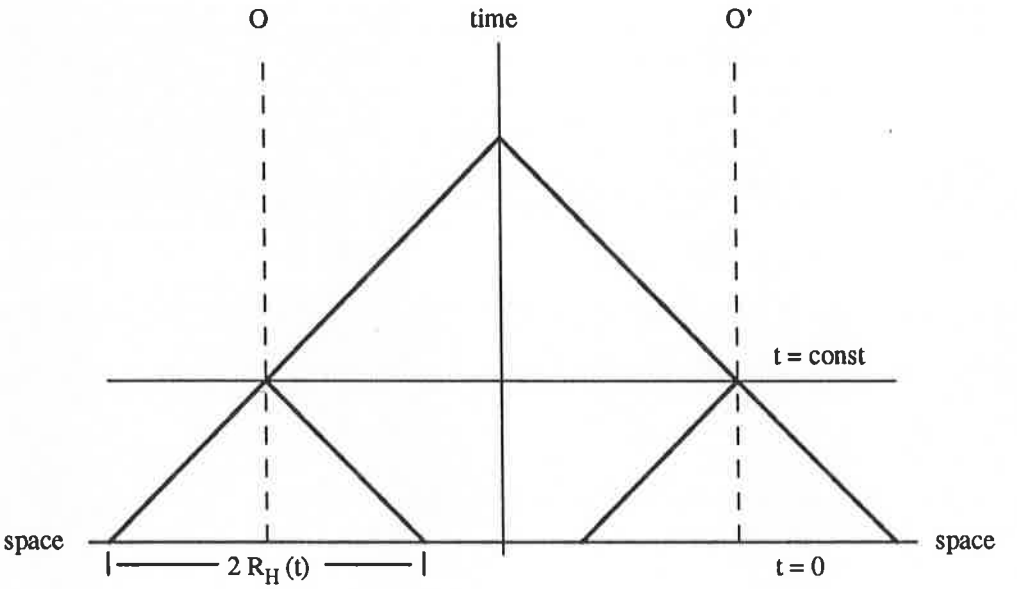

Figure 2.1: Illustration of the horizon problem

2.3 Inflation

Regardless the achievements of the hot big bang model, there are several difficulties which can be solved in an inflationary universe [21]. We will pose the problems first, before we have a look at how inflation works and solves these problems.

One of the problems is known as the *horizon problem*. The past light cone of a fundamental observer O at a time t is cut off at $t = 0$. The epoch we are considering is radiation dominated, so the proper distance a photon could travel is

$$R_{\mathrm{H}}(t) = S(t) \int_0^t \frac{cdt'}{S(t')} = 2ct. \tag{2.33}$$

R_{H} is called the particle horizon, which separates causally connected from disconnected areas. Two observers O and O' at time t are totally causally disconnected, if they are separated by a proper distance larger than $2R_{\mathrm{H}}(t)$ (Figure 2.1). It should be stressed that causal connection is a necessary condition for homogeneity in a given region. There is no conclusive reason for the same initial conditions in two disconnected regions.

Let us regard the example of CMB. The expansion factor since the time of GUT up to now can be calculated for example by using the temperature to be $\approx 4 \cdot 10^{26}$. Now, at $t \approx 10^{-35}$ s the particle horizon is $2R_{\mathrm{H}} = 6 \cdot 10^{-25}$ cm. In present time we get therefore a length scale of homogeneity of ≈ 240 cm. This

does not match at all with observations, as we see the universe to be more or less homogeneous over scales of 10^{28} cm. The analysis of data collected by the satellite COBE has recently shown that the CMB has an anisotropy of $\Delta T/T \approx 10^{-5}$ [51]. On an angular scale of a few degrees this corresponds to a length scale of 10^{27} cm.

Next we may consider the *flatness problem*. It can also be stated as "Why is Ω_0 so close to unity?" In the previous section we neglected the term kc^2/S^2, the influence of curvature. However, this is not valid for all times, as this term is scale dependent. When we use the density parameter Ω, we can express (2.19) as

$$\Omega - 1 = \frac{\dot{S}_0^2}{\dot{S}^2}(\Omega_0 - 1). \tag{2.34}$$

As for $t \to 0$, $\dot{S} \to \infty$ for the radiation dominated epoch, the convergence of $\Omega \to 1$ is very rapidly, in numbers

$$\left.\frac{\dot{S}_0^2}{\dot{S}^2}\right|_{t_{GUT}} \approx 10^{-48}. \tag{2.35}$$

Or the other way around: if Ω had not been extremely fine-tuned to unity at very early times, it would have evolved much further away from the observed values $0.1 < \Omega_0 < 2$. This means the universe would have contracted back to $S = 0$ or expanded to $S \to \infty$ much before the present epoch.

There are some other problems of the standard model, like the magnetic monopol problem, but we may constrain ourselves to these two.

The way inflation solves these difficulties is by introducing a temporary phase of exponential expansion into the dynamics of the very early universe. Suppose, the expansion starts at t_i and lasts until t_f. The scale factor looks like

$$S(t) \sim \begin{cases} t^{1/2} & t < t_i \\ \exp H(t - t_i) & t_i < t < t_f \\ t^{1/2} & t_f < t \end{cases} \tag{2.36}$$

for the universe is radiation dominated before and after inflation. Typical values for t_i, t_f and H are

$$t_i \approx 10^{-35}\text{s}, \quad H \approx 10^{10}\text{GeV}, \quad t_f \approx 70H^{-1}. \tag{2.37}$$

In the end we get an overall expansion of $\approx \exp(70) \approx 2.5 \cdot 10^{30}$.

Inflation deals with the previously stated problems as follows. The horizon problem is trivially solved: due to the exponential expansion the entire observed region since decoupling is brought into a causally connected area. The large scale isotropy is guaranteed. Also for the flatness problem inflation provides a natural solution. The deviation from euclidean space is given by the term kc^2/S^2. Even if one starts with some reasonable large term, inflation brings it down to merely zero for $t \approx t_f$. The $\Omega_0 = 1$ solution is a strong attractor for an universe, which

had an inflationary phase in its past. We can illustrate the "flattening" of space by an easy example. Assume we are two dimensional and live on the surface of a 3-sphere, whose radius is comparable to our size. In that case we might notice its curvature by measuring the well known deviations from euclidean geometry for instance. Once the radius of our sphere is increased by a factor of the order of 10^{30}, say, we will hardly be able to make out any effect of curvature. The same argument naturally holds for hyperbolical space, too. Notice that we did not change the topology of space, i.e., setting the value of k from 1 to 0. Inflation just reduces the contribution of curvature.

The idea of inflation is quite appealing and several mechanisms have been suggested to realize this idea. It is clear, e.g., from equation (2.19), that we need a (at least approximately) constant energy density to get an exponentially increasing scale factor.

We can obtain such a density from a phase transition at a temperature of about 10^{14} GeV connected to the spontaneous breaking of GUT symmetry. The theories which describe this symmetry breaking contain a massless scalar field ϕ, the so-called Higgs field. The behaviour of this field is guided by a potential $V(\phi, T)$, which itself interacts with the temperature of the surrounding.

For very high temperatures $T \gg 10^{14}$ GeV the potential has only one minimum at $\phi = 0$ with $V(0) \approx (10^{14}\text{GeV})^4$. When we reduce the temperature to $T \approx 10^{14}$ GeV a second minimum occurs at $\phi = \sigma$. For $T \ll 10^{14}$ GeV this is the true minimum with $V(\sigma) = 0$.

However, the Higgs field may not transit immediately from $\phi = 0$ to $\phi = \sigma$, when the universe is cooling down. It might get stuck in the false vacuum state $\phi = 0$. If that happens, the energy density is dominated by the constant term $V(0)$ and the universe expands rapidly. Finally quantum tunneling and thermal fluctuations will lead to a transition of the Higgs field to the true minimum $V(\sigma)$ and inflation stops.

One particular potential which was suggested is the Coleman-Weinberg potential [11]. For $T = 0$ it is given by

$$V(\phi) = \frac{1}{2}\lambda\sigma^4 + \lambda\phi^4\left(\ln\frac{\phi^2}{\sigma^2} - \frac{1}{2}\right), \qquad \lambda \approx 10^{-3}, \sigma \approx 2 \cdot 10^{15}\ \text{GeV}. \tag{2.38}$$

This potential is very flat near $\phi = 0$ and drops rapidly to $V = 0$ near $\phi = \sigma$. For finite temperatures there is a small barrier near $\phi = 0$ with a height of $\mathcal{O}(T^4)$ between the false and true vacuum (Figure 2.2). When the temperature of the universe dropped sufficiently, to about 10^9 GeV, say, the Higgs field tunnels rather quickly through this potential well and slowly 'rolls down' the gentle slope of the potential. During this time the energy density remains (nearly) constant and the universe expands exponentially. The total expansion factor is $\approx \exp(\mathcal{O}(10^2))$ for typical values of the Coleman-Weinberg potential.

When the Higgs field finally falls down and oscillates around the minimum $\phi = \sigma$, the decay of Higgs particles into secondaries damps the oscillation and

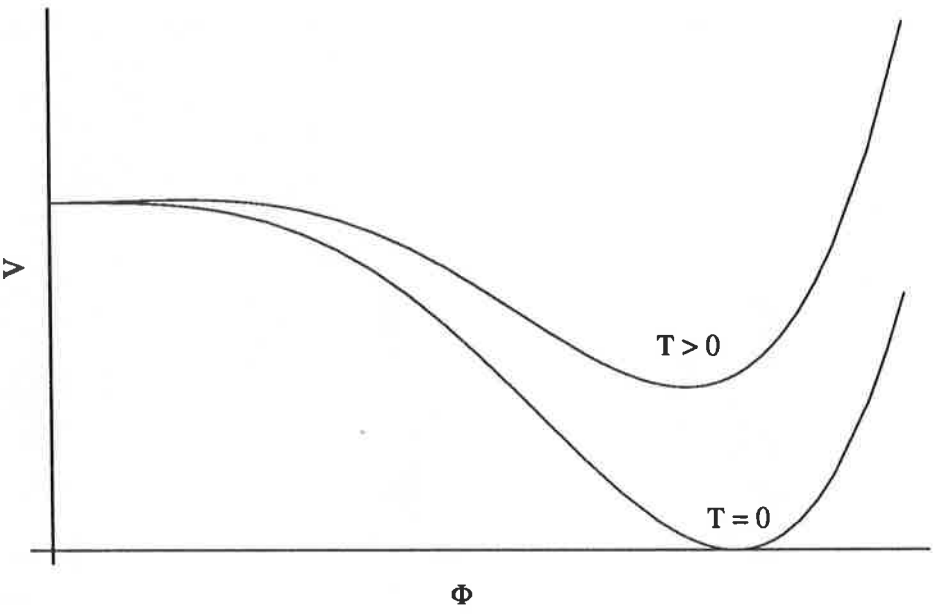

Figure 2.2: The Coleman-Weinberg potential for $T = 0$ and $T > 0$.

leads to a reheating of the universe to $T \approx T_{\text{initial}} \approx 10^{14}$ GeV. The decay process also explains, why the entropy of the universe is so large. At present we have $s \approx 10^{85}$ in the observable region. With the main contribution coming from photons the entropy goes like $T^3 \sim S^{-3}$, so the entropy per proper volume is conserved in an adiabatically expanding universe. Therefore we would have to explain, why a conserved dimensionless quantity has such a large value. During reheating a lot of entropy is released by the decaying Higgs field, whereas the scale factor and consequently the proper volume remains nearly constant. Inflation provides a natural explanation for the large entropy density today.

A problem in general with all versions of inflation is the growth of density perturbations, which only works, if the parameters are fine-tuned. Remember that one of the motivations of inflation was to avoid fine-tuning. So far, no model of inflation can be considered completely satisfactory [41].

Anyway, the combination of inflation with the Einstein-de Sitter model is referred to as the standard model, which shows the confidence physicists have in it. There are, as we have already seen and will see in the next chapter, still some puzzles left, known for a long time as well as recently occurred. Thus there is enough justification for the search for alternative and eventually more satisfying theories [6, 43].

Chapter 3

Motivations for Alternative Cosmologies

3.1 The Cosmological Constant

Browsing through the history of GR we find that especially one feature behaves just like a jinn in the bottle. The cosmological constant, released by Einstein, is always invoked when there are problems to solve. Let us have a closer look at this mystic constant.

It justifies its existence simply by the mathematical possibility of being included in the Lagrangian (2.2). And it is attacked by the aesthetics among physicists, who do not like its appearance making the theory less elegant. By the way, we could have also included higher orders of R, but naturally one always looks for the simplest case and includes higher order terms only if they are technically demanded or on other reasons, e.g., convenience, philosophy.

As mentioned above, Einstein [16] himself introduced the cosmological constant guided by the imagination of a static universe at that times. It can easily be shown that a static universe corresponds to the $k = +1$ case in the FRW context with $p_{\text{matter}} = 0$ and

$$\lambda_{\text{static}} = \frac{1}{S^2}, \tag{3.1}$$

where the scale factor is naturally a constant. Obviously λ is positive and acts as a repulsive force to prevent the static universe from collapsing under the influence of gravitational attraction of the dust particles. Unfortunately this solution turned out to be unstable, as minor deviations in S caused the universe either to expand to infinity or to contract back to zero [14]. When Hubble observed the redshifts of galaxies, which could easily be understood in an expanding universe à la Friedmann, the cosmological constant disappeared.

In the 1960's λ became popular again, when observations seemed to reveal the fact, that there was an excessively large number of quasars at redshifts of $z \approx 1.95$. So cosmologists concluded the universe should have had a phase of

constant scale factor like in the *Lemaître* model [33]. Therein the scale factor starts from zero, reaches a plateau and remains there for some time until it expands further to infinity. This behaviour can be realised, if one chooses λ to be slightly larger than λ_{static}.

Apparently this was the first time when quantum effects were said to be responsible for the cosmological constant, where λ can be regarded as a vacuum energy density. This is not contradictory, as in quantum field theories there exists no "perfect" vacuum. Quantum fluctuations give rise to an energy density. These fluctuations are the origin of the Casimir effect [10], which was first observed by Spaarnay in 1957 [53]. Obviously physicists had a possible explanation for the cosmological constant from quantum theory but unfortunately it does not work out conclusively at all.

Equation (2.14) including the λ-term can be written for the present epoch as

$$\left(\frac{\dot{S}}{S}\right)^2\Bigg|_{t_0} = -\left.\frac{kc^2}{S^2}\right|_{t_0} + \frac{\lambda c^2}{3} + \frac{8\pi G}{3}\rho_0 \tag{3.2}$$

or with use of the density parameter

$$\begin{aligned} 1 &= \Omega_k + \Omega_\lambda + \Omega_{\text{m}} \\ \Omega_{\text{tot}} &= \Omega_\lambda + \Omega_{\text{m}} = 1 - \Omega_k. \end{aligned} \tag{3.3}$$

Here we defined

$$\Omega_k = -\frac{kc^2}{S_0^2 H_0^2}, \quad \Omega_\lambda = \frac{\lambda c^2}{3H_0^2}, \quad \Omega_{\text{m}} = \frac{8\pi G}{3H_0^2}\rho_0 \tag{3.4}$$

for the present epoch. Observations show that Ω_{m} does not differ much from unity and major effects from the curvature term are not expected. So we get for the contribution of λ

$$|\Omega_\lambda| \lesssim 1 \tag{3.5}$$

or in units of length

$$|\lambda| \lesssim 10^{-56}\,\text{cm}^{-2}. \tag{3.6}$$

This is the total vacuum energy contribution. We want to look at λ as consisting of a bare cosmological constant and a part arising from quantum theory

$$\lambda = \lambda_{\text{bare}} + \lambda_{\text{QT}}. \tag{3.7}$$

λ_{QT} can be calculated and, if we trust GR up to the Planck scale, the puzzling result is

$$\lambda_{\text{QT}} = 10^{62}\,\text{cm}^{-2} \tag{3.8}$$

We face the fact that λ_{bare} and λ_{QT} have to cancel each other at an accuracy of 118 orders of magnitude. There is no obvious reason why some constant should be so extremely fine-tuned.

One may not like our separation of λ into two parts and argue that there is only one λ, namely from quantum fluctuations. But this moves the problem to that the particle physics' prediction is wrong by a factor of at least 10^{118}! This enormous discrepancy leads us to the conclusion that there is either something wrong with the standard model of particle physics, its application to the very early universe, or that there is an unknown relation between the free parameters of particle physics and cosmology, which has yet to be discovered.

Up to now particle physics was quite successful in the context of big bang, regarding for example the abundances of light nuclei or the number of neutrino species as mentioned in the previous chapter. Furthermore the symmetry breaking during the GUT epoch leads to an explanation for a phase transition and therefore for inflation.

So we tend to look for the third alternative, a still hidden relation between the parameters, that leads to an unexpected cancellation. We should draw our attention to the fact that we calculated λ_{QT} only for one sort of particles, whereas in reality a whole zoo of elementary particles contributes and consequently has to cancel out.

A viable solution for λ should also explain the inflationary phase, during which a rather large cosmological constant drives the exponential expansion, and its small value at present. A small but non-vanishing λ might be demanded by present observations as we will see in the next section. Promising solutions of the λ-problem may possibly be found in quantum cosmology, particularly through the contribution of wormholes. As this is not part of the work to be done here, we refer to a review article by Carroll et al. [9] for example. We will also see, how QSSC provides an elegant solution for λ.

3.2 The Age Problem

Of all the cosmological parameters the Hubble constant is the most popular one. The discussion about the exact value started in the 1930's and will continue to the day, when someone will have found a watertight method to measure it.

The value Edwin Hubble found was about $530\,\mathrm{km\,s^{-1}\,Mpc^{-1}}$. Nowadays the experts' opinions converge to an interval from

$$H_0 = 100\,h_0\,\mathrm{km\ s^{-1}Mpc^{-1}} \tag{3.9}$$

in the usual notation with

$$0.5 < h_0 < 1. \tag{3.10}$$

How can we determine h_0 and why is it so important? To deduce the Hubble constant from the relation

$$z = HD \tag{3.11}$$

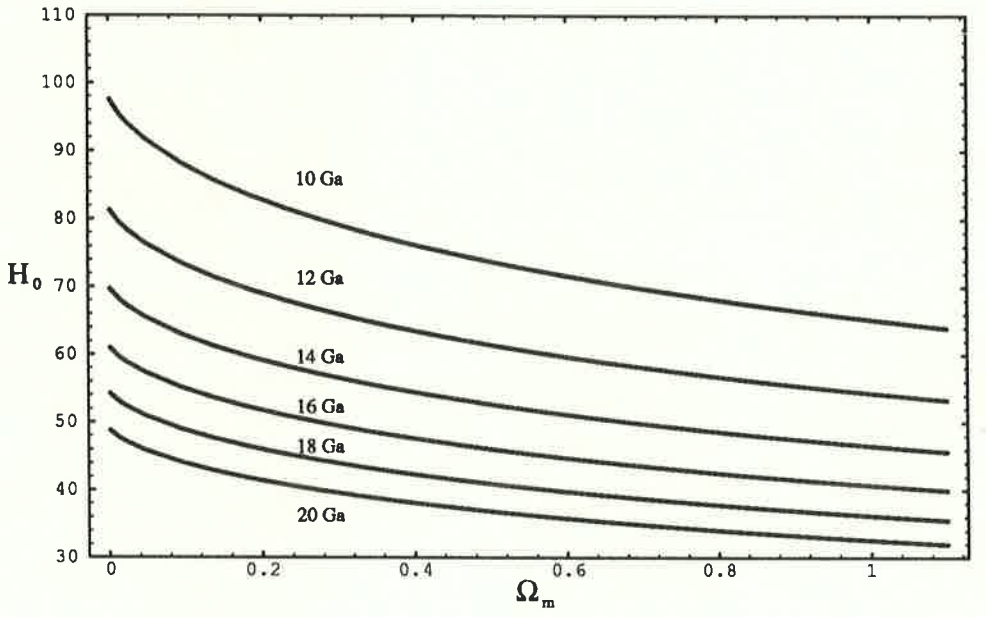

Figure 3.1: The Hubble constant as function of the density parameter Ω_m ($\lambda = 0$).

we obviously need the redshift and the proper distance of the extragalactic object. Note that we did not take into account the object's peculiar velocity, i.e., with respect to the cosmic rest frame. We assumed this velocity to be known and already removed from (3.11). While it is rather simple to measure the redshift, the proper distance is not at all easy to obtain. For a good description of different methods see for example Fukugita et al. [18].

The importance of H_0 lies in the fact that it allows us to estimate one fundamental property of the universe in big bang cosmology, its age. We see that H_0 has the dimension of inverse time, hence H_0^{-1} is a time interval, the Hubble time. Closer examination shows, as is naturally expected, that the matter content has certain influence on the dynamical evolution of the universe. Like in the previous section we characterize matter density by Ω_m. Large Ω_m leads to short life time of the universe and vice versa. Some numerical values for different choices of parameters are given in Table 3.1. The $H_0 - t_0$ dependence is more complicated for all other values of Ω_m.

We should recall that $\Omega_m < 1$ universes are open, $\Omega_m > 1$ closed. Nowadays we have to cope with the missing mass rather than with the exceeding mass problem, so we constrain our discussion to the interval $0 < \Omega_m < 1$.

Figure 3.1 shows H_0 as a function of Ω_m. The graphs are labeled with the corresponding age. Note that we have put $\lambda = 0$ in the preceding discussion.

There are various other methods to estimate the age of the universe. It is obvious that the universe can not be younger than a single object inside. So if

Ω_m	t_0	$t_0(h_0 = 0.5)$	$t_0(h_0 = 0.8)$
0	$\frac{1}{H_0}$	19.6 Ga	12.2 Ga
1	$\frac{2}{3H_0}$	13.0 Ga	8.1 Ga

Table 3.1: Age of the universe for different values of Ω_m and h_0.

we know the age of some contents we have a lower limit for t_0.

Stellar evolutionary theory is a reasonably reliable branch of astrophysics. From the Hertzsprung-Russell diagram of globular clusters, we are able to determine the age of these apparently oldest structures in the universe. There is a broad consensus that the oldest globular clusters are around 15 – 18 Ga old. The lower limits of all these ages range between 12 and 14 Ga.

Nuclear dating methods are unfortunately not very accurate, if they are applied to the whole universe. One has to rely on some speculative assumptions regarding the nucleosynthesis of these heavy elements, like ^{238}U, ^{235}U, ^{232}Th, and the uncertainties in their abundances. Nevertheless one can obtain a lower limit of 9.6 Ga [49]. This limit is clearly less restrictive than the ones obtained from globular clusters. However, the physics of nuclear decay is much better understood than stellar evolution and galaxy formation, so that this limit is more secure.

We would like to mention a third method, not very reliable at all, but interesting in its argumentation. It is based on the *anthropic principle*. One can find a lot of different versions of this "principle", we may use a sort of weak variant: The universe or parts of it must be such that we can inhabit it or them in principle. To be specific, some stars must have completed their life and produced the heavy elements, that are necessary for our life, which gives a lower limit. On the other hand, the universe must be young enough that some stars can still provide energy through nuclear reactions. Estimates from these assumptions yield at least the right order of magnitude for t_0, several times 10 Ga.

Returning to the beginning of this section, the Hubble constant, we see that either a low h_0 or a low Ω_m is necessary to obtain an age of the universe which is consistent with the limits above. For $\Omega_m = 0.1$ we require $0.63 < h_0 < 0.73$, for $\Omega_m = 1$ we need $0.46 < h_0 < 0.54$. The last case is the favourite of promoters of inflation, as it corresponds to an euclidean universe.

Recent analysis of data obtained by the Hubble Space Telescope (HST) yielded the result shown in Figure 3.2 [17]. Distance measurements to the Virgo cluster galaxy M100 using the Cepheid method leads to 17.1 ± 1.8 Mpc and consequently to a Hubble constant of 80 ± 17 km s^{-1}Mpc^{-1}. We can see that only $0.1 < \Omega_m <$

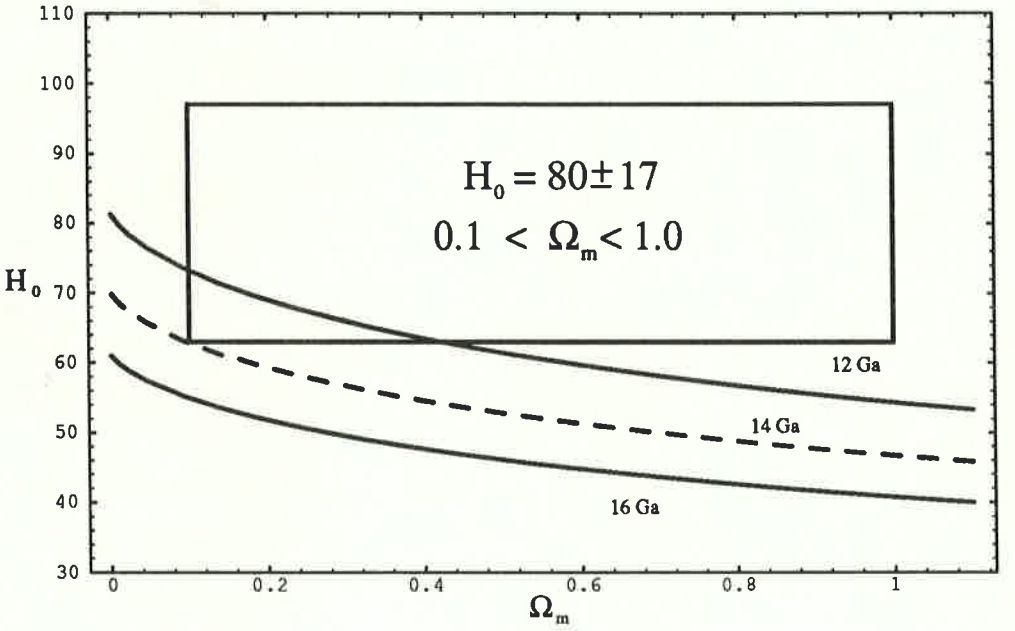

Figure 3.2: Current limits on H_0 (in km s^{-1} Mpc^{-1}) and the age and matter density of the Universe. The box denotes the result obtained by Freedman et al. [17]

0.4, a low density universe is compatible with this value of H_0 and a lower age limit of 12 Ga. For a $\Omega_m = 1$ model as demanded by inflationary theory, $h_0 = 0.8$ leads to $t_0 = 8.1$ Ga, far below the limits.

In order to save big bang theory we have three possibilities: we could either doubt this result and believe more in the existing measurements of a low Hubble constant. Or we could reexamine the theory of stellar evolution. Finally, seemingly the last remaining solution, we can revive the cosmological constant.

For $\lambda \neq 0$ and $\Omega_{tot} = 1$ the age of an object at redshift z is given by [56]

$$t_0(z) = \frac{2}{3}\left(1+\frac{\Omega_m}{\Omega_\lambda}\right)^{\frac{1}{2}} H_0^{-1}\left\{\sinh^{-1}\left(\frac{\Omega_\lambda}{\Omega_m}\right)^{\frac{1}{2}} - \sinh^{-1}\left[\left(\frac{\Omega_\lambda}{\Omega_m}\right)^{\frac{1}{2}}(1+z)^{-\frac{3}{2}}\right]\right\}. \tag{3.12}$$

In order to get $\Omega_{tot} = \Omega_m + \Omega_\lambda = 1$ for inflation, we can chose $\Omega_m = 0.1$ and $\Omega_\lambda = 0.9$, in accordance with observations for Ω_m.

$$t_0(z \to \infty) \approx 1.3\, H_0^{-1} = 15.9\,\text{Ga} \tag{3.13}$$

So we could reach the limits given by globular clusters and the recent measurement of H_0, but the price we pay is the occurrence of λ with all its implications mentioned in the previous section.

Chapter 4

Quasi-Steady State Cosmology

4.1 The Steady State Theory

Before we come to QSSC we would like to give, as a historical remark, an outline of its predecessor and godfather, the steady state theory.

In 1948 there were two major reasons that gave rise to this theory, developed by Hoyle [23], Bondi and Gold [7]. From the value of Hubble's constant known at that time, the age of the universe turned out to be

$$t_0 = H_0^{-1} = 1.9 \cdot 10^9 \mathrm{a}, \tag{4.1}$$

considerably less than the age of the Earth, the latter being well known from radioactive dating methods.

The other reason was the appearance of a singularity, the big bang itself. It seemed to be artificial. Further we have the freedom to choose initial conditions on a spacelike hypersurface, which should not be possible in a complete theory. Finally, the laws of physics should remain the same for all times, but exactly this is violated when we encounter a singularity.

One approach to the steady state theory is the *perfect cosmological principle* (PCP). It is an extension of the common CP and states that the universe should have the same properties not only in all directions for all fundamental observers, but also for all times. We therefore get

$$H = \frac{\dot{S}}{S} = const = H_0, \quad q = -1 \tag{4.2}$$

and

$$S \sim \mathrm{e}^{Ht}. \tag{4.3}$$

As the curvature is given by the expression k/S^2 and it should also remain unchanged in time, we arrive at an euclidean spacetime ($k = 0$) with the line element

$$ds^2 = c^2 dt^2 - e^{2Ht}\left(dr^2 + r^2(d\theta^2 + sin^2\theta d\phi^2)\right) \tag{4.4}$$

The steady state theory provides also an argument for the sign of H_0, until now undetermined, without measuring the redshift of galaxies. If $H_0 = 0$ was true, the universe would be infinitely old. As already pointed out by Olbers in 1826 [40], such an universe should have reached thermal equilibrium already and sky at night should be as bright as during the day. For $H_0 < 0$ the situation would be even worse. So $H_0 > 0$ remains the only possibility.

Regarding the matter density in the universe, one obviously needs matter to be created, in order to keep the density constant. The rate of creation is quantified by the following calculation. The proper volume increases as

$$\frac{\dot{V}}{V} = 3H_0. \tag{4.5}$$

So the total mass M must increase as $M = V\rho_0$, or

$$\dot{M} = 3H_0 V \rho_0. \tag{4.6}$$

The rate of creation per unit volume is therefore

$$\begin{aligned} Q &= 3H_0\rho_0 \\ &= 2 \cdot 10^{-46}\, h_0^3\, \Omega_0\, \mathrm{g\,cm^{-3}\,s^{-1}}. \end{aligned} \tag{4.7}$$

For present values of $h_0 \approx 0.8$, $\Omega_0 \approx 0.2$ we get an average creation of *one* nucleon per day and km^3. This creation of matter is basically a violation of the energy conservation law.

$$T^{ik}{}_{;k} \neq 0\,! \tag{4.8}$$

One way of describing the matter creation is to use a scalar field. As this feature is also incorporated in the quasi-steady state theory, we will postpone the discussion to the next section.

Steady State was finally abandoned on grounds of counts of radio sources, the discovery of the CMB, its perfect Planckian spectrum [35] and the abundance of light nuclei, which are said to be primordial in the context of big bang, whereas in steady state they are formed in stars only. Nevertheless, one of the merits of steady state is that it enlived the discussion on different cosmological models and acted as a stimulant for research. In Popper's sense it is a good theory, because it made clear-cut predictions that could be proved or disproved.

4.2 Field Equations

We will now derive the field equations of QSSC, a theory proposed by Hoyle, Burbidge and Narlikar [27, 28, 29, 30] as an alternative to big bang cosmology. Again, as in usual GR, we start with an action A to derive the field equations.

The difference now is that we look for conformal invariant equations. A conformal transformation is given by

$$g^*_{ik} = \Omega^2(X)\, g_{ik}, \tag{4.9}$$

which scales distances between two points by $\Omega(X)$, but leaves angles and orientation unchanged.

The reason to demand conformal invariance is that the causal structure of spacetime is not changed under these transformations. The light cones remain the same. Nonetheless it is clearly not valid to use the extreme cases $\Omega = 0$, $\Omega = \infty$. It is not possible to extend the metric down to a singularity, for example to the big bang or beyond.

It can be calculated from (4.9) with more or less effort

$$\begin{aligned} da^* &= \Omega\, da \\ \sqrt{-g^*} &= \Omega^4 \sqrt{-g} \\ R^* &= \Omega^{-2}(R + 6\Omega^{-1}\Box\Omega). \end{aligned} \tag{4.10}$$

The last relation clearly destroys the conformal invariance of the action used in Section 2.1

$$A_{\text{grav}} = \frac{c^3}{16\pi G} \int_V (R - 2\lambda)\sqrt{-g}\, d^4x. \tag{4.11}$$

Our *Ansatz* for the action is

$$A = -\sum_a \int M^{(a)}(A)\, da, \tag{4.12}$$

where a denotes particle 'a', A its location in 4-space and $M^{(a)}$ its inertia. According to Ernst Mach [34] inertial forces should arise entirely by motion of a particle with respect to the background matter. Here we take the particle's inertia determined by other particles present in the universe

$$M^{(a)}(A) = \sum_b \mu^2 \int G(A, B)\, db \tag{4.13}$$

μ is a coupling constant, $G(A, B)$ a Green function. It is a biscalar which propagates the contribution of particle b from B to A. $G(X, B)$ obeys the conformal invariant wave equation

$$\Box_x G(X, B) + \frac{1}{6} R(X)\, G(X, B) = \frac{\delta_4(X, B)}{\sqrt{-g(B)}}. \tag{4.14}$$

Under conformal transformations we require $G(X, B)$ to scale like

$$G^*(X, B) = \frac{1}{\Omega(X)\Omega(B)} G(X, B). \tag{4.15}$$

From (4.13) it is clear that $M(X)$ obeys the transformation law

$$M^*(X) = \frac{1}{\Omega(X)} M(X), \tag{4.16}$$

hence the action (4.12) is conformally invariant.

The field equations can be obtained in the usual way. We vary A and set $\delta A = 0$. In this case we have

$$\begin{aligned} \delta A &= -\sum_a \int [\delta(M^{(a)}(A))\, da + M^{(a)}(A)\, \delta(da)] \\ &= -\int [G_{ik} + T_{ik}] \sqrt{-g}\, \delta g^{ik}\, d^4x \\ &= 0 \end{aligned} \tag{4.17}$$

The energy-momentum tensor T_{ik} has the form of a set of relativistic moving particles

$$T^{ik} = \sum_a \int M^{(a)}(A) \frac{\delta_4(X, A)}{\sqrt{-g(A)}} \frac{da^i}{da} \frac{da^k}{da}\, da \tag{4.18}$$

The Einstein tensor G_{ik} looks now more complicated as in the standard case. Equation (4.14) has retarded and advanced solutions. We write the retarded solution as

$$M^{\text{ret}}(X) = \sum_a \mu \int G^{\text{ret}}(X, A)\, da \tag{4.19}$$

and M^{adv} analogous. The result after a rather tedious but straightforward calculation is [26]

$$\begin{aligned} G_{ik} &= \frac{1}{6}(R_{ik} - \frac{1}{2} g_{ik} R) M^{\text{ret}} M^{\text{adv}} \\ &\quad -\frac{1}{2}(M^{\text{adv}}_{,i} M^{\text{ret}}_{,k} + M^{\text{ret}}_{,i} M^{\text{adv}}_{,k} - g_{ik} g^{ab} M^{\text{adv}}_{,a} M^{\text{ret}}_{,b}) \\ &\quad +\frac{1}{6}\left[(M^{\text{ret}} M^{\text{adv}})_{;ik} - g_{ik} \Box (M^{\text{ret}} M^{\text{adv}})\right] \end{aligned} \tag{4.20}$$

Both M^{ret} and M^{adv} are not completely determined as the homogeneous wave equation can yield different solutions. By the physical requirement that fields without sources have to be zero this ambiguity is removed. From (4.14) we get for the retarded and advanced solution

$$\Box(M^{\text{adv}} - M^{\text{ret}}) + \frac{1}{6} R (M^{\text{adv}} - M^{\text{ret}}) = 0. \tag{4.21}$$

With the boundary condition this gives

$$M^{\text{ret}} = M^{\text{adv}} = M \tag{4.22}$$

We can therefore write (4.20) as

$$\begin{aligned} G_{ik} &= \frac{1}{6}M^2(R_{ik} - \frac{1}{2}g_{ik}R) \\ &\quad -M_{,i}M_{,k} + \frac{1}{2}g_{ik}g^{ab}M_{,a}M_{,b} \\ &\quad +\frac{1}{6}\left[(M^2)_{;ik} - g_{ik}\Box(M^2)\right] \end{aligned} \tag{4.23}$$

In contrast to Einstein's field equations in Section 2.1, (4.23) is conformally invariant. The masses of particles depend on their coordinates X. We can get constant particle masses, if we choose a particular conformal factor $\Omega(X)$ such that

$$m = \frac{1}{\Omega(X)}M(X) = const. \tag{4.24}$$

All derivatives of M drop out in (4.23) and we get the well known result

$$R_{ik} - \frac{1}{2}g_{ik}R = -\kappa T_{ik} \tag{4.25}$$

with $\kappa = 6/m^2$. We will obtain the usual form of this coupling constant in a minute. First note that the action (4.12) should be a dimensionless quantity as required by quantum mechanics, where $\exp(iA)$ gives the probability amplitude for the occurrence of a particular configuration in a volume V. The mass field M had units of inverse length in our calculation so far, hence (4.12) was dimensionless. When we want to restore conventional units for masses, we have to replace

$$m \mapsto \frac{mc}{\hbar} \tag{4.26}$$

in κ and T_{ik}. We can see that the Compton wavelength was used as a natural unit for particle masses. After this transformation the constant κ looks like

$$\kappa = \frac{6\hbar}{m^2c^3}. \tag{4.27}$$

It takes its usual form $\kappa = 8\pi G/c^4$, provided we *define* the gravitational constant G as

$$G = \frac{3\hbar c}{4\pi m^2}. \tag{4.28}$$

We note that, if G has its usual value, the particle's mass is the Planck mass

$$m_{\mathrm{p}} = \left(\frac{3\hbar c}{4\pi G}\right)^{1/2} \approx 10^{-5}\,\mathrm{g}. \tag{4.29}$$

This relationship can be looked upon in two different ways. If we assume G to be one of the fundamental constants then it determines the mass of particles of our gravitational theory. Or we regard the value of m_{p}, which is the result of our scaling to obtain constant particle masses, as fundamental. In this case the gravitational constant is fixed by the matter content of the universe.

4.3 The Cosmological Constant Revisited

We have already seen that G can be related to the background matter in the universe. What about λ? So far there was no reason for the cosmological constant to appear.

It turns out that we can actually derive λ in the right order of magnitude, if we choose a more general case of the wave equation (4.14). Without destroying the conformal invariance we can include a term proportional to $G^3(X, B)$. The resulting equation for one particle a then reads like

$$\Box M^{(a)} + \frac{1}{6} R M^{(a)} + M^{(a)^3} = \int \frac{\delta_4(X, A)}{\sqrt{-g(A)}}\, da. \tag{4.30}$$

This is unfortunately not a linear equation any more, so we can not obtain a solution for $M = \sum_a M^{(a)}$ by superposition of all one particle equations. Assumed all particles have the same mass, we can write the wave equation for M as

$$\Box M + \frac{1}{6} R M + \Lambda M^3 = \sum_a \int \frac{\delta_4(X, A)}{\sqrt{-g(A)}}\, da \tag{4.31}$$

with $\Lambda = N^{-2}$, the inverse square of all Planck particles present in the universe. Now we have to relate Λ to the cosmological constant. Consider the action

$$\begin{aligned} A \;=\; & -\frac{1}{2} \int \left(M^{,i} M_{,i} - \frac{1}{6} R M^2 \right) \sqrt{-g}\, d^4x \\ & + \frac{1}{4} \Lambda \int M^4 \sqrt{-g}\, d^4x \\ & - \sum_a \int \frac{\delta_4(X, A)}{\sqrt{-g(A)}}\, M\, da. \end{aligned} \tag{4.32}$$

Variation with respect to M leads to (4.31) and if we set $M = m = const$ and use the definition of G we get

$$A = \frac{c^3}{16\pi G} \int \left(R + 3\Lambda \left(\frac{mc}{\hbar} \right)^2 \right) \sqrt{-g}\, d^4x + \int L_{\text{phys}} \sqrt{-g}\, d^4x. \tag{4.33}$$

Comparison with (4.11) leads to

$$\lambda = -\frac{3}{2} \Lambda \left(\frac{mc}{\hbar} \right)^2. \tag{4.34}$$

A rough estimate gives that the total observed mass in the universe is about 10^{80} nucleons. These could be theoretically combined to $\sim 10^{61}$ Planck particles. Λ is therefore of the order 10^{-122} and the result for the cosmological constant is

$$\lambda \approx -10^{-56}\,\text{cm}^{-2}, \tag{4.35}$$

which matches fairly well with the observational constraints. Note that λ is negative. It acts as additional gravitating mass, unlike in Einstein's static universe, and slows down the expansion.

4.4 Creation of Matter

Until now we did not depart drastically from the standard picture of GR. We obtained the field equations, which are scale invariant and which reduce to the standard form in a particular scale with $M(X) = m = const.$ In what follows we put $c = \hbar = 1$ unless mentioned explicitly.

However, in QSSC we have the phenomenon of matter to be created like in steady state theory. In the latter creation was necessary to combine the PCP with the expansion of space, the matter content had to remain constant. Creation occurred throughout spacetime at a small rate. In QSSC, as we will see, creation takes place only in regions with strong curvature and is of explosive nature.

The concept of creation of particles, i.e., broken world lines, can also be related to requirements from quantum mechanics. When calculating the quantity $\exp(iA)$ in a volume V, this volume should be entirely arbitrary. Instead, in standard big bang cosmology V is chosen such that $t > 0$ for all interior points. All world lines start at $t = 0$, a point which is placed outside V. In QSSC the more general case is considered, that world lines of particles start at different points and all these points are included.

The process of creation can be described by including a mass less scalar field $c(X)$ in the mass field $M(X)$. This formalism was developed and widely used by Hoyle and Narlikar in the 60's [24, 25]. So we regard $M(X)$ to consist of two components

$$M(X) = m(X) + c(X). \tag{4.36}$$

The contribution of the c-field is due to short living primaries, that decay into n stable secondary particles, such as baryons. To be specific, matter is created as Planck particles with mass $m_p = 10^{-5}$ g and mean life time $\tau = 10^{-43}$ s. The stable particles give rise to $m(X)$, which we will make constant by a suitable choice of scale like in the previous section.

$$c(X) = \sum_a c^{(a)}(X) \tag{4.37}$$

$$m(X) = \sum_a \sum_{r=1}^{n} m^{(a_r)}(X) \tag{4.38}$$

From the action for this inertia field we can obtain a conservation law for the creation process. We vary the action with respect to the starting point of the particle's world line.

$$\begin{aligned} A &= -\sum_a \int_{A_0} (m + c)\, da \\ &= -\sum_a \int_{A_0+\delta A_0} m\, da - \sum_a \int_{A_0}^{A_0+\delta A_0} c\, da \end{aligned}$$

$$= -\sum_a \int_{A_0+\delta A_0} m\,da - \sum_a c(A_0)\tau \tag{4.39}$$

The last step is justified, as the life time of a Planck particle is very short. In the steady state theory a similar action has been considered

$$A = -\sum_a \int_{A_0+\delta A_0} m\,da - \sum_a C(A_0). \tag{4.40}$$

The analogy is easy to see: $C = c\tau$.

The conservation law is now given by

$$-m\frac{dx^i}{da}g_{ik} + c_{,k}\tau = 0 \tag{4.41}$$

or

$$c_{,k}c^{,k} = \frac{m^2}{\tau^2}. \tag{4.42}$$

In general, i.e., in flat space, this condition is not satisfied like in steady state. In the latter creation was possible throughout spacetime but at a much smaller rate. However, in the vicinity of a massive body spacetime can be described by the Schwarzschild metric

$$ds^2 = \left(1 - \frac{2M}{r}\right)dt^2 - \frac{dr^2}{\left(1 - \frac{2M}{r}\right)} - r^2 d\Omega^2. \tag{4.43}$$

On grounds of symmetry we regard only time and radial derivatives of $c(X)$ and it can be shown that the left hand side of (4.42) increases as one goes to smaller r, while m^2/τ^2 remains constant. Thereby creation should only occur near massive objects.

How do the field equations (4.23) look when we use the form (4.36) for the inertia field? Let us first recall, that $m(X) = m = const$, so all derivatives of $m(X)$ drop out. We further note the very small contribution of $c(X)$ to $M(X)$ compared to $m(X)$, as the life time of Planck particles is very short. Nevertheless, we can not neglect the derivatives of $c(X)$. However, when we average over many Planck particles, terms linear in $c_{,i}(X)$ will cancel each other. Under these assumptions and including the cosmological constant we get from (4.23) and (4.28)

$$R_{ik} - \frac{1}{2}g_{ik}R + \lambda g_{ik} = -\frac{8\pi G}{c^4}\left[T_{ik} + C_{ik}\right]. \tag{4.44}$$

The contribution of the c-field part on the right hand side is given by

$$C_{ik} = -\frac{2\hbar c}{3}\left(c_{,i}c_{,k} - \frac{1}{4}g_{ik}c_{,l}c^{,l}\right). \tag{4.45}$$

Its (0,0)-component clearly shows that $c(X)$ is a negative energy field.

$$C_0^0 = -\frac{\hbar}{2c}\dot{c}^2. \tag{4.46}$$

If we furthermore make the usual assumption of homogeneity and isotropy for the universe, spatial derivatives in (4.44) will vanish and we get

$$C_\alpha^\alpha = \frac{\hbar}{6c}\dot{c}^2. \tag{4.47}$$

Negative pressure occurs through the c-field, the former driving the expansion of spacetime. The process of matter creation looks now as follows. In a region with strong curvature condition (4.42) is satisfied. Planck particles are produced and the c-field transits down to a lower state. Usually this would lead to an instability, as there is no lowest energy state and the field would continue cascading down. The process will be explosive, anyway, but due to the negative pressure space expands. The c-background will decrease and fall below the threshold, thus creation stops.

Chapter 5

The Dynamics of QSSC

5.1 The Field Equations in Robertson-Walker Metrics

Like in Chapter 2 we make simplifying assumptions to obtain solutions of the field equations (4.44). We regard the cosmological principle to be valid. It will turn out thay even Weyl's postulate is obeyed World lines of fundamental observers do not intersect like in big bang.

Our energy-momentum tensor is the same as in the FRW-models, dust without pressure,

$$T_{ik} = \rho c^2 u_i u_k. \tag{5.1}$$

We have already seen in the previous chapter that the contribution of the c-field looks like

$$C_{ik} = -\frac{2\hbar c}{3}(c_{,i}c_{,k} - \frac{1}{4}g_{ik}c_{,l}c^{,l}). \tag{5.2}$$

The CP demands spatial derivatives in (5.2) to vanish, leading to

$$C^i_k = -\frac{2\hbar c}{3}(c^{,i}c_{,k} - \frac{1}{4c^2}\delta^i_k\dot{c}^2). \tag{5.3}$$

The only non-zero components of C^i_k are

$$C^0_0 = -\frac{\hbar}{2c}\dot{c}^2 \tag{5.4}$$

$$C^\alpha_\alpha = \frac{\hbar}{6c}\dot{c}^2. \tag{5.5}$$

Using the form of Robertson-Walker metrics (2.13) together with these results and (5.1) we get from (4.44) two equations for the scale factor.

$$3\frac{\dot{S}^2 + kc^2}{S^2} = \lambda c^2 + 8\pi G\rho - \frac{4\pi G\hbar}{c^3}\dot{c}^2 \tag{5.6}$$

$$2\frac{\ddot{S}}{S} + \frac{\dot{S}^2 + kc^2}{S^2} = \lambda c^2 + \frac{4\pi G\hbar}{3c^3}\dot{c}^2. \tag{5.7}$$

Even in the case of mass creation, i.e., $T^{ik}{}_{;k} \neq 0$, in this model, a more general conservation law still holds.

$$(T^{ik} + C^{ik})_{;k} = 0 \tag{5.8}$$

We can calculate this straight away or derive it from (5.6) and (5.7) to

$$\frac{\hbar}{2c^3}\left(4\frac{\dot{S}}{S}\dot{c}^2 + \partial_t \dot{c}^2\right) = 3\frac{\dot{S}}{S}\rho + \partial_t \rho. \tag{5.9}$$

If we set the right hand side of (5.9) to zero, we get the conservation law of standard big bang, namely no creation of matter and $\rho \sim S^{-3}$. For the c-field (5.9) leads to $\dot{c}^2 \sim S^{-4}$. Generally spoken, for small S the background of the c-field could be large enough to satisfy the creation condition (4.42). In order to deal with the solution of (5.6) and (5.7) we regard two separate cases, one with matter creation, the other without, and combine these two solutions afterwards.

5.2 The Creative Mode

We assume that condition (4.42) is satisfied everywhere and for all times, thus we have an overall and continuous creation of matter.

$$\dot{c}\tau = \frac{mc}{\hbar} \tag{5.10}$$

We regard only time derivatives in accordance with the CP. This scenario is similar to the steady state theory, so we use

$$S = S_0 \exp\left(\frac{t}{P}\right) \tag{5.11}$$

as *Ansatz* for the scale factor to solve (5.6) and (5.7) for $k = 0$:

$$3\frac{1}{P^2} = \lambda c^2 + 8\pi G\rho - \frac{4\pi G}{\hbar c}\frac{m^2}{\tau^2} \tag{5.12}$$

$$3\frac{1}{P^2} = \lambda c^2 + \frac{4\pi G}{3\hbar c}\frac{m^2}{\tau^2} \tag{5.13}$$

leading to

$$\rho = \frac{2m^2}{3\hbar c\tau^2} \tag{5.14}$$

$$\frac{1}{P^2} = \frac{\lambda c^2}{3} + \frac{2\pi G\rho}{3}. \tag{5.15}$$

Now, let $m = m_{\mathrm{p}}, \tau = \tau_{\mathrm{p}}$ and we get a result which seems puzzling at first glance.

$$\rho = 6 \cdot 10^{92}\,\mathrm{g\,cm^{-3}}$$

$$P \approx \tau_{\mathrm{p}}$$

The universe would be as dense as a Planck particle and would expand with a characteristic time scale of the order of the Planck time. But this result is expected under the assumption, that (4.42) holds at all points in spacetime. It shows that the creation process is of explosive nature and extremely violent. If we make the more realistic assumption of matter creation to take place only in strongly curved regions, we expect that the average of all these single creation events lowers to a reasonable level.

In case $k \neq 0$ we get similar results, the scale factor looks like

$$S = cP\cosh\left(\frac{t}{P}\right), \qquad k = +1 \tag{5.16}$$

$$S = cP\sinh\left(\frac{t}{P}\right), \qquad k = -1 \tag{5.17}$$

P is again given by (5.15).

It is a well known feature of de Sitter solutions that spacetime has a constant curvature in four dimensions. The three solutions for $k = 0, \pm 1$ are in fact just three different sections of the same space.

5.3 The Non-Creative Mode

In this case condition (4.42) does not hold anywhere. The covariant derivative of (5.8) vanishes for both terms separately

$$\begin{aligned} T^{ik}{}_{;k} &= 0 \\ C^{ik}{}_{;k} &= 0. \end{aligned} \tag{5.18}$$

From (5.9) we see for the non-creative mode

$$\begin{aligned} \rho &\sim S^{-3} \\ \dot{c}^2 &\sim S^{-4}. \end{aligned} \tag{5.19}$$

We can write (5.6) as follows.

$$3\frac{\dot{S}^2 + kc^2}{S^2} = \lambda c^2 + \frac{8\pi G\bar{\rho}\bar{S}^3}{S^3} - \frac{4\pi G\hbar}{c^2}\frac{\bar{c}^2\bar{S}^4}{S^4}. \tag{5.20}$$

The barred quantities are constants from integration of (5.9). We will look at them when we consider the composite solution.

In the following section we will discuss the general behaviour of the scale factor as determined by (5.20). After that we will find an exact solution for the scale factor.

5.3.1 Phase Space Analysis

For simplicity we denote (5.6) and (5.7) in the following way:

$$\frac{\dot{S}^2+k}{S^2} = \lambda + \frac{A}{S^3} - \frac{B}{S^4} \tag{5.21}$$

$$2\frac{\ddot{S}}{S} + \frac{\dot{S}^2+k}{S^2} = 3\lambda + \frac{B}{S^4} \tag{5.22}$$

We have put $\hbar = c = 1$, $\lambda \to 3\lambda$ and

$$A = \frac{8\pi G}{3}\bar{\rho}\bar{S}^3 \tag{5.23}$$

$$B = \frac{4\pi G}{3}\bar{c}^2\bar{S}^4. \tag{5.24}$$

Most of the following analysis will be done with use of (5.21) only.

Let us consider the case $k = 0$ first. (5.21) gives

$$\dot{S}^2 = \lambda S^2 + \frac{A}{S} - \frac{B}{S^2}. \tag{5.25}$$

The roots of the right hand side of this equation, i.e., the extrema of the scale factor are approximately

$$S_{\min} \approx \frac{B}{A} \tag{5.26}$$

$$S_{\max} \approx \left(-\frac{A}{\lambda}\right)^{1/3}. \tag{5.27}$$

In the first case we neglected the influence of λ for small S, in the latter the influence of B for large S. As we expect approximately equal contributions from all three 'sources' A, B and λ, the results are fairly accurate. However, these values are exact for either $\lambda = 0$ or $B = 0$ respectively. For $\lambda = 0$ the scale factor becomes minimal at $S = S_{\min}$, but has no upper limit. Without the c-field S has a single extremum at $S = S_{\max}$.

If we look at

$$\frac{d}{dS}\dot{S}^2 = 2\lambda S - \frac{A}{S^2} + 2\frac{B}{S^3} \equiv 0, \tag{5.28}$$

which gives the extrema of the 'velocities' $\dot{S}$, we find that there exists no extremum for $B = 0$, but for $\lambda = 0$.

$$B = 0: \qquad S = \left(\frac{A}{2\lambda}\right)^{1/3} < 0 \tag{5.29}$$

$$\lambda = 0: \qquad S = \frac{2B}{A} \tag{5.30}$$

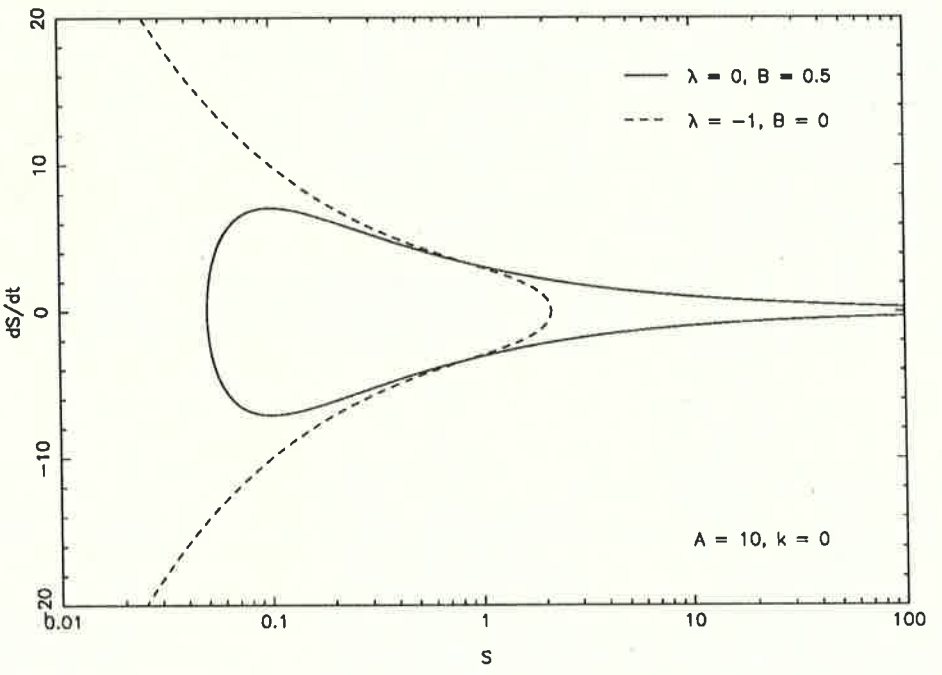

Figure 5.1: Two typical possibilities for the scale factor in absence of either the c-field or the cosmological constant.

These two extreme cases can be characterized as follows. The c-field acts as a repulsive force, which prevents the scale factor from reaching zero. There is a lower limit, given approximately by $S_{\min}$. The negative cosmological constant tends to slow down the expansion. As its influence does not decrease with increasing S, like the influence of matter, we get an upper boundary $S_{\max}$. Absence of the c-field yields to a singularity. Without λ we have a bouncing universe, i.e., the scale factor starts at infinity, contracts to $S_{\min}$ and expands again to infinity. Figure 5.1 shows these two possibilities.

Therefore, in order to get closed trajectories, i.e., an oscillating scale factor, we require

$$\begin{aligned} \lambda &< 0 \\ B &> 0. \end{aligned}$$

In fact, there is a third condition. Looking at (5.25) we notice that there is an upper limit for B. If $B > B_{\max}$ we can not get any real solution for $\dot{S}$. For $k = 0$ this limit can be calculated from $\dot{S} = 0$ and $\frac{d}{dS}\dot{S}^2 = 0$ and yields

$$B_{\max} = \frac{3}{4}\left(-\frac{A^4}{4\lambda}\right)^{1/3}. \tag{5.31}$$

If $B < B_{\max}$ we have an oscillating scale factor as shown in Figure 5.2 for different values of the parameters A, B and λ.

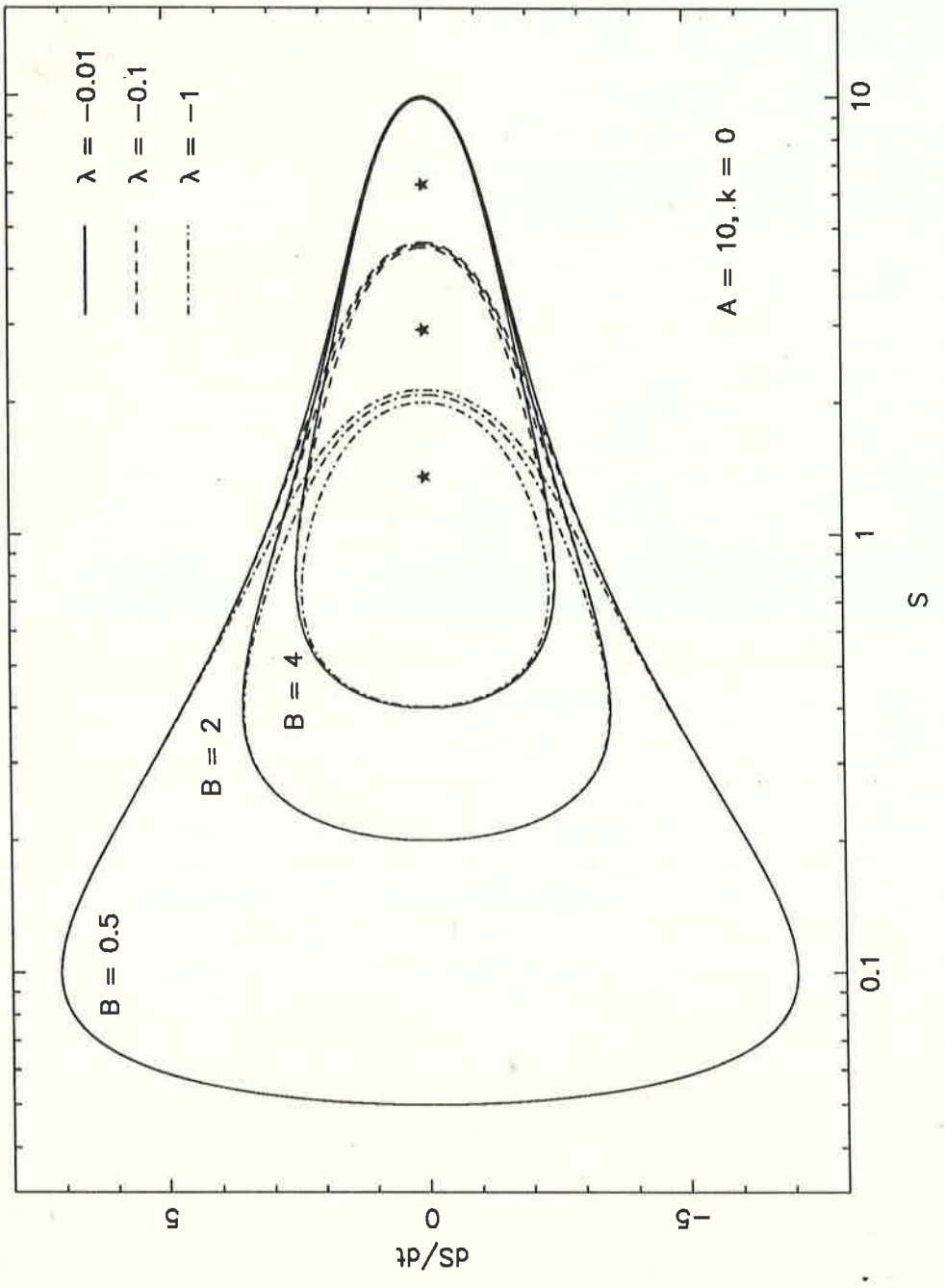

Figure 5.2: Trajectories in phase space for different values of A, B and λ. The '$\star$'s denote a static universe.

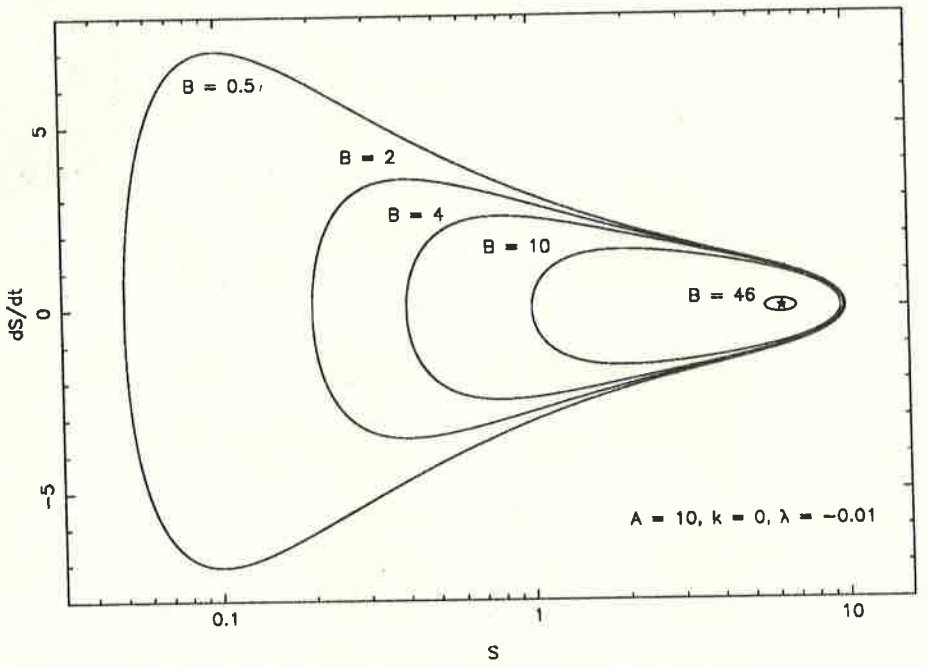

Figure 5.3: Increasing B leads to a static universe

As a curiousity we can obtain a static universe, marked by '$\star$' in the figures. These solutions are stable unlike the static universe of Einstein. We have set $\dot{S} \equiv 0$ and $\ddot{S} \equiv 0$ in (5.21) and (5.22). We easily find

$$S_{\text{static}} = \left(-\frac{A}{4\lambda}\right)^{1/3}. \tag{5.32}$$

To reach such a solution, we can for example keep A and λ fixed and increase B until

$$B \equiv B_{\text{max}} = \frac{3}{4}\left(-\frac{A^4}{4\lambda}\right)^{1/3} \tag{5.33}$$

as in the previous discussion. Some trajectories for this procedure are shown in Figure 5.3. The static universe is an extremely fine-tuned state. It corresponds to a single point in parameter space. For smaller B we have small oscillations, for larger B we will not have any solution at all. The universe behaves similar to a pendulum which gets slightly pushed from a stable position of rest.

Including the curvature term k shows no difference in principle. For $k = +1$ it is easy to see, that S_{min} increases and S_{max} decreases. It is the other way around for $k = -1$. In Figure 5.4 we show the influence of k on the behaviour of the scale factor.

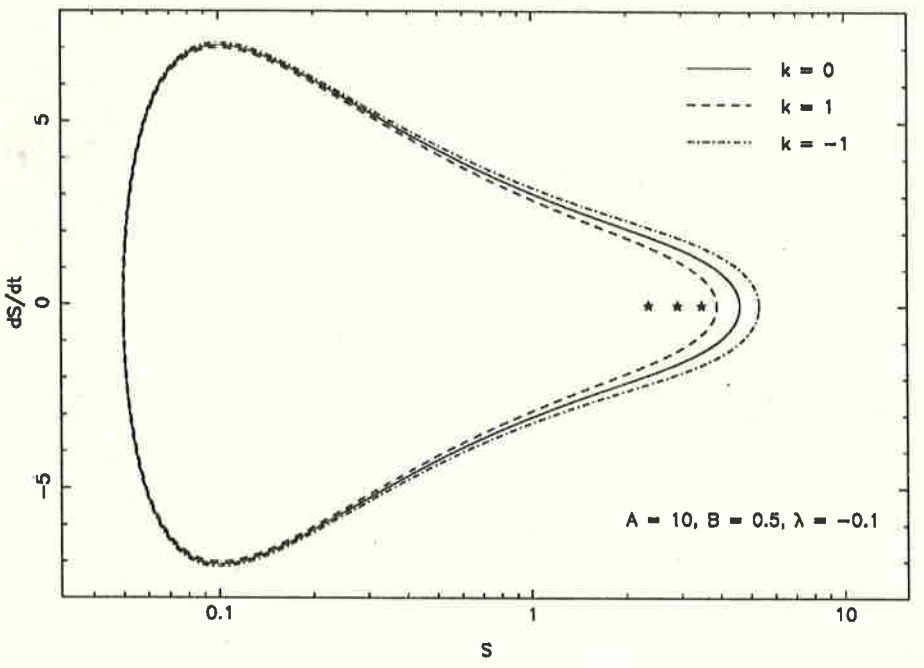

Figure 5.4: Influence of the curvature term k on trajectories

Now S_{static} is given by

$$S_{\text{static}} = \left(\frac{-A}{8\lambda} + \sqrt{\left(\frac{-k}{6\lambda}\right)^3 + \left(\frac{A}{8\lambda}\right)^2}\right)^{1/3} + \left(\frac{-A}{8\lambda} - \sqrt{\left(\frac{-k}{6\lambda}\right)^3 + \left(\frac{A}{8\lambda}\right)^2}\right)^{1/3} \tag{5.34}$$

and the maximal value for B by

$$B_{\max} = -3\lambda S_{\text{static}}^4 + kS_{\text{static}}^2. \tag{5.35}$$

We should note that for $k = -1$ Equation (5.34) is only valid as long as λ is smaller than

$$\lambda_{\max} = -\frac{8}{27A^2}. \tag{5.36}$$

For $\lambda = \lambda_{\max}$ we get from (5.34)

$$S_{\text{static}} = \frac{3}{2}A, \tag{5.37}$$

which is the upper turn-around point for S in the phase space diagram. There are actually two more solutions, but these are not of any physical relevance as they lead to a negative scale factor.

$$S_{2/3} = -\frac{3}{4}A \tag{5.38}$$

Finally, if $\lambda > \lambda_{\max}$, we get three solutions again, and again there is only one positive.

$$S = \frac{2}{\sqrt{-6\lambda}} \cos\left[\frac{1}{3}\cos^{-1}\left(\frac{3}{4}A\sqrt{-6\lambda}\right)\right] \tag{5.39}$$

5.3.2 Exact Solution

From the qualitative analysis in the preceding section we expect an oscillatory solution for the scale factor. In the series of papers concerning the QSSC [27, 28, 29] Hoyle et al. assumed the form

$$S(t) = \bar{S}\left(1 + \eta\cos\frac{2\pi t}{Q}\right) \tag{5.40}$$

during the interval without creation of matter. The parameter η satisfies the condition

$$0 < \eta < 1$$

to avoid a singularity. This is in accordance with the discussion above. The oscillation period Q is of the order of several billion years. The meaning of $\bar{S}$ will be discussed later. Basically, $\bar{S}$ is related to an overall exponential expansion.

We will now calculate an exact solution for $S(t)$ and we start with the form

$$S(t) = \bar{S}\,(1 + \eta\cos\theta(t))\,. \tag{5.41}$$

The linear relation between t and θ and the free parameter Q are replaced by a function $\theta(t)$, which has to be determined. If we put (5.41) into (5.20) we get

$$3\eta^2\dot{\theta}^2\sin^2\theta + 3\frac{kc^2}{\bar{S}^2} = \lambda c^2(1+\eta\cos\theta) + \frac{8\pi G\bar{\rho}}{1+\eta\cos\theta} - \frac{4\pi G\hbar\bar{c}^2}{c^3(1+\eta\cos\theta)^2}. \tag{5.42}$$

Two more conditions can be obtained, when we make use of the extrema of S. We set $S_{\max} = S(\theta = 0)$ and $S_{\min} = S(\theta = \pi)$, and note that $\dot{S} = 0$ at these points. From (5.42) we then have

$$\lambda c^2 + \frac{8\pi G\bar{\rho}}{(1\pm\eta)^3} - \frac{4\pi G\hbar\bar{c}^2}{c^3(1\pm\eta)^4} - 3\frac{kc^2}{\bar{S}^2(1\pm\eta)^2} = 0. \tag{5.43}$$

In the end these relations yield $\bar{\rho}$ and $\bar{c}^2$ as functions of η, k, λ and $\bar{S}$

$$\bar{\rho} = -\frac{\lambda c^2}{2\pi G}(1+\eta^2) + \frac{3kc^2}{4\pi G\bar{S}^2} \tag{5.44}$$

$$\bar{c}^2 = -\frac{\lambda c^5}{4\pi G\hbar}(1-\eta^2)(\eta^2+3) + \frac{3kc^5}{4\pi G\hbar\bar{S}^2}(1-\eta^2). \tag{5.45}$$

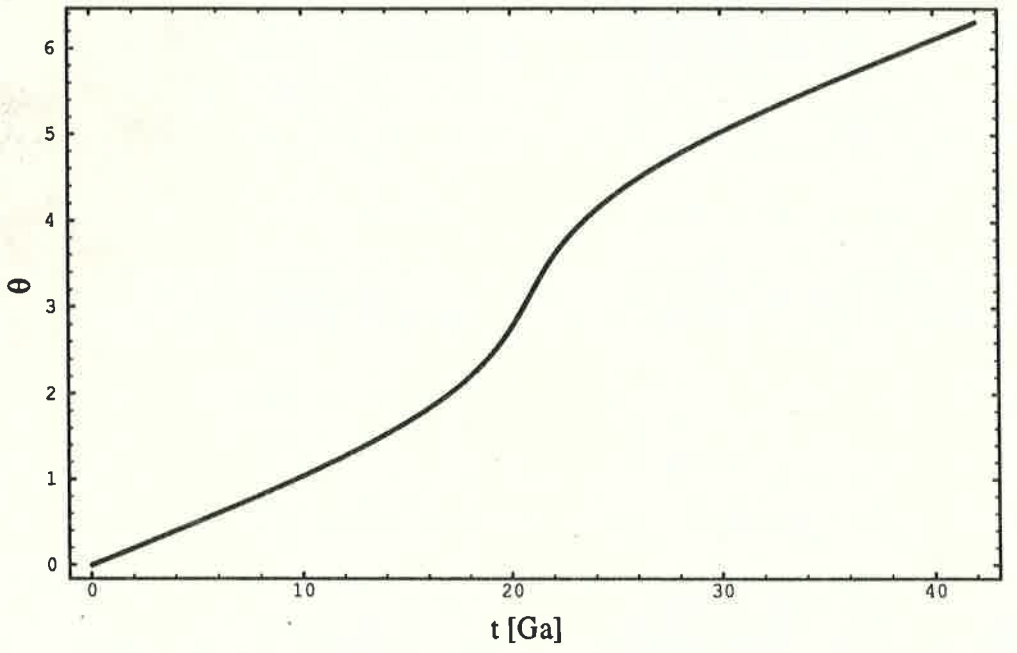

Figure 5.5: $\theta(t)$ for $k = 0$ and $\eta = 0.75$. We set $\lambda = -10^{-56}\,\mathrm{cm}^{-2}$, to get a time scale in Ga.

After some calculation we get an equation for $\dot{\theta}$, which is unfortunately not analytically to integrate. This could have already been seen from (5.25), as that equation leads to an elliptical integral.

$$\dot{\theta} = \frac{\sqrt{-\lambda}\,c}{\sqrt{3}(1+\eta\cos\theta)}\left(\eta^2\cos^2\theta + 4\eta\cos\theta + 6 + \eta^2 - \frac{3k}{\lambda\bar{S}^2}\right)^{1/2} \tag{5.46}$$

or

$$\begin{aligned} t &= \frac{\sqrt{3}}{\sqrt{-\lambda}\,c}\int_0^\theta \frac{1+\eta\cos\theta'}{\sqrt{\eta^2\cos^2\theta' + 4\eta\cos\theta' + 6 + \eta^2 - \frac{3k}{\lambda\bar{S}^2}}}\,d\theta' \\ &\equiv \frac{\sqrt{3}}{\sqrt{-\lambda}\,c}\xi(\eta,\theta). \end{aligned} \tag{5.47}$$

The integral can be evaluated numerically. All results for t scale with $(-\lambda)^{-1/2}$, so we set $\lambda = -10^{-56}\,\mathrm{cm}^{-2}$ for this section in accordance with Section 4.3. A more accurate determination will be given later, when we relate the theoretical results to observations.

In Figure 5.5 we show the θ-t-dependence for $k = 0$ and $\eta = 0.75$. The deviation from a linear relation is apparently maximal around the minimum of the scale factor, at $\theta = \pi$. It is easy to see from (5.47) that for $\eta = 0$ we have

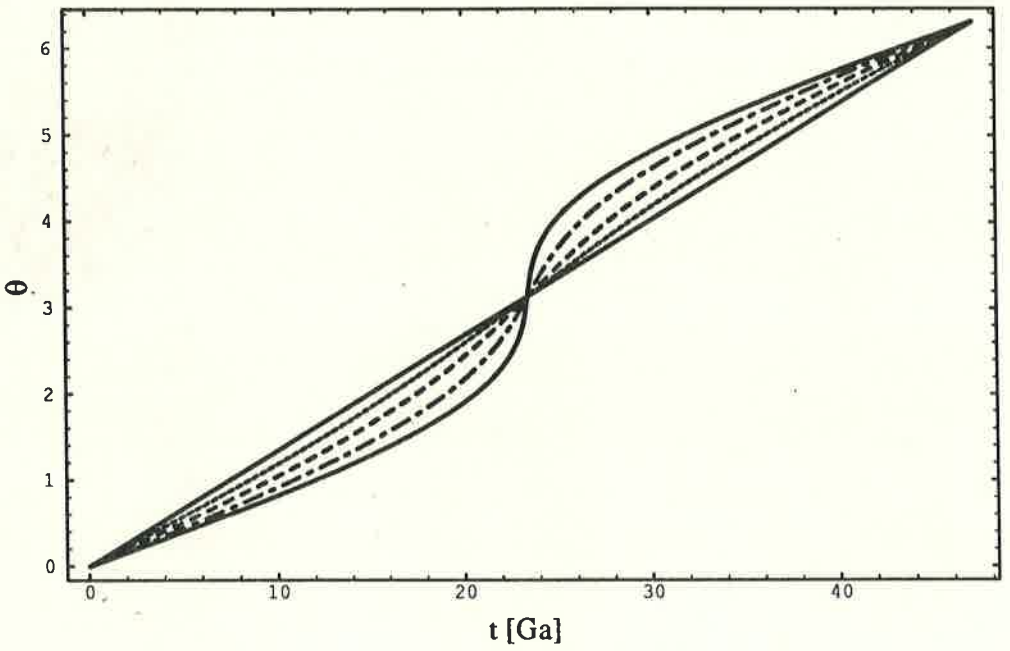

Figure 5.6: Larger η lead to more deviation from a linear relation between θ and t. λ takes different values to get the same oscillation period for the different values of $\eta = 0, 0.25, 0.5, 0.75, 0.95$.

again θ proportional to t. Figure 5.6 illustrates the influence of η on the non-linearity of $\theta(t)$. Here we used different values for λ to get the same oscillation period Q. The latter is obviously given by (5.47) with the upper limit $\theta = 2\pi$.

$$Q = \frac{\sqrt{3}}{\sqrt{-\lambda}c}\xi(\eta, 2\pi) \tag{5.48}$$

The change of Q with η is shown in Figure 5.7 for the three different curvatures $k = 0, \pm 1$. For the numerical evaluation in case $k \neq 0$ we assumed $\bar{S} = 10^{28}$ cm, the Hubble radius.

It can be seen that the oscillation period is larger for $k = -1$ and smaller for $k = +1$ than in the euclidean case. The period decreases for all three possibilities with increasing amplitude η. We note that the previous mentioned analogy with a pendulum does not match perfectly, as the period is independent of the amplitude for the latter. However, the change in Q is not very large.

The difference of $\theta(t)$ for $k = 0, \pm 1$ for the same values for η and λ is illustrated in the next Figure 5.8. At first sight it seems to be possible to go from one case to another by a simple rescaling of time. This is not the case as one can see from Table 5.1, where we calculated several ratios of time for different k and equal η. Rescaling fo time would be successful only if there would be the same ratio for all θ.

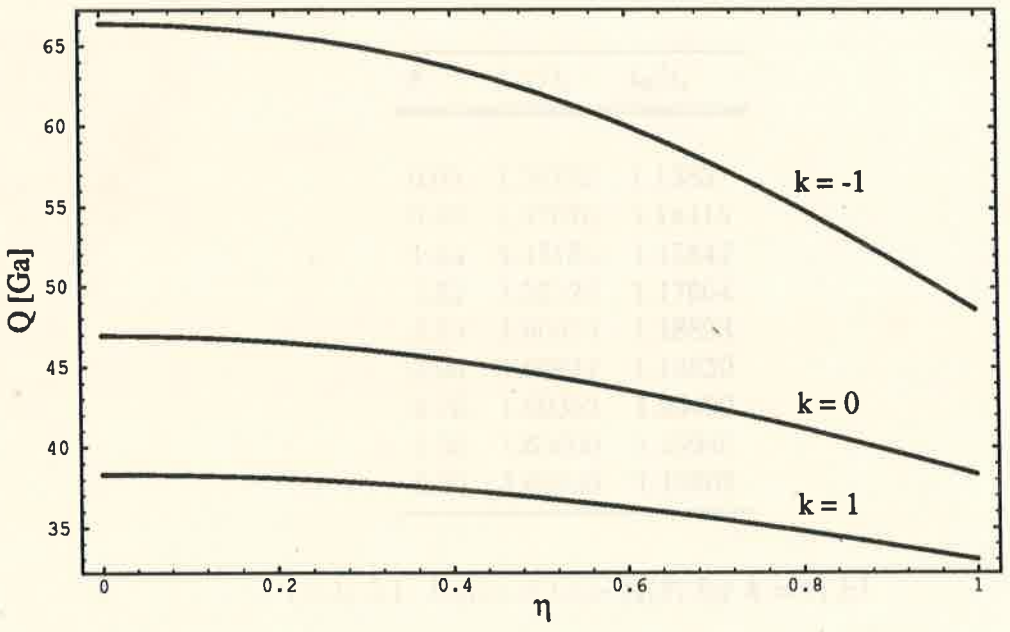

Figure 5.7: Oscillation period Q as a function of η

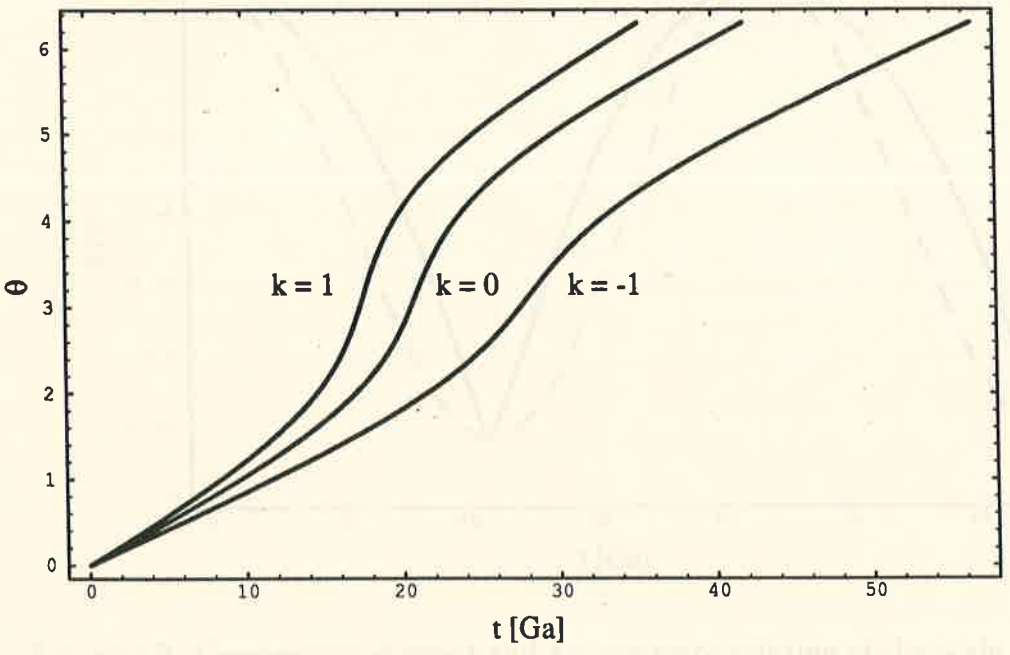

Figure 5.8: $\theta(t)$ for the three possibilities $k = 0, \pm 1$ ($\eta = 0.75$).

θ	t_{-1}/t_1	t_0/t_1
0.05	1.35732	1.13857
0.80	1.37670	1.14415
1.55	1.43185	1.15842
2.35	1.52126	1.17664
3.15	1.60313	1.18893
3.90	1.66647	1.19839
4.70	1.69362	1.20499
5.50	1.65600	1.19946
6.30	1.60135	1.18862

Table 5.1: Ratio of time $t_k(\theta)$ for $k = 0, \pm 1$

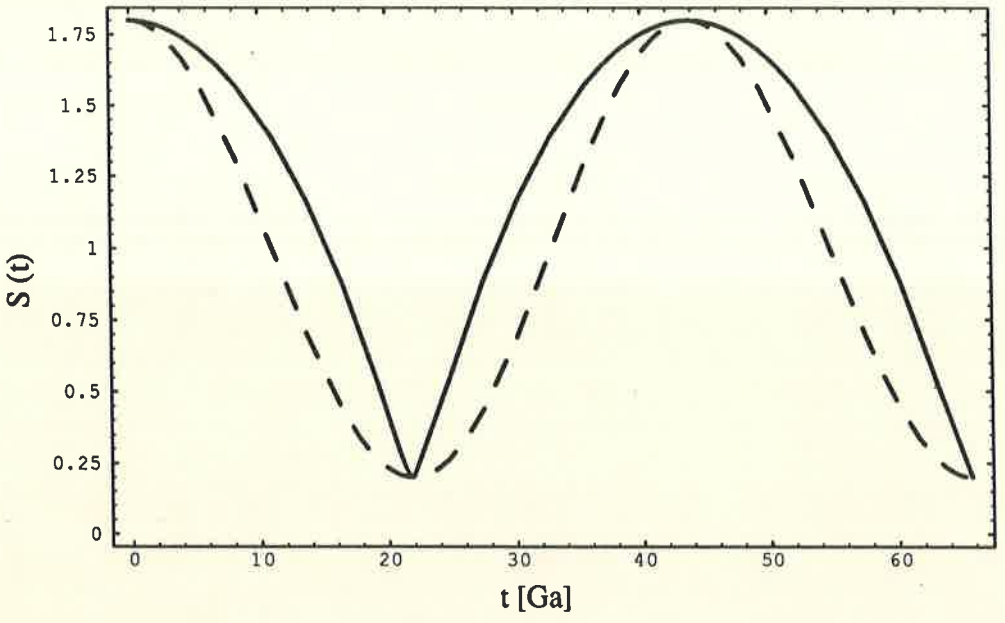

Figure 5.9: Comparison of exact and approximate solution of the scale factor in a non-creation interval

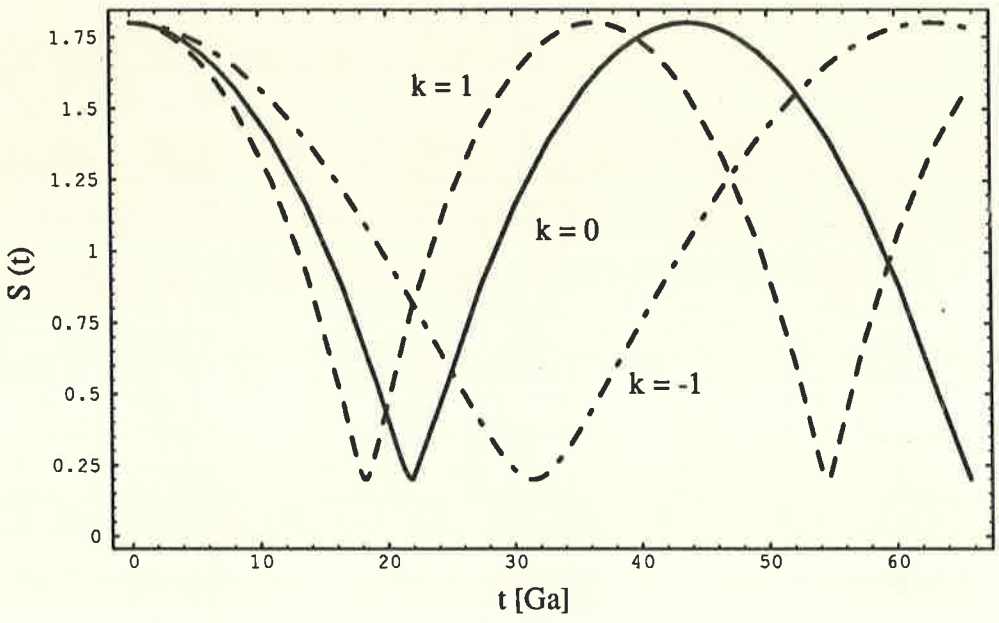

Figure 5.10: The influence of curvature k on the scale factor

Until now we have looked only at $\theta(t)$ but not at the scale factor and its difference to the approximate solution (5.40). We adjusted amplitude and period of both solutions and show the result in Figure 5.9. The amplitude is $\eta = 0.8$ and $\lambda = -0.88 \cdot 10^{-56}\,\mathrm{cm}^{-2}$, but these exact values will be important only when we deal with observations. We notice the narrower troughs and flatter crests as compared to the approximate solution, which is represented by the dashed line.

Figure 5.10 illustrates the influence of k. Again we have the difference in Q, but additionally even narrower troughs for $k = 1$ than for $k = 0, -1$. The contraction and expansion is more rapid in a closed universe.

Recalling the parameter B from the preceding phase space analysis, we can illustrate the general behaviour of the scale factor in Figure 5.11. The static solution corresponds to $B = B_{\mathrm{max}}$ or $\eta = 0$ respectively. For decreasing B we get oscillations with small amplitude η and long period Q. Even smaller B are equivalent to large η and shorter period. It can be seen that solutions with large η deviate more from a pure cosine solution.

5.4 The Composite Solution

In general we will not have just one of the previously discussed modes but a mixture of both. Creation of matter is very likely to occur around the minima of the scale factor as the c-field background is then the highest. We expect a series

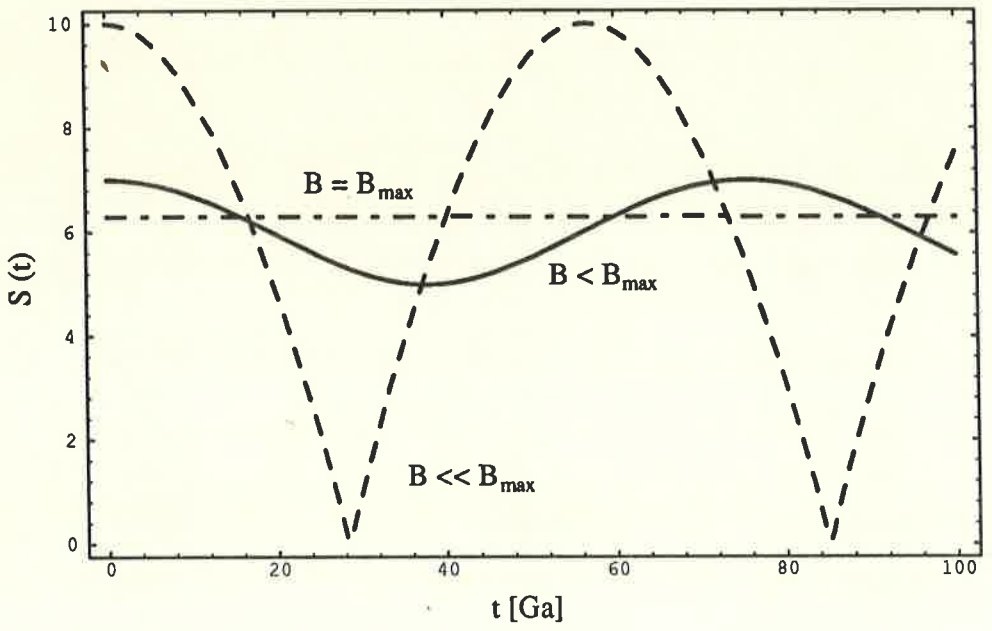

Figure 5.11: Solutions for different values of B

of free oscillations in between which matter is created.

In order to find a combined solution, we have to relate barred quantities like $\bar{\rho}$ to the corresponding non-barred. From the de Sitter like solution we have

$$2\pi G\rho_{\mathrm{DS}} = \frac{3}{P^2} - \lambda c^2 \tag{5.49}$$

and from the oscillation

$$2\pi G\bar{\rho} = -\lambda c^2(1+\eta^2) + \frac{3kc^2}{2\bar{S}^2} \tag{5.50}$$

$$-\lambda c^2 = \frac{3\xi^2(\eta)}{Q^2}. \tag{5.51}$$

With these equations we get

$$\frac{\rho_{\mathrm{DS}}}{\bar{\rho}} = \left(1 + \frac{Q^2}{\xi^2 P^2}\right)\left(1 + \eta^2 + \frac{kc^2Q^2}{2\bar{S}^2\xi^2}\right)^{-1}. \tag{5.52}$$

As we expect the time scale of exponential expansion to be much longer than one oscillation, $P \ll Q$, the second term in the numerator can be neglected. The third term in the denominator can essentially be written as k.

$$\frac{\rho_{\mathrm{DS}}}{\bar{\rho}} \approx \frac{1}{1+\eta^2+k} \tag{5.53}$$

During one oscillation we had $\rho_{\text{osc}} \sim S^{-3}$, leading to $\rho_{\text{min}} = \bar{\rho}(1+\eta)^{-3}$ and $\rho_{\text{max}} = \bar{\rho}(1-\eta)^{-3}$, ergo

$$\frac{1}{(1+\eta)^3} < \frac{\rho_{\text{osc}}}{\bar{\rho}} < \frac{1}{(1-\eta)^3}. \tag{5.54}$$

$\bar{\rho}$ has been sort of a mean density during one cycle. It can be seen from the last two relations, that ρ_{DS} also lies between these two limits. It therefore suggests itself to identify ρ_{DS} with this mean density.

The rate of creation can be calculated in the following way. According to the principle that every cycle should be an exact repetition of the previous one, we need creation of mass as space has expanded due to the de Sitter like solution after one particular oscillation. The amount of new matter is therefore

$$(\rho + \Delta\rho)\mathrm{e}^{-3Q/P} = \rho \tag{5.55}$$

or, as $P \ll Q$,

$$\frac{\Delta\rho}{\rho} \approx \frac{3Q}{P}. \tag{5.56}$$

In the end we find that a solution of the form

$$S(t) = \mathrm{e}^{t/P}\,(1 + \eta\cos\theta(t)) \tag{5.57}$$

is very well suited for the quasi-steady state cosmological model (Figure 5.12). For the future calculations we choose $k = 0$, for convenience and for it was shown that there is no major difference to the other cases.

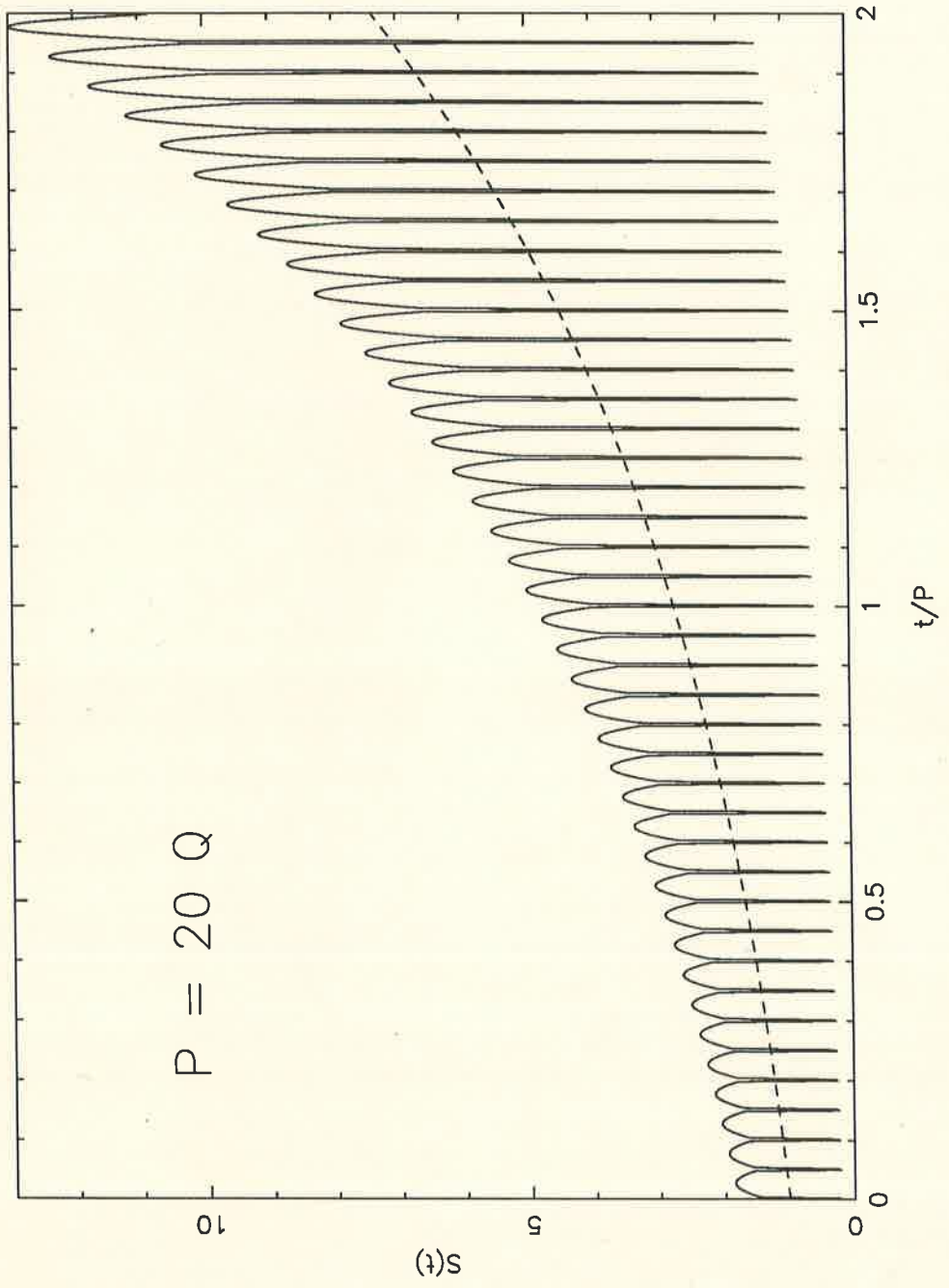

Figure 5.12: Illustration of the scale factor in QSSC. The expansion time scale is $P = 20\,Q$, the oscillation amplitude $\eta = 0.8$. The dashed line (- - - -) shows the exponential expansion.

Chapter 6

Observational Tests

6.1 Parameters of QSSC

We have seen that the general solution for the scale factor in QSSC is an exponential expansion superposed with an oscillation. We will now relate the parameters of the theory λ, η, P, and t_0 to observations. P will be determined later by radio source counts. The present epoch t_0 is measured in units of the oscillation period Q since the last maximum, $\theta(t=0)=0$.

The Hubble constant is given by

$$H = \frac{1}{P} - \frac{\eta \sin\theta}{1+\eta\cos\theta}\dot{\theta}. \tag{6.1}$$

Assuming a maximal redshift for sources located at the minima we get a condition for η, when we for the moment neglect the exponential expansion.

$$\cos\theta = z_{\max}\left(\frac{1}{\eta}-1\right)-1 \tag{6.2}$$

or

$$0 \le z_{\max}\left(\frac{1}{\eta}-1\right) \le 2. \tag{6.3}$$

We will use these two quantities to determine the other free parameters. We recall from (5.47) that $\dot{\theta}\sim\sqrt{-\lambda}$ and therefore $Q\sim 1/\sqrt{-\lambda}$ and $H\sim\sqrt{-\lambda}$. The Hubble constant can be scaled with the cosmological constant. This is, however, not possible for the deceleration parameter q. The latter is given by

$$\begin{aligned} q &= -\frac{1}{H^2}\frac{\ddot{S}}{S} \\ &= -\frac{1}{H^2}\left(\frac{1}{P^2} - \frac{\eta\sin\theta\left(\frac{2}{P}\dot{\theta}+\ddot{\theta}\right)-\eta\cos\theta\,\dot{\theta}^2}{1+\eta\cos\theta}\right) \end{aligned} \tag{6.4}$$

with

$$\ddot{\theta} = \frac{\eta \sin\theta}{(1+\eta\cos\theta)^2}(\dot{\theta} - \eta\cos\theta - 2). \tag{6.5}$$

Note that q is a function of η and θ only. In Table 6.1 we started with the values for $h_0 = 0.75$, $z_{max} = 5$ and $P = 20Q$. For η within the possible range as given by (6.3) we calculated the dimensionless oscillation period ξ, the angle θ from (6.2) and the present epoch t_0. Using h_0 we get λ and therefore Q in units of time. Finally we obtain from θ and η the deceleration parameter q.

It is interesting to see that for the minimal possible η we have to go close to the scale factor maximum at $\theta = 2\pi$ for the demanded z_{max}. As $\dot{S}$ approaches zero at this limit, the Hubble constant becomes very small. A large cosmological constant is required to scale h_0 to its desired value, leading therefore to a very short oscillation period in physical units. We showed already in Chapter 5.3 that ξ does not vary significantly with η. However, q_0 is independent of λ, so that the small 'scaleless' Hubble constant causes a considerable rise for θ approaching 2π, where q_0 diverges.

At the large η end we are closed to the minimum, $\theta = \pi$. The scale factor shows a steep incline, therefore h_0 becomes large. We need λ to be small, on the other hand leading to very long oscillation periods. Whereas q is very sensitive for smaller η, it does not vary much in this region.

In previous papers Hoyle et al. [28, 29] had used the approximate solution and they had chosen the following values for the parameters:

$$\begin{aligned} \eta &= 0.75, \qquad t_0 = 0.85 \\ P &= 20\,Q, \qquad Q = 40 \cdot 10^9\,\mathrm{a} \end{aligned}$$

They obtained a Hubble constant of $h_0 = 0.65$ and a rather high deceleration parameter $q_0 = 1.725$. The maximal redshift was $z_{max} = 4.86$. This choice of parameters also took care of the age of globular clusters, which are about 14 Ga old. Hoyle et al. assumed these structures to have formed during oscillatory minima.

Table 6.1 clearly shows that this set of parameters is not compatible with the exact solution. We could, however, change λ to get the same Hubble constant, but Q would be generally too small and q far too large.

In accordance with recent measurements of the Hubble constant [17] we take

$$\begin{aligned} h_0 &= 0.75, \qquad t_0 = 0.7 \\ \eta &= 0.80, \qquad P = 20\,Q \end{aligned}$$

Hence the other parameters take the values

$$\begin{aligned} z_{max} &= 5.1 \\ \lambda &= -0.88 \cdot 10^{-56}\,\mathrm{cm}^{-2} \\ Q &= 43.8 \cdot 10^9\,\mathrm{a} \\ q_0 &= 0.99 \end{aligned}$$

η	ξ	θ	t_0	λ $[10^{-56}\mathrm{cm}^{-2}]$	Q [Ga]	q_0
0.72	2.30467	5.94829	0.920961	-24.6175	8.50393	17.6998
0.73	2.29789	5.72708	0.869036	-8.84399	14.1461	6.5631
0.74	2.29104	5.57073	0.832619	-5.09866	18.5754	3.92922
0.75	2.28413	5.44212	0.802928	-3.41455	22.6301	2.74865
0.76	2.27715	5.32983	0.777271	-2.45952	26.5827	2.08118
0.77	2.27012	5.22851	0.754392	-1.84718	30.5793	1.6545
0.78	2.26302	5.13512	0.73359	-1.42365	34.7232	1.3603
0.79	2.25587	5.04775	0.714424	-1.11546	39.1039	1.14692
0.8	2.24866	4.96507	0.6966	-0.883007	43.8101	0.986555
0.81	2.24139	4.8861	0.679912	-0.703084	48.9381	0.862913
0.82	2.23407	4.81011	0.664208	-0.561151	54.5996	0.765801
0.83	2.22669	4.73649	0.649375	-0.447637	60.9298	0.688513
0.84	2.21926	4.66475	0.635328	-0.355974	68.0977	0.626452
0.85	2.21178	4.59447	0.622002	-0.281499	76.3198	0.576354
0.86	2.20425	4.52525	0.609348	-0.220799	85.8807	0.535831
0.87	2.19668	4.45674	0.59733	-0.171316	97.1626	0.503094
0.88	2.18905	4.38858	0.585921	-0.131082	110.692	0.476765
0.89	2.18138	4.32041	0.575103	-0.0985489	127.215	0.455761
0.9	2.17367	4.25183	0.564869	-0.0724766	147.818	0.439212
0.91	2.16591	4.18243	0.555215	-0.0518473	174.145	0.426402
0.92	2.15811	4.11169	0.546148	-0.035809	208.791	0.416731
0.93	2.15027	4.03898	0.537683	-0.0236332	256.074	0.409683
0.94	2.1424	3.96346	0.529842	-0.0146841	323.675	0.404805
0.95	2.13448	3.884	0.52266	-0.00839468	426.504	0.401691
0.96	2.12653	3.79886	0.516188	-0.00425013	597.177	0.399966
0.97	2.11854	3.70515	0.510499	-0.00177433	920.776	0.399279
0.98	2.11053	3.59728	0.505708	-0.000520502	1693.61	0.399292
0.99	2.10248	3.46077	0.502015	-0.0000644326	4795.25	0.399665

Table 6.1: Parameters for $h_0 = 0.75$, $z_{\mathbf{max}} = 5$ and $P = 20\,Q$

Taking the exponential expansion into account, the maximal observed redshift is slightly higher than 5. It should be mentioned that the time elapsed since the last minimum in this case is about 8.8 Ga.

In the following sections we work out observational features of QSSC, using the exact solution for the scale factor and the above values for the parameters.

6.2 Counts of Radio Sources

6.2.1 · Principles

The number counts of radio sources is one of the classical cosmological tests. As the results depend on the geometry of spacetime, we should be able to distinguish between different cosmological models. We will give a general overview about the underlying principles, after that we will apply the formalism to the QSSC.

In a static euclidean space there is a simple relation for the flux from a source with luminosity L at distance r

$$\mathcal{F} = \frac{L}{4\pi r^2}. \tag{6.6}$$

For the number of sources up to a given distance we have

$$N = \frac{4}{3}\pi n r^3, \tag{6.7}$$

where $n = const$ is the density of sources per unit volume. We can combine these two relations to

$$N^2\mathcal{F}^3 = const \tag{6.8}$$

or, equivalently

$$\frac{d\log N}{d\log \mathcal{F}} = -\frac{3}{2}. \tag{6.9}$$

It is nothing else than the well known volume-surface relationship in euclidean geometry.

In a FRW-like universe the formulae above look of course different. Due to the expansion of space we expect less faint sources, whereas the deviation from the euclidean result should be less striking in our neighbourhood.

The simplest case is the matter dominated Einstein-de Sitter (EdS) model, $k = 0$, $\Omega = 1$. It is convenient to use the redshift z as a distance parameter. We can write the flux reaching us from a distant source as

$$\mathcal{F} = \frac{L}{4\pi D_L^2}. \tag{6.10}$$

Here we defined the luminosity distance D_L as

$$D_L = S_0 r(z)(1+z) \tag{6.11}$$

in order to make (6.10) look similar to (6.6). In an EdS universe D_L looks like

$$D_L = \frac{2c}{H_0}\left((1+z) - (1+z)^{1/2}\right). \tag{6.12}$$

Astronomers do not measure the total (bolometric) flux $\mathcal{F}$, i.e., integrated over all wavelengths, but only in a frequency range given by the bandwidth of the instrument. The appropriate quantity is therefore the flux density F. The objects of interest are extragalactic, like radio galaxies, so the flux quantities are very small. The common unit is Jansky, where $1\,\mathrm{Jy} = 10^{-26}\,\mathrm{W\,m^{-2}\,Hz^{-1}}$. We find the flux density as a function of frequency to be

$$F(\nu) = \frac{L\,I(\nu(1+z))}{4\pi S_0^2 r^2 (1+z)}. \tag{6.13}$$

Here $I(\nu)$ is the intensity function, which gives the luminosity in the emission frequency range $\nu \ldots \nu + d\nu$ in the rest frame of the source

$$dL = L\,I(\nu)d\nu. \tag{6.14}$$

In order to make calculations easier, it is very common to use a power law for $I(\nu)$ with a spectral index α

$$I(\nu) = \nu^{-\alpha} \tag{6.15}$$

For a power law spectrum we can write (6.13) in the simpler form

$$F(\nu) = \frac{L_\nu}{4\pi S_0^2 r^2 (1+z)^{1+\alpha}}. \tag{6.16}$$

The quantity L_ν is called power and is the luminosity per frequency. In the case $\alpha = 1$ the spectrum is also referred to as a logarithmic spectrum. We will assume this form for the remainder of the chapter.

The number of sources in a shell with volume dV is generally given by

$$dN = n_{\mathrm{CM}} dV_{\mathrm{CM}}. \tag{6.17}$$

The index CM denotes quantities in a comoving frame. Expressing n_{CM} through today's proper density we get

$$dN = n_0 S_0^3\, 4\pi r^2 dr. \tag{6.18}$$

With the coordinate radius

$$r = \frac{2c}{S_0 H_0}\left(1 - (1+z)^{-1/2}\right) \tag{6.19}$$

and

$$\frac{dr}{dz} = \frac{c}{S_0 H_0}(1+z)^{-3/2} \tag{6.20}$$

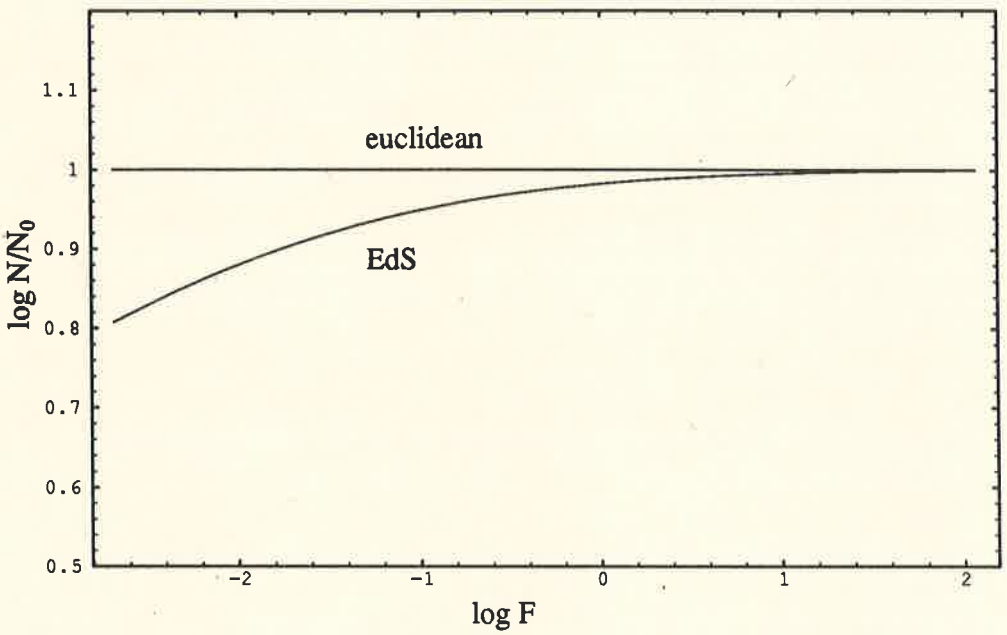

Figure 6.1: Integral source counts as expected in an EdS universe. $N_0 = \bar{N}F^{-3/2}$ is the normalization factor.

(6.18) yields

$$dN = 16\pi n_0 \left(\frac{c}{H_0}\right)^3 \left((1+z)^{-3/2} + (1+z)^{-5/2} - 2(1+z)^{-2}\right) dz. \qquad (6.21)$$

This result can easily be integrated and we get the number of sources in a redshift interval from z_1 to z_2

$$N(z_2, z_1) = 32\pi n_0 \left(\frac{c}{H_0}\right)^3 \left[(1+z)^{-1} - (1+z)^{-1/2} - \frac{1}{3}(z+1)^{-3/2}\right]_{z_1}^{z_2}. \qquad (6.22)$$

Figure 6.1 shows the expected results for an euclidean and an EdS universe. Number counts are usually normalized to the value expected in an uniformly filled static euclidean universe. As euclidean source counts show a slope of -1.5 on a log-log scale (cf. (6.9)), it is convenient to multiply N with $F^{3/2}$ to get a horizontal line instead. Another possibility is to show differential source counts, $dN/dF \equiv \Delta N$ against F, multiplied with $F^{5/2}$, thus not introducing an arbitrary normalization factor. We will use both conventions.

In this very simplified picture we assumed that n, the density of sources is constant and independent of the luminosity. A more realistic model involves a luminosity function ϕ, which gives the mean number of sources per unit volume with luminosity in the range $L \ldots L + dL$

$$dn = \phi(L)dL. \qquad (6.23)$$

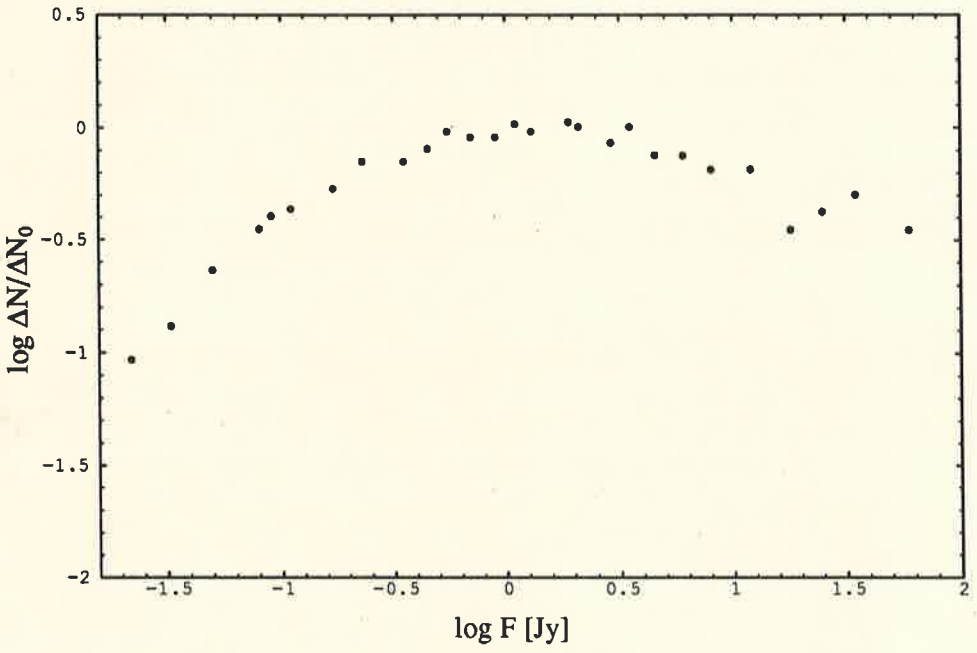

Figure 6.2: Observational data at 408 MHz. The differential count is normalized to an uniformly filled euclidean universe with $\Delta N_0 = 1125\, F^{-5/2}$.

As for the spectrum, a simple power law is frequently used, $\phi \sim L^{-\beta}$. For small β the counts are dominated by strong sources, for large β by weak sources.

However, even these assumptions can not fit observations. In Figure 6.2 we have redrawn the data for a frequency of 408 MHz obtained by Kellermann et al. [32]. There is a clear excess of faint sources, which can in principle be explained in two ways. First, we sit in a region of smaller source density. This explanation is also known as the "local hole" interpretation. Second, the luminosity and/or the density of sources evolve with time. Faint sources as distant and hence older objects could have had different properties than fairly nearby brighter sources. Evolution of galaxies seems to be plausible. There is increasing evidence, but still no conclusive proof, that galaxy properties correlate with redshift.

Historically, the deduction of galaxy evolution went against the steady state theory, as it is clearly inconsistent with the perfect cosmological principle.

It is now extremely difficult, if not impossible to untangle the geometry, the form of the luminosity function and its evolution with time from the observational data. The fact that we deal with an inhomogeneous mixture of quasars, radio galaxies, compact and extended sources, which all have different luminosity characteristics, does not make the task easier. Evolutionary models that fit the observations contain some 30–40 parameters [42].

6.2.2 Source Counts in QSSC

Contrary to big bang cosmology we start with the rather simple assumption of no evolution. Using the same formulae as in the standard case, we compute tables for coordinate radius and flux density. Instead of redshift we take time as distance parameter, as the redshift is ambiguous owing to the oscillating scale factor. We can see from Eq. (6.16) that the flux density $F \sim (1+z)^{-2}$. With the redshift being an oscillating function the flux density shows periodic variations, too. It turns out that besides the present half cycle we receive the largest fluxes from sources located around the maxima of previous cycles. These sources will therefore have a major effect on number counts in QSSC.

Due to the expected creation of matter around the minima of the scale factor, we do not assume a constant comoving density as usual. The density evolves on the time scale of the exponential expansion, while it remains constant during a particular oscillation. Or in terms of proper density, n_{proper} evolves $\sim S^{-3}$ during one oscillation. In accordance with the steady state principle n_{proper} does not change from one oscillation to the next. The comoving density changes exponentially

$$n_{\mathrm{CM}} = n_0 \, S_0^3 \, \mathrm{e}^{3(t-t_0)/P}, \tag{6.24}$$

where n_0 again is the present proper density. The number of sources in a time interval $t \ldots t + dt$ can therefore be calculated from

$$dN(t) = 4\pi \, \phi(L) \, n_0 \, S_0^3 \, \mathrm{e}^{3(t-t_0)/P} \, \frac{r(t)^2}{S(t)} \, cdt. \tag{6.25}$$

The algorithm is the following. For a flux density F_{scan} we calculate from the flux table by interpolation all times t_i, at which sources with this flux are located.

$$t_i \ni F(t_i) = F_{\mathrm{scan}}. \tag{6.26}$$

The number of solutions t_i will be odd. When going back in time, the first solution will be during the present half cycle before the last minimum. The second will be before the last maximum, marking the starting point of sources with flux higher than F_{scan}. The third solution marks the end of this population, in general prior the last maximum. The same holds for all cycles back. For smaller and smaller F_{scan} we get contributions from earlier and earlier cycles. Figure 6.3 illustrates the situation.

For all times t_i we will compute the corresponding number of sources back to that time, i.e., up to that distance and get the total number from an alternating series

$$N = N(t_1) - N(t_2) + N(t_3) \mp \cdots \tag{6.27}$$

This has been done for various sets of source populations with different luminosities L and abundances $\phi(L)$.

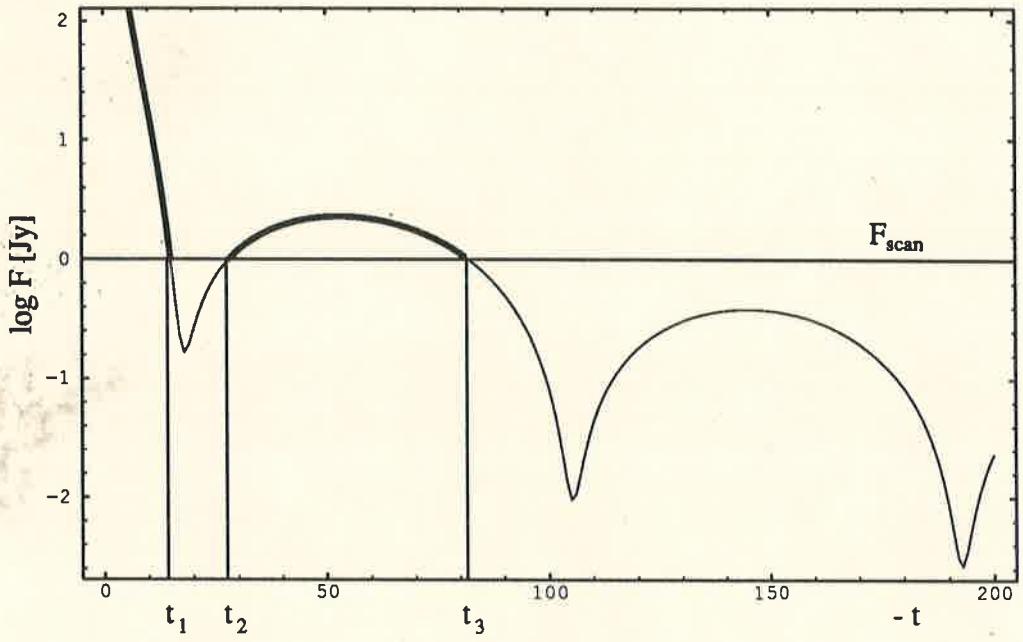

Figure 6.3: We plotted log F against t (arbitrary units), where t decreases to the right, to illustrate the calculation. The bold part marks the total contribution. $F_{\mathbf{scan}}$ is 1 Jy in this example.

For the first calculation we assumed the luminosity function $\phi \sim L^{-2.1}$. The population of sources consisted of eleven classes with power L_ν ranging from $3 \cdot 10^{28} - 3 \cdot 10^{29}$ W Hz^{-1} in equidistant steps on a logarithmic scale. Figure 6.4 shows the result as differential number count. The theoretical result resembles the observational data in Figure 6.2 fairly closely.

The most obvious features of this figure are

- the decrease down to fluxes of 50 Jy,
- the sharp rise that starts at about 30 Jy,
- the flattening at around 5 Jy,
- the plateau between 0.4 and 2 Jy,
- the gradual decline for even fainter sources.

As in the calculation done with the approximate solution by Hoyle et al. [28], we determined the ratio P/Q to differ not much from 20. It turns out that for larger values of P the decline towards the faint end is more gentle. For smaller P we will have the opposite effect, less faint sources. We see that the differences in source counts are only marginal as compared to the result obtained by Hoyle

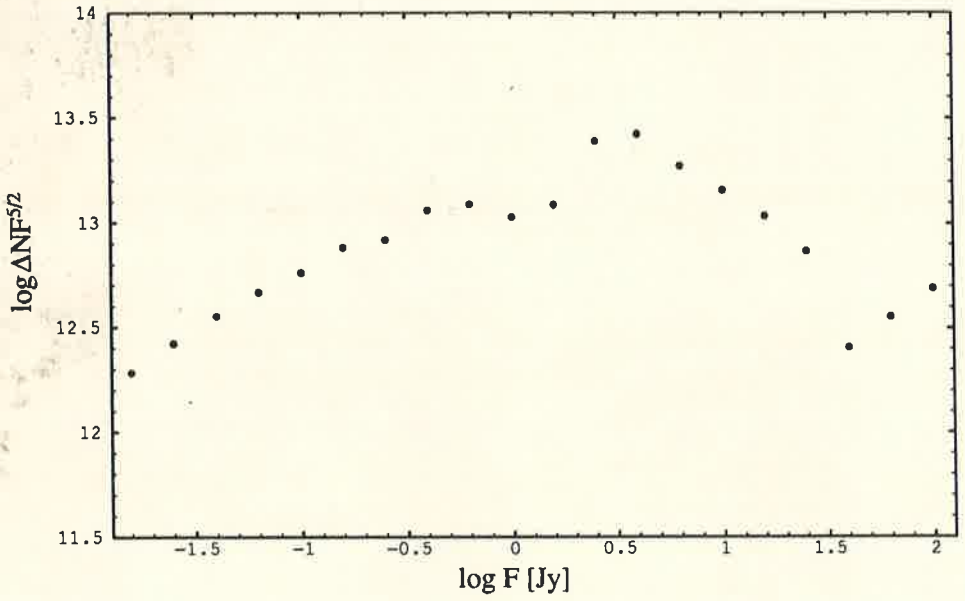

Figure 6.4: Differential counts of radio sources for the first scenario

et al. (op.cit.). But we should keep in mind that the luminosities we used are reduced by a factor 0.3.

Unlike in big bang cosmology, where evolution is said to be responsible for the excess of faint sources, the novel feature of the QSSC is the addition of sources from previous cycles, mainly the last one. As we have already pointed out earlier these sources are from epochs where the scale factor was larger than today. The very peculiar result of this calculation is that the majority of the sources in the steeper than euclidean flux range is blueshifted. In Figure 6.5 we computed the fraction of blueshifted sources for the first scenario. Clearly, more than 80% of sources in the flux range from 1 to 6 Jy should be blueshifted. In order to determine the redshift, or blueshift respectively, of one of the sources, we have to make an optical identification, since the measurement of shifts in frequency requires a line spectrum.

Such an identification has been done, e.g., by Allington-Smith [2, 3]. They had selected 59 sources at 408 Mhz from the B2 catalog with flux densities between 1 and 2 Jy. The aim was to study that particular part of the population that exceeds the non-evolutionary prediction by the greatest amount. The result was that 36 members of the sample have measured redshifts, corresponding to 61%.

It is tempting to conclude that the QSSC prediction is wrong. However, Allington-Smith's sample is very small, hence statistically not extremely relevant. It has been pointed out by McCarthy [36] that it is incomplete in its redshift content. Finally, there is always a non-zero probability of misidentifications of

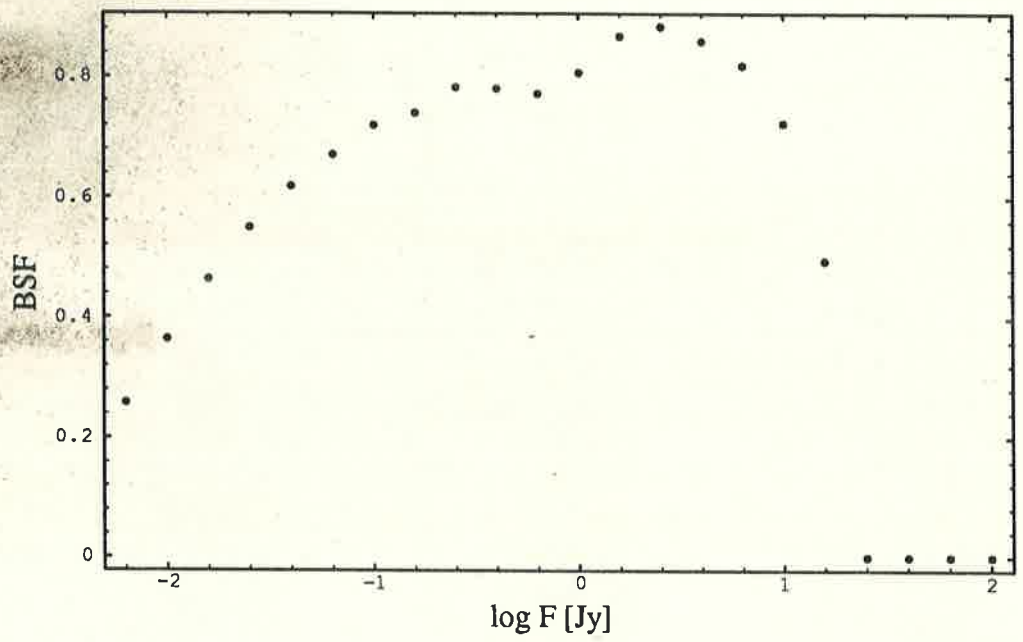

Figure 6.5: Fraction of blueshifted sources for the first scenario

radio sources with optical ones. In the next section we will see that the blueshifted galaxies tend to be very faint optically and hence they may be missed out in favour of the nearby redshifted ones in an optical identification program.

Nevertheless, to avoid blueshift dominated counts, we considered a second scenario analogous Hoyle et al. [31], but with the new solution for the scale factor and different numerical values. We regarded only three populations of sources. Their characteristics are shown in Table 6.2. The timings have to be understood in the following way. Regard a single oscillation from one maximum to the next. If we measure time in units of Q, the first maximum is at $t = 0$, the next at $t = 1$. Hence population I exists for all times, whereas II and III are only present in symmetric intervals around the minima. The occurrence of more luminous sources is correlated with the oscillation and the creation of matter. Note that the least luminous sources are the most abundant. We show the result of this calculation in Figure 6.6.

The jump in numbers at $\approx$ 2 mJy is due to the starting contribution of population II from the previous cycle. According to the timings there are clearly no blueshifted sources in this result. Looking at the data for a frequency of 1.4 Ghz (Figure 6.7), again redrawn from Kellermann et al. [32], we can notice obvious similarities. In particular, there seems to be an upward tendency at fluxes of about 1 mJy, which might correspond to the jump in the QSSC result, smeared out by observational errors.

For comparison we did an analogous computation for similar populations for

Population	L_ν [W Hz^{-1}]	n	t_{min}	t_{max}
I	$5 \cdot 10^{24}$	5000	0	1
II	$5 \cdot 10^{25}$	1000	0.32	0.68
III	$5 \cdot 10^{27}$	1	0.40	0.60

Table 6.2: Properties of radio sources for the second scenario. n denotes a relative number density, the timings are in units of Q.

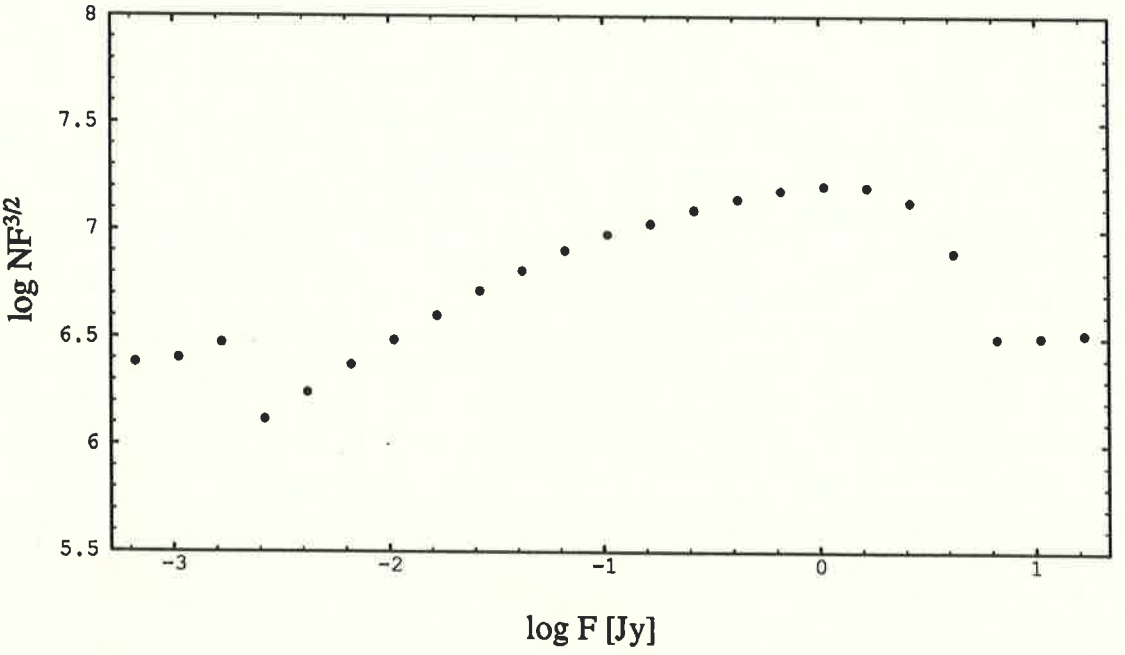

Figure 6.6: Integral counts of radio sources for the second scenario

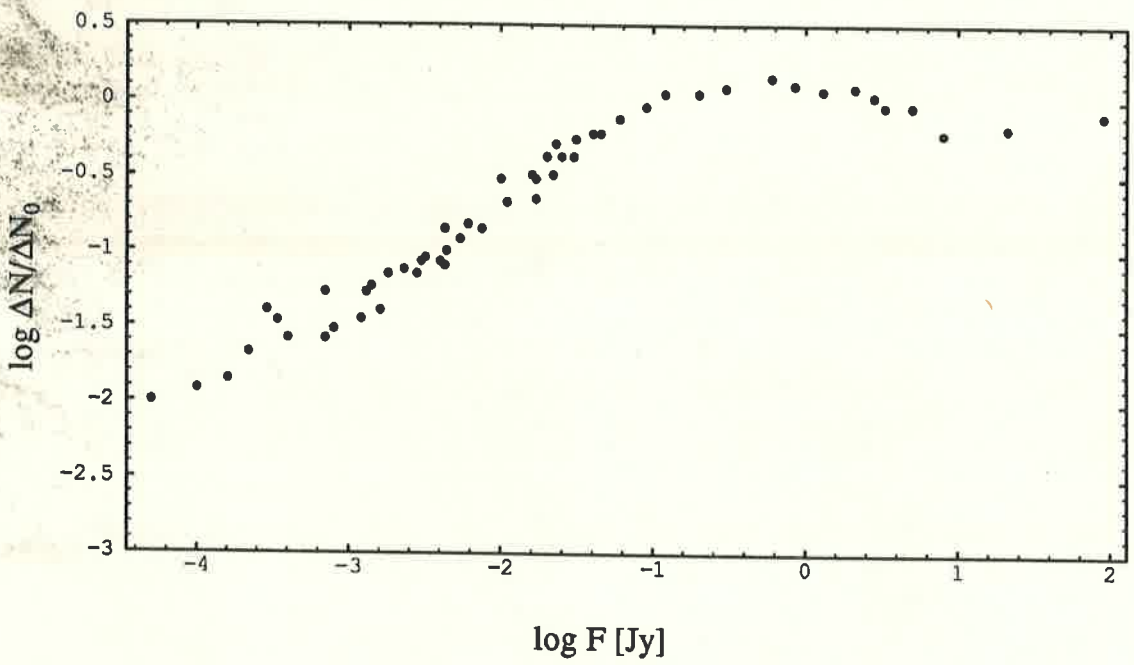

Figure 6.7: Observational data at 1.4 GHz. The differential count is normalized to an uniformly filled euclidean universe with $\Delta N_0 = 225\, F^{-5/2}$.

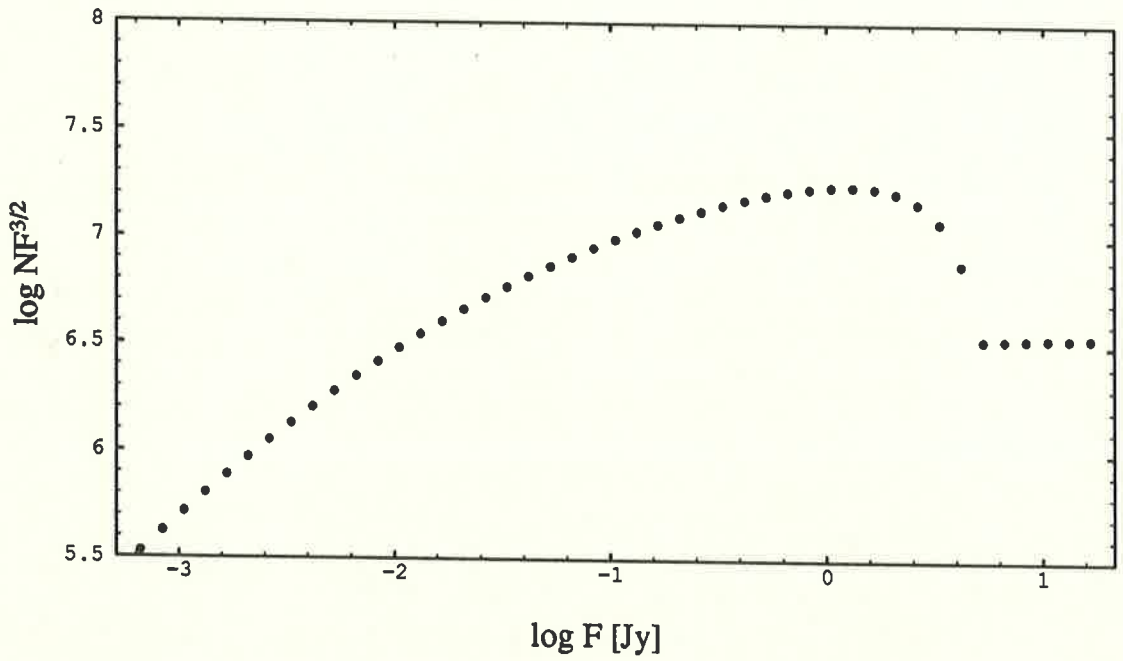

Figure 6.8: Integral counts of radio sources analogous the second scenario in an EdS universe.

the EdS model with $h = 0.75$. In order to determine the switch-off epoch of II and III prior to the present epoch, we calculated the redshift for II and III at $t = 0.68$ and $t = 0.60$ respectively in the QSSC case, and used these redshifts, $z = 0.073$ for II, $z = 0.63$ for III, for the present calculation. Figure 6.8 shows the outcome of this computation and the similarity is obvious, except that there is no steep rise at $F \approx 2$ mJy. The steeper than euclidean counts at $F \approx 2$ Jy are without exception produced by the timing of population II and III. Evolution is responsible for this non-standard feature.

For clarification we show in Figures 6.9 for QSSC and 6.10 for EdS the result for three populations separately. We can clearly see that in both cases sources from II dominate the number counts. For fluxes higher than ≈ 4 Jy only sources from I are present. In the EdS model I has some influence for very small fluxes around 2 mJy, too. The contribution of III is more or less negligible because of the least occurrence. For QSSC there are contributions from previous cycles that change the situation. First, we have the already mentioned rise at $F = 10$ mJy originating from II around the last maximum. Second, the contribution of III is in general larger. Effects from previous cycles from I do not occur in this picture. They will show about one decade later than effects from II, around 0.2 mJy.

It is interesting to notice that in both cases the results look very similar, at least for fluxes higher than the threshold of contribution from previous cycles. The reason is the close resemblance between the respective scale factors back to close to the last minimum. For Figure 6.11 we plotted S_{qssc} and S_{EdS}, the latter for $h = 0.75$ and identical S_0. The similarity is obvious. We illustrate the difference in more detail in the next Figure 6.12, where we show the relative deviation $\delta S = (S_{\mathrm{qssc}} - S_{\mathrm{EdS}})/S_{\mathrm{qssc}}$ against redshift $z = S_0/S_{\mathrm{qssc}}$. For $z \lesssim 3.5$ the difference does not exceed 5%, explaining the similarity in source counts. For II and III we have marked the sources with $z = 3$ and $z = 4$ in Figure 6.10. Differences should show from here on towards larger redshifts. Comparing with Figure 6.9 we see that in the case of QSSC sources from previous cycles have already changed the situation at these redshifts. In the end we find, that there are no major differences in source counts, when we compare the present half cycle of the QSSC with the EdS model.

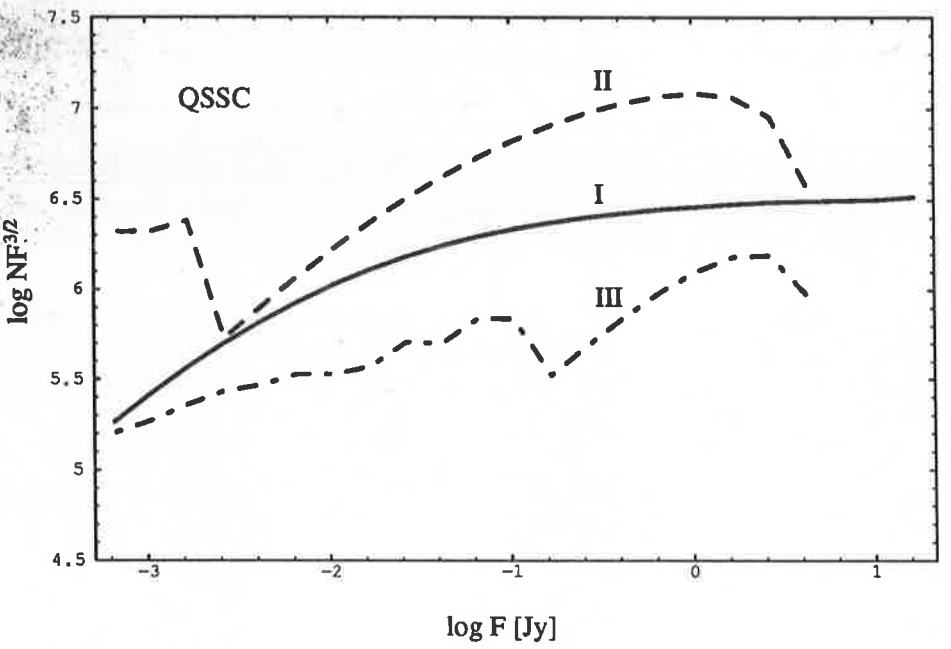

Figure 6.9: The contribution of the three populations separately in QSSC.

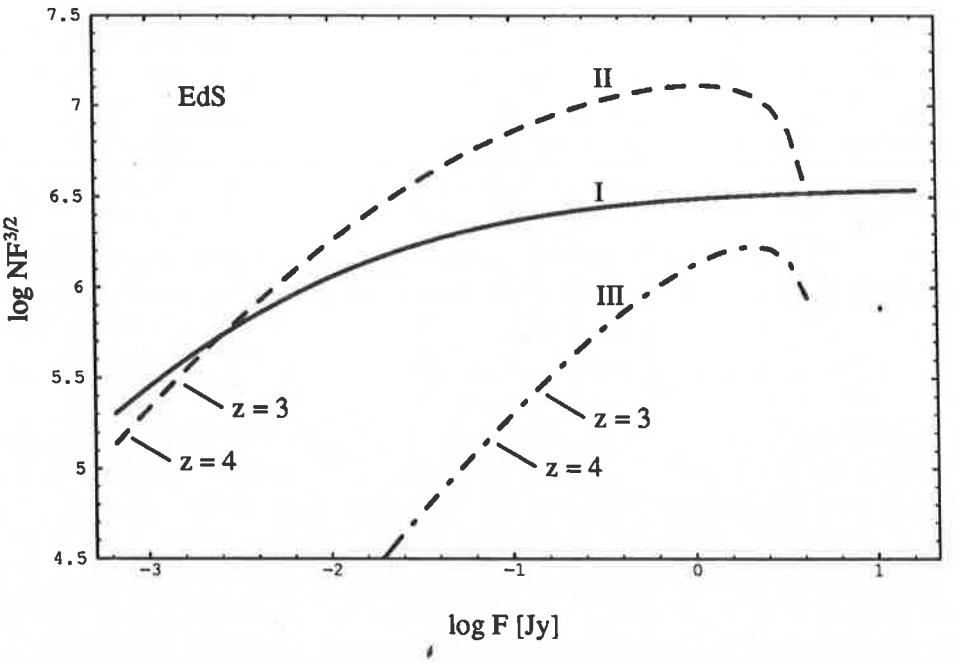

Figure 6.10: The analogous picture for an EdS universe.

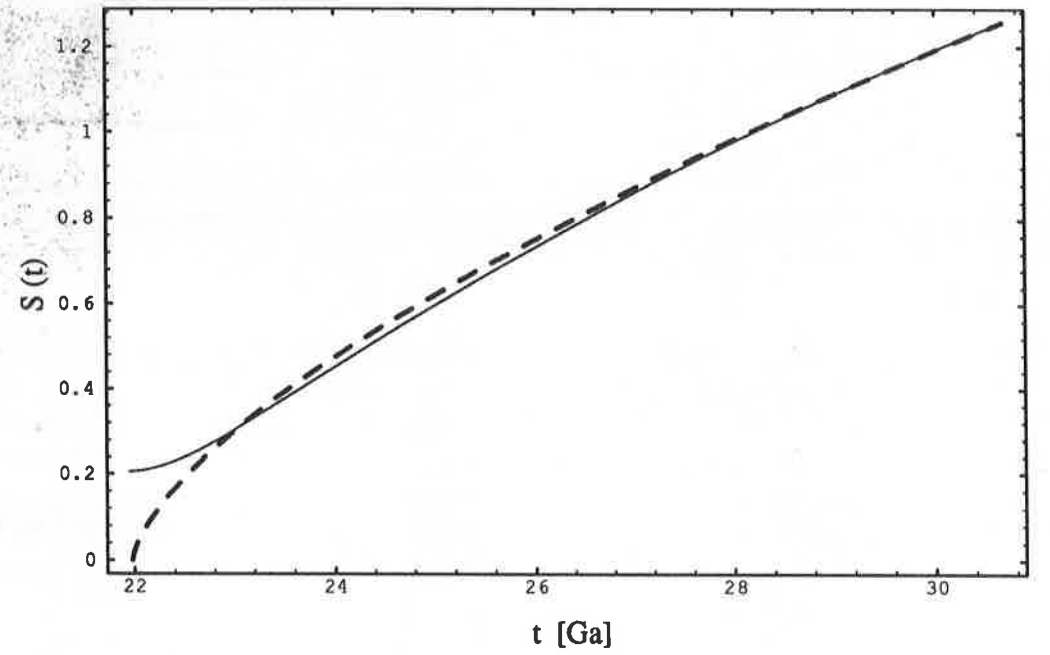

Figure 6.11: Scale factor for the previous half cycle (—) in QSSC and for an EdS model with $h = 0.75$ (– –)

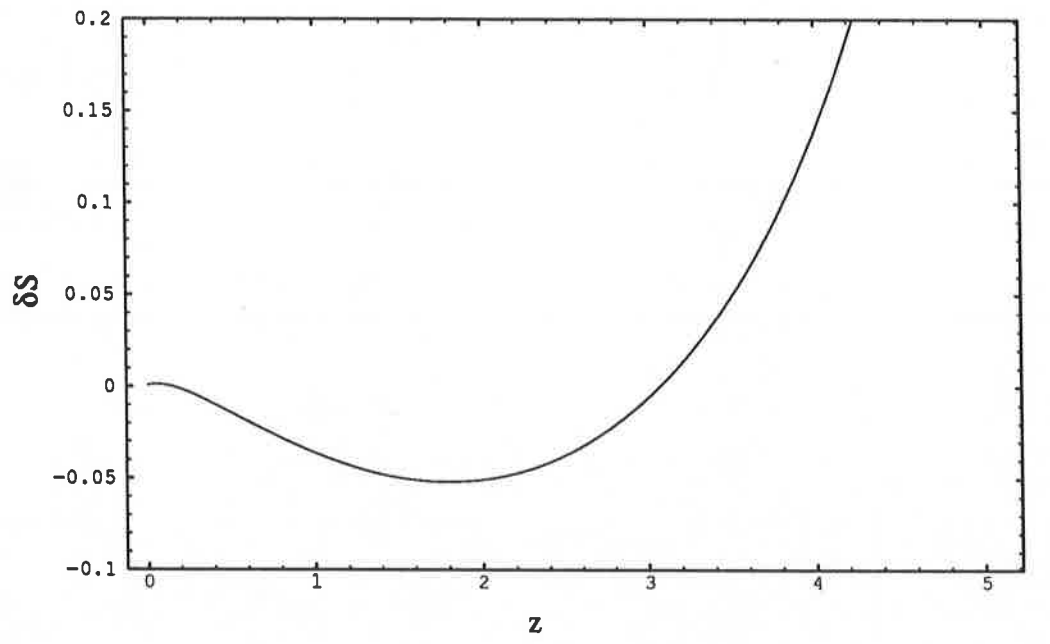

Figure 6.12: Relative deviation $\delta S = (S_{\text{qssc}} - S_{\text{EdS}})/S_{\text{qssc}}$ against redshift $z = S_0/S_{\text{qssc}}$.

6.3 Magnitude-Redshift Relation

It is very common among optical astronomers to measure bolometric fluxes not in absolute units on a linear scale, but relative to a standard source on a log-scale. The resulting quantity is called apparent magnitude m_{bol},

$$m_{\mathrm{bol}} = -2.5 \log \left(\frac{\mathcal{F}_{\mathrm{bol}}}{\mathcal{F}_0} \right) \tag{6.28}$$

with $\mathcal{F}_0 = 2.48 \cdot 10^{-5}\,\mathrm{erg\,cm^{-2}\,s^{-1}}$. Additionally one defines the absolute magnitude M by

$$m_{\mathrm{bol}} - M_{\mathrm{bol}} = 5 \log D_L - 5. \tag{6.29}$$

D_L is the already mentioned luminosity distance, here in units of parsecs. The absolute magnitude equals the apparent magnitude for a source at a distance of 10 pc. M specifies the intrinsic luminosity of the source.

With D_L being a function of redshift, we can plot m against z for a given absolute magnitude M. For small z there is a linear relation between z and m. This can be seen for example by Taylor expanding D_L for the EdS model. This linear region is basically the classical Hubble diagram. Hubble measured velocities as a function of distance, which corresponds to the magnitude-redshift relation for small z. For increasing redshifts we expect increasing influence of the geometry of spacetime, especially the corrections coming from the deceleration parameter q. The hope to determine the value of q and thus distinguish between different cosmological models was destroyed due to the uncertainties in the data.

In QSSC we have a drastic departure from the standard picture of a basically linear relation with small deviations towards the high-redshift end. Because of the oscillations in the scale factor there is a maximum redshift and very distant, only weakly redshifted and even blueshifted objects are present. It shows in the $m-z$ relation as a bending down at high redshifts. In Figure 6.13 we plotted the theoretical points for an absolute magnitude $M = 22.44$.

Clearly, going to an apparent magnitude of 23 one should detect a large number of sources with very small redshift or even blueshift. Of course, Figure 6.13 does not show blueshifted sources explicitly, as we used the conventional log-log scale.

The difference to the result by Hoyle et al. [28] is that small redshifts occurred only at $m = 24.5$, about 1.5 magnitudes later. However, due to enhanced absorption in the optical range by dust around the last minimum, where the density is greater by a factor of about 200, these sources should be dimmed by another 2 to 3 magnitudes. This dimming could be the reason why blueshifted sources have not been detected so far and have been missed out in optical identification programs. Their magnitude might have been shifted to $m \approx 26$. Identification of blueshifted sources would be a striking confirmation of the QSSC prediction.

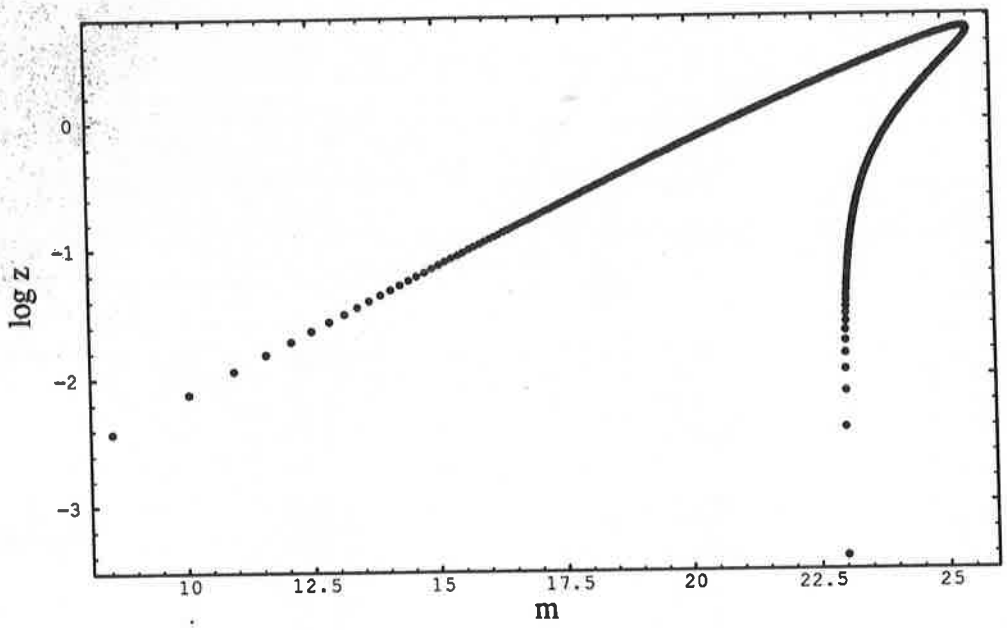

Figure 6.13: Magnitude-redshift relation in QSSC for $M = 22.44$.

6.4 Iron Whiskers

In big bang cosmology the CMB is interpreted as relic from very early times of the universe. As there is no corresponding epoch in QSSC, from which a CMB could have originated, it is assumed that the CMB is thermalized starlight. As a thermalizing agent Hoyle et al. [28] suggested iron whiskers, formed in supernovae. These have the property of being nearly transparent in the optical and radio range, but very opaque in the millimeter range.

In this chapter we will not deal with the thermalizing process and the CMB itself, but with the optical depth of these iron whiskers and their influence on high redshift objects.

The optical depth τ is generally given by the integral of the absorption coefficient α along the line of sight.

$$\tau = \int_0^r \alpha \, dr'. \tag{6.30}$$

α is also written as

$$\alpha = \rho\kappa, \tag{6.31}$$

where ρ is the density and κ the mass absorption coefficient. κ is in general a function of wavelength λ. In the cosmological case we have

$$\tau(\lambda, z) = \int_0^z c\,\rho_0 (1+z')^3 \,\kappa\!\left(\frac{\lambda}{1+z'}\right) \left|\frac{dt}{dz'}\right| dz'. \tag{6.32}$$

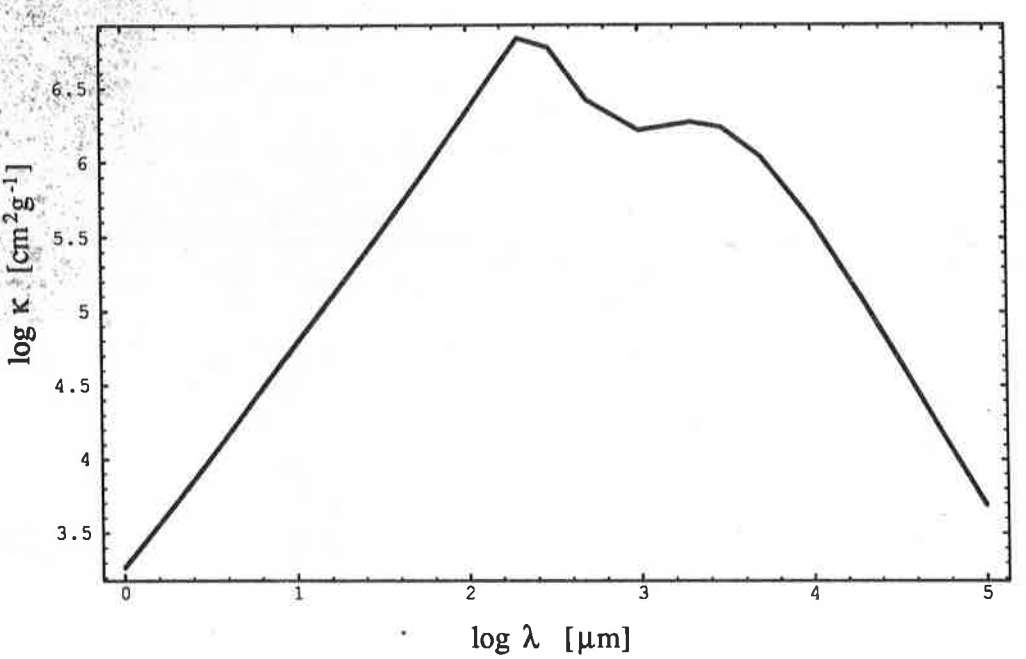

Figure 6.14: Mass absorption coefficient α for a mixture of whiskers of length 100 μm and 1000 μm in a ratio by mass of 50 : 1.

λ is the observed wavelength, ρ_0 the present density of absorbing matter. We used again the redshift as a distance parameter. As we go back only to the last minimum, there is no problem even in QSSC with ambiguities. The argument of κ takes care of the fact, that λ is a function of redshift.

In our case the absorbing material are iron whiskers. Wickramasinghe and Hoyle [58] calculated the mass absorption coefficient of these structures. Their result is shown in Table 6.3. The data were computed for a whisker radius $a = 0.01\,\mu$m and a cyrogenic DC-conductivity $\sigma = 6.8 \cdot 10^{18}\,\mathrm{s}^{-1}$.

Hoyle et al. [27, 28] took a mixture of $l = 100\,\mu$m and $l = 1000\,\mu$m needles in a ratio by mass of 50 : 1. The resulting total mass absorption coefficient is shown in Figure 6.14 on a log-log scale.

The optical depth τ can also be expressed as a change in apparent magnitude Δm. Obviously holds

$$\begin{aligned} \Delta m &= 2.5\,\tau \log e \\ &\approx 1.086\,\tau. \end{aligned} \tag{6.33}$$

Using (6.32) and (6.33) we calculated Δm for redshifts back to the last minimum at different wavelengths of observation (Table 6.4). With increasing redshift the maximal Δm changes from about $\lambda = 300\,\mu$m to $\lambda = 1000\,\mu$m. For high redshifts, i.e., close to the minimum, we have a very large optical depth in the

λ [μm]	κ [cm^2 g^{-1}]					
	l [μm]					
	1000	500	300	200	100	50
$1 \cdot 10^0$	$1.86 \cdot 10^3$	$1.86 \cdot 10^3$	$1.86 \cdot 10^3$	$1.86 \cdot 10^3$	$1.86 \cdot 10^3$	$1.86 \cdot 10^3$
$2 \cdot 10^0$	$5.00 \cdot 10^3$	$5.00 \cdot 10^3$	$5.00 \cdot 10^3$	$5.00 \cdot 10^3$	$5.00 \cdot 10^3$	$5.00 \cdot 10^3$
$3 \cdot 10^0$	$9.24 \cdot 10^3$	$9.24 \cdot 10^3$	$9.24 \cdot 10^3$	$9.24 \cdot 10^3$	$9.24 \cdot 10^3$	$9.24 \cdot 10^3$
$5 \cdot 10^0$	$2.04 \cdot 10^4$	$2.04 \cdot 10^4$	$2.04 \cdot 10^4$	$2.04 \cdot 10^4$	$2.04 \cdot 10^4$	$2.04 \cdot 10^4$
$1 \cdot 10^1$	$6.00 \cdot 10^4$	$6.00 \cdot 10^4$	$6.00 \cdot 10^4$	$6.00 \cdot 10^4$	$6.00 \cdot 10^4$	$6.00 \cdot 10^4$
$2 \cdot 10^1$	$1.72 \cdot 10^5$	$1.72 \cdot 10^5$	$1.72 \cdot 10^5$	$1.72 \cdot 10^5$	$1.72 \cdot 10^5$	$1.72 \cdot 10^5$
$3 \cdot 10^1$	$3.19 \cdot 10^5$	$3.19 \cdot 10^5$	$3.19 \cdot 10^5$	$3.19 \cdot 10^5$	$3.19 \cdot 10^5$	$3.19 \cdot 10^5$
$5 \cdot 10^1$	$7.12 \cdot 10^5$	$7.12 \cdot 10^5$	$7.12 \cdot 10^5$	$7.12 \cdot 10^5$	$7.12 \cdot 10^5$	$7.12 \cdot 10^5$
$1 \cdot 10^2$	$2.21 \cdot 10^6$	$2.21 \cdot 10^6$	$2.21 \cdot 10^6$	$2.21 \cdot 10^6$	$2.21 \cdot 10^6$	$2.21 \cdot 10^6$
$2 \cdot 10^2$	$6.89 \cdot 10^6$	$6.89 \cdot 10^6$	$6.89 \cdot 10^6$	$6.89 \cdot 10^6$	$6.89 \cdot 10^6$	$1.01 \cdot 10^6$
$3 \cdot 10^2$	$1.30 \cdot 10^7$	$1.30 \cdot 10^7$	$1.30 \cdot 10^7$	$1.30 \cdot 10^7$	$5.81 \cdot 10^6$	$4.49 \cdot 10^5$
$5 \cdot 10^2$	$2.68 \cdot 10^7$	$2.68 \cdot 10^7$	$2.68 \cdot 10^7$	$2.42 \cdot 10^7$	$2.14 \cdot 10^6$	$1.62 \cdot 10^5$
$1 \cdot 10^3$	$5.73 \cdot 10^7$	$5.73 \cdot 10^7$	$2.73 \cdot 10^7$	$6.99 \cdot 10^6$	$5.39 \cdot 10^5$	$4.04 \cdot 10^4$
$2 \cdot 10^3$	$8.88 \cdot 10^7$	$3.96 \cdot 10^7$	$8.11 \cdot 10^6$	$1.82 \cdot 10^6$	$1.35 \cdot 10^5$	$1.01 \cdot 10^4$
$3 \cdot 10^3$	$8.54 \cdot 10^7$	$2.13 \cdot 10^7$	$3.73 \cdot 10^6$	$8.14 \cdot 10^5$	$6.00 \cdot 10^4$	$4.49 \cdot 10^3$
$5 \cdot 10^3$	$5.50 \cdot 10^7$	$8.63 \cdot 10^6$	$1.37 \cdot 10^6$	$2.94 \cdot 10^5$	$2.16 \cdot 10^4$	$1.62 \cdot 10^3$
$1 \cdot 10^4$	$2.06 \cdot 10^7$	$2.27 \cdot 10^6$	$3.45 \cdot 10^5$	$7.37 \cdot 10^4$	$5.40 \cdot 10^3$	$4.04 \cdot 10^2$
$2 \cdot 10^4$	$5.89 \cdot 10^6$	$5.76 \cdot 10^5$	$8.65 \cdot 10^4$	$1.84 \cdot 10^4$	$1.35 \cdot 10^3$	$1.01 \cdot 10^2$
$3 \cdot 10^4$	$2.69 \cdot 10^6$	$2.57 \cdot 10^5$	$3.84 \cdot 10^4$	$8.19 \cdot 10^3$	$6.00 \cdot 10^2$	$4.49 \cdot 10^1$
$5 \cdot 10^4$	$9.81 \cdot 10^5$	$9.26 \cdot 10^4$	$1.38 \cdot 10^4$	$2.95 \cdot 10^3$	$2.16 \cdot 10^2$	$1.62 \cdot 10^1$
$1 \cdot 10^5$	$2.47 \cdot 10^5$	$2.32 \cdot 10^4$	$3.46 \cdot 10^3$	$7.37 \cdot 10^2$	$5.40 \cdot 10^1$	$4.04 \cdot 10^0$

Table 6.3: Mass absorption coefficient α for iron whiskers at various lengths l and wavelengths λ.

z	Δm																
	λ [μm]																
	10	20	30	50	100	200	300	500	1000	2000	3000	5000	10000	20000	30000	50000	100000
.2	.00143	.00412	.00762	.0169	.0523	.174	.177	.0853	.0467	.0509	.0494	.0337	.0132	.00387	.00178	.000649	.000163
.4	.00259	.00747	.0138	.0305	.0939	.322	.377	.205	.0994	.102	.103	.0756	.0311	.00942	.00435	.0016	.000403
.6	.00358	.0103	.0191	.0422	.129	.445	.588	.364	.161	.156	.161	.126	.0547	.0171	.00797	.00294	.000742
.8	.00445	.0129	.0238	.0524	.16	.548	.791	.564	.234	.211	.222	.183	.0845	.0274	.0129	.00478	.00121
1.	.00523	.0152	.0281	.0617	.187	.635	.978	.798	.322	.27	.285	.248	.121	.0407	.0194	.00722	.00183
1.2	.00595	.0173	.032	.0702	.212	.712	1.15	1.06	.43	.333	.352	.318	.165	.0575	.0277	.0104	.00265
1.4	.00661	.0193	.0357	.0781	.235	.784	1.3	1.34	.566	.403	.421	.394	.217	.0783	.0382	.0144	.00369
1.6	.00724	.0211	.0391	.0855	.257	.85	1.44	1.64	.732	.48	.494	.474	.278	.104	.0511	.0195	.00499
1.8	.00782	.0228	.0423	.0925	.277	.912	1.57	1.93	.935	.565	.57	.56	.347	.134	.0669	.0257	.00662
2.	.00839	.0245	.0454	.0993	.297	.971	1.69	2.23	1.18	.661	.651	.65	.424	.169	.0859	.0333	.00861
2.2	.00893	.0261	.0484	.106	.315	1.03	1.8	2.51	1.46	.768	.739	.744	.511	.211	.108	.0425	.011
2.4	.00945	.0276	.0513	.112	.333	1.08	1.9	2.79	1.79	.888	.833	.843	.607	.26	.135	.0535	.014
2.6	.00996	.0291	.0541	.118	.351	1.13	2.	3.06	2.16	1.02	.936	.947	.712	.315	.166	.0666	.0175
2.8	.0105	.0306	.0569	.124	.368	1.19	2.1	3.32	2.57	1.18	1.05	1.06	.827	.379	.203	.082	.0216
3.	.011	.032	.0596	.13	.385	1.24	2.2	3.57	3.03	1.35	1.17	1.17	.952	.452	.245	.1	.0266
3.2	.0115	.0335	.0623	.136	.402	1.29	2.3	3.82	3.53	1.55	1.31	1.3	1.09	.535	.294	.122	.0324
3.4	.012	.0349	.065	.142	.42	1.34	2.4	4.06	4.08	1.79	1.46	1.43	1.24	.63	.351	.147	.0394
3.6	.0125	.0364	.0678	.148	.437	1.39	2.49	4.3	4.68	2.07	1.64	1.57	1.4	.739	.417	.176	.0476
3.8	.013	.0379	.0706	.155	.455	1.44	2.59	4.53	5.34	2.39	1.83	1.73	1.57	.863	.493	.211	.0575
4.	.0135	.0394	.0735	.161	.473	1.49	2.7	4.78	6.06	2.78	2.05	1.9	1.77	1.01	.583	.253	.0692
4.2	.0141	.0411	.0766	.168	.493	1.55	2.81	5.03	6.86	3.25	2.31	2.1	1.99	1.17	.689	.302	.0835
4.4	.0147	.0428	.08	.175	.514	1.61	2.92	5.3	7.75	3.82	2.62	2.32	2.24	1.37	.816	.363	.101
4.6	.0154	.0448	.0837	.183	.538	1.68	3.05	5.6	8.76	4.55	3.	2.59	2.53	1.61	.974	.439	.123
4.8	.0162	.0472	.0881	.193	.566	1.76	3.21	5.96	9.98	5.51	3.5	2.94	2.9	1.93	1.18	.541	.154
5.	.0174	.0505	.0943	.207	.606	1.88	3.43	6.45	11.7	7.01	4.27	3.46	3.44	2.4	1.5	.7	.201

Table 6.4: Change in apparent magnitude Δm as a function of redshift z and wavelength λ.

mm-range, whereas radio and optical range, at the right and left end of the table, are only weakly affected.

Wright has raised the issue of optical depth as a referee of one of Hoyle et al.'s paper [60]. He did not give absolute values for τ, but only the ratio of the values for observed wavelengths 1.25 mm and 21 cm, the latter corresponding to 1.4 Ghz, the frequency of radio source counts. He obtains a ratio of 63 through a full oscillation. It is not clear how he could calculate this number, as there are no data given for the mass absorption coefficient at $\lambda = 21\,\mathrm{cm}$. He could, however, have extrapolated to obtain these data. A linear extrapolation seems plausible.

We repeated this calculation without any such assumptions and used only the available data. The result depends crucially on the solution of the scale factor. We went back to the last minimum, as the objects of interest are in the previous half cycle. It turned out, that there is a significant difference in the results, whether we use the approximate or the exact solution. The optical depth is more sensitive than for example source counts.

Wright was in particular concerned with McMahon et al.'s observation of the high redshift QSO BR 1202–0725 [37]. They detected this QSO with redshift $z = 4.69$ at $\lambda = 1.25\,\mathrm{mm}$. The redshifts shows that this QSO is close to the last minimum and the absorption by iron whiskers should be strong at this wavelength.

When we use the approximate solution, we get an optical depth of 25.1 at $\lambda = 1.25\,\mathrm{mm}$. The exact solution with its different set of parameters leads to $\tau = 7.82$ for the same redshift and wavelength. This discrepancy originates from two reasons. First, the time interval in the approximate case is 13.1 Ga as compared to 8.8 Ga. The derivative $|dt/dz|$ in (6.32) is therefore always larger for the approximate solution. Second, the QSO with its high redshift lies very close to the last minimum for the approximate solution and $|dt/dz|$ diverges at that point. The contribution of this factor in the region close to the minimum is hence very large. Due to the parameter choice for the exact solution the QSO is further away from the minimum.

Using data given by McMahon et al. and Andreani et al. [5] we calculated luminosities, optical depth and the necessary increase in luminosities for several QSOs. It should be noted that the luminosity distance D_L in big bang is different from the one in QSSC. For the big bang case we used (6.12), for QSSC coordinate and redshift data from tables, which we had computed for radio source counts. This is, however, only a minor correction as we have seen that the scale factors are very similar in both cases. The main influence is from absorption as expected. We show the result in Table 6.5. For redshifts between 3 and 4 the effect is not extremely large. But when we look at $z = 4.69$ there is already a difference of a factor ≈ 2500.

In one of their papers Hoyle et al. [28] were also considering the ultraluminous IRAS galaxy F10214+4724 with $z = 2.286$. Since its detection by Rowan-Robinson et al. [46] this galaxy has caused a lot of discussions because of its

quasar	z	F [mJy]	$(\nu L_\nu)_{\rm bb}$ $[h^{-2} L_\odot]$	τ	e^τ	$(\nu L_\nu)_{\rm qssc}$ $[L_\odot]$	Ref.
2132+0126	3.19	11.5	$1.44 \cdot 10^{11}$	2.48	11.9	$3.24 \cdot 10^{12}$	1
0344+0222	3.38	5.7	$8.11 \cdot 10^{10}$	2.9	18.2	$2.83 \cdot 10^{12}$	1
0345+0130	3.64	6.1	$1.02 \cdot 10^{11}$	3.57	35.5	$7.11 \cdot 10^{12}$	1
0307+0222	4.38	6.6	$1.68 \cdot 10^{11}$	6.17	478	$1.73 \cdot 10^{14}$	1
1202-0725	4.69	10.5	$3.11 \cdot 10^{11}$	7.82	2490	$1.77 \cdot 10^{15}$	2

Table 6.5: Luminosities in BB and QSSC for quasars at $\lambda = 1.25$ mm from (1) Andreani et al. [5] and (2) McMahon et al. [37]

λ [μm]	F [mJy]	$(\nu L_\nu)_{\rm bb}$ $[h^{-2} L_\odot]$	τ	e^τ	$(\nu L_\nu)_{\rm qssc}$ $[L_\odot]$	Ref.
61700.	0.36	$4.32 \cdot 10^{7}$	0.0291	1.03	$7.84 \cdot 10^{7}$	1
35500.	0.27	$5.64 \cdot 10^{7}$	0.0821	1.09	$1.08 \cdot 10^{8}$	1
1400.	0.03	$1.60 \cdot 10^{8}$	0.952	2.59	$7.25 \cdot 10^{8}$	3
1200.	9.6	$5.93 \cdot 10^{10}$	1.15	3.16	$3.29 \cdot 10^{11}$	2
1100.	24.	$1.62 \cdot 10^{11}$	1.29	3.62	$1.04 \cdot 10^{12}$	1
800.	50.	$4.63 \cdot 10^{11}$	1.94	6.96	$5.70 \cdot 10^{12}$	1
450.	273.	$4.50 \cdot 10^{12}$	2.36	10.6	$8.38 \cdot 10^{13}$	1
100.	$< 510.$	$< 3.78 \cdot 10^{13}$	0.298	1.35	$< 8.97 \cdot 10^{13}$	1
60.	190.	$2.35 \cdot 10^{13}$	0.133	1.14	$4.72 \cdot 10^{13}$	1
25.	$< 90.$	$< 2.67 \cdot 10^{13}$	0.0347	1.04	$< 4.87 \cdot 10^{13}$	1
20.	$< 45.$	$< 1.67 \cdot 10^{13}$	0.0246	1.02	$< 3.01 \cdot 10^{13}$	1
12.	$< 90.$	$< 5.56 \cdot 10^{13}$	0.0112	1.01	$< 9.90 \cdot 10^{13}$	1
10.	$< 12.$	$< 8.89 \cdot 10^{12}$	0.00844	1.01	$< 1.58 \cdot 10^{13}$	1

Table 6.6: Luminosities for different wavelength for IRAS F10124+4724 with flux data from (1) Rowan-Robinson et al. [47], (2) Downes et al. [13], (3) Solomon et al. [52]

very high luminosity in far infrared. In the rest-frame range from 6–36 μm it is $3 \cdot 10^{14} L_{\odot}$, assumed $h = 0.5$, $\Omega = 1$, making F10214+4724 by a factor of 10 the most luminous IRAS galaxy.

We will look at the influence of iron whiskers on this galaxy, which is expected to be not very strong, as the redshift is comparably low. Table 6.6 gives luminosities for big bang and QSSC for wavelengths from 10–61700 μm. The maximum effect is at wavelengths of around 500 mm, where the QSSC luminosity is higher by a factor 10 than the big bang luminosity. Like in Table 6.5 the difference in D_L has been taken into account. The luminosities for big bang are given with the parameter h. When we assume a Hubble constant of $h = 0.75$, then these values are larger by 1.78.

Recent observations seem to reveal the fact that F10214+4724 is actually a gravitationally lensed galaxy [8, 20, 50]. With a proposed magnification of about 10 the luminosity in the standard case would be reduced to normal. The probability that it is a lensed system with a magnification of 2 to 10 is about 25%, provided the local luminosity function is valid up to this redshift and luminosity. The probability would considerably increase, if the luminosity function would become steeper at high redshifts. Magnifications of 20 or more are essentially ruled out unless the luminosity function is very steep, $\phi(L) \sim L^{-6}$ or so [54].

Gravitational lensing does not change the spectrum of the lensed object, unless different parts of the spectrum, e.g., emission lines, radio continuum, originate from different regions of the object, as magnification is a function of the position. Features from small size regions might also be distorted by microlensing. Anyway, F10214+4724 is said to be an ordinary obscured AGN with the infrared luminosity arising from the obscuring dust torus, a fairly extended region, hence we do not expect significant distortions.

In the QSSC case the absorption by iron whiskers leads to an additionally required luminosity of a factor 10, especially around 500 μm, where absorption has its maximum. However, if one adopts the view of redshifts being non-cosmological, both this cases, QSO BR 1202-0725 and IRAS F10214+4724, can be solved trivially by bringing them closer to us.

Chapter 7

Conclusion

7.1 Summary

We have derived field equations from an conformal invariant, dimensionless action. The mass of a particle was determined by the presence of other particles in the universe, thus taking Mach's view into account. The field equations could be reduced to their standard form as obtained by Einstein, when we took the particle masses to be constant. We have related the particle mass — the Planck mass m_p — to the gravitational constant G.

A massless scalar field has been introduced to give a field theoretical description of the mass creation process that takes place in QSSC. It turned out that this mass field has negative energy and pressure. The influence of this c-field as part of the energy-momentum tensor in the field equations in a Robertson-Walker metric has been a major part of this work.

We obtained an exact solution for the scale factor. It has been shown that there is no singularity in this cosmological model under the assumed conditions, the presence of (1) ordinary matter, which additionally leads to a cosmological constant, and (2) the c-field. All non-creative solutions are of oscillatory nature or static, the latter being stable unlike Einstein's static universe. The creative mode solutions correspond to exponentially expanding, de Sitter-like models. Combination of both modes leads to a superposition of an endless series of short term oscillations and a long term exponential expansion. In between the oscillations new matter is created, especially around the minima, in accordance with the steady state principle.

We have used the exact solution for a flat spacetime, i.e., $k = 0$, to work out various observational features of the universe.

The parameters of QSSC have been related to recent observations of the Hubble constant $h_0 = 0.75$ and the maximum observable redshift. We have changed the parameter values as compared to the set used by Hoyle et al. [28] for the approximate solution. The exact solution provides a better rationale for

these values. The time elapsed since the last minimum has been reduced from 14 Ga for the approximate solution to 8.8 Ga at present. Hence globular clusters should have formed prior to the last minimum.

We have repeated the calculation for counts of radio sources and found the following. For a scenario analogous Hoyle et al. (op.cit.) with no evolution of sources there are only marginal deviations from the calculation done with the approximate solution, provided the luminosities are generally reduced by a factor 0.3. We have found that the region of interest, the steeper than euclidean range around 1 Jy, is dominated by 80% blueshifted sources. Those have not been identified so far. We have estimated the magnitude of blueshifted sources to be definitely larger than 23, very likely around $m \approx 25$, today's limit of optical identification. Thus these sources might have escaped their identification in favour of relatively nearby faint redshifted objects.

To avoid possible blueshifts, we have introduced periodic evolution. The excess of faint sources arises solely from the timings during the present half cycle. The contribution from previous cycles shows only at very low fluxes of about 1 mJy. A similar computation has been done for an EdS universe. We have shown that the close resemblance follows from our particular choice of parameters. Both the scale factor for QSSC and the EdS model are very similar back to a redshift $z \approx 4$. No blueshifts are present in this scenario down to sub-mJy fluxes, but evolution is needed to fit the observational data. However, one of the arguments in favour of QSSC was that evolution could be avoided and a simpler picture with contributions from previous cycles would be sufficient.

We have investigated the influence of iron whiskers, the thermalizing agent to produce the CMB, on high redshift objects, especially in the mm-range. We have considered particularly two objects. The first is the QSO BR 1202-0725 at a redshift of $z = 4.69$. The optical depth up to this redshift, which is close to the last minimum, is 7.8 for the exact solution as compared to 25 for the approximate solution. The QSO would be more luminous than in the standard case by a factor 2500. Hence its luminosity would be extraordinary large, about $10^{15}\ L_{\odot}$.

The IRAS galaxy F10214+4724 is not so heavily affected, as its redshift is comparably low, $z = 2.29$. The maximum increase in luminosity is by a factor 10. Thus cancelling the suggested magnification by gravitational lensing, it would still remain the most luminous object in the infrared. Moreover, its extreme luminosity and additional gravitational lensing would make F10214+4724 to a most unusual object in the universe. On the contrary, if not have been lensed, F10214+4724 would have easily escaped its detection. There is a considerable bias in flux limited samples to pick magnified objects.

However, in both these cases we have made the conventional assumptions and used the redshift as a distance indicator. Non-cosmological redshifts would solve the problem of high luminosities trivially.

7.2 Ideas for Future Investigations

On the theoretical side, a full quantum description of the creation process would remove one stumbling-block to further progress.

Concerning observations, the origin and properties of the CMB would be very interesting topics. It has been demonstrated, e.g., [27, 28], that it is in principle possible to create background radiation through thermalization of starlight. The recent analysis of data collected by COBE makes two aspects of the CMB particularly interesting for detailed investigation. First, the spectrum in Planckian to a very high degree of accuracy. It would be worthwhile to calculate the transition from a line spectrum to a black body spectrum by means of iron whiskers. Comparing the result with observational data we should be able to infer density and mixture of the thermalizing agent more reliably. Second, big bang cosmology predicts a certain anisotropy in the CMB by tracing back today's observable structures to the last scattering surface at time of decoupling. On small scales, $\theta \lesssim 1°$, anisotropies should come from fluctuations in the energy density at t_{dec}. However, these might have been eventually wiped out. On larger scales, $\theta \gtrsim 1°$, fluctuations in the gravitational potential at the last scattering surface give rise to an anisotropy of $\delta T/T \approx 10^{-6}$ at the present epoch. This agrees well with the COBE result. An analogous prediction from QSSC would be desirable.

The formation of structures should be calculated in the QSSC. The infinite amount of time available and the creation of matter should cause considerable differences to the results in the standard context.

It is clear that a large optical depth, $\tau \approx 10$, in the mm-range back to the last minimum is required to adequately blacken the CMB. Increasing detection of high redshift objects in this wavelength range might put upper limits on the density of iron whiskers. This could be cross-checked with the optical depth needed for the CMB.

Optical identification programs should be carried out at very low fluxes. The QSSC predicts a large number of blueshifted sources, which are optically very faint. Depending on the scenario, blueshifted sources could be present at around 1 Jy for no evolution, abound 0.2 mJy for periodic evolution in the radio range. These numerical values are, however, subject to the assumed luminosities. Eventual detection of blueshifted sources would be a serious contradiction to the kinematics of the standard model and a strong argument in favour of QSSC.

On the astrophysical side one could investigate IRAS F10214+4724 in more detail. Its redshift is not extremely high but still sufficient for considerable influence of iron whiskers. With the range of data from different parts of the spectrum available, one could try to model the spectrum after subtraction of the absorption by iron whiskers.

Appendix A

Conventions and Notation

Minkowski metric	$ds^2 = c^2dt^2 - dx^2 - dy^2 - dz^2$
signature	$(+\,-\,-\,-)$
Latin indices	$i, j, k, \ldots = 0, 1, 2, 3$
Greek indices	$\lambda, \mu, \nu, \ldots = 1, 2, 3$
Riemann tensor	$R^i{}_{klm} = \Gamma^i_{km,l} - \Gamma^i_{kl,m} + \Gamma^i_{sl}\,\Gamma^s_{km} - \Gamma^i_{sm}\,\Gamma^s_{kl}$
Ricci tensor	$R_{kl} = g^{im}\,R_{iklm} = R^m{}_{klm}$
curvature scalar	$R = g^{ik}\,R_{ik} = R^k{}_k$
Einstein tensor	$G_{ik} = R_{ik} - \frac{1}{2}g_{ik}\,R$
$S(t)$	scale factor
k	sign of curvature: $0, \pm 1$
t_0	present epoch
X_0	quantity X at $t = t_0$
H	Hubble constant $H = 100\,h\,\mathrm{km\,s^{-1}\,Mpc^{-1}}$
ρ_c	critical density $\rho_c = 3H_0^2/(8\pi G)$
Ω	mass density in units of ρ_c
CMB	cosmic microwave background
CP	cosmological principle
EdS	Einstein-de Sitter
FRW	Friedmann-Robertson-Walker
GR	general relativity
GUT	grand unified theories
PCP	perfect cosmological principle
QSSC	quasi-steady state cosmology

Appendix B

Source Counts Codes

We have used *Mathematica* [59] for calculations. This appendix contains the codes that have been written to compute theoretical results for counts of radio sources in Chapter 6.2. We had investigated three different scenarios.

1. The first code is for QSSC with no evolution of sources. We considered eleven classes with power ranging from $3 \cdot 10^{28} - 3 \cdot 10^{29}\,\mathrm{W\,Hz^{-1}}$. This code is built of an interactive main routine, which reads all required parameters and eventually available data from previous calculations and a set of subroutines. Those have been written for calculation of tables for redshift, coordinate radius, flux density, number of sources and the final routine, where the contributions from all classes and cycles are added up. The final output is a table which contains flux density F and differential number counts multiplied with $F^{5/2}$ for the desired flux density range.

2. The second code is basically a combination of the previous subroutines for the number of sources and the final loop. Additionally required input, e.g, constants, coordinate radius, results from previous calculations, is read in the beginning. The basic parameters like η, t_0 did not change anymore, thus the first part of the previous code has been omitted. In this code we were particularly concerned with the respective timings and luminosities of the three different populations. The output is a table that contains integral number counts $NF^{3/2}$ against F.

3. The third code is the standard calculation for source counts in an EdS universe. The only non-standard feature is the combination of three classes of sources, which start contributing from different redshift onwards. The output is again an integral number count.

```
(*  MATHEMATICA program QSSC predictions *)
(*              Rainer Sachs              *)
(*                26.03.95                *)

  Clear[c,deltat,ip,k,eta,instream,T1,q,period,
        t0,P,m,plabel,s0,ral,fl,nu,file,imax,
        rshift,R1,F]
  Remove[theta,scale]

(* constants *)
(* units generally used are length in Mpc, time in Ga *)

  c=306.61
  deltat=.5

(* data-table T1 [time,theta] *)

  ip=InputString["use theta_t program y/n "]
  If[ip=="n",{file=InputString["data file for theta[t] "],
              k=Input["curvature "],
              eta=Input["amplitude "],
              lambda=10^-56 Input["lambda [10^-56 cm^-2] "],
              instream=OpenRead[file],
              T1=Flatten[ReadList[instream],1],
              Close[instream],
              SetDirectory["~/math/predictions/main"]
             },
             {<<theta_t3.m}
    ]

(* functions and variables *)

  theta=Compile[{x},Interpolation[T1][x]]
  period=q /. FindRoot[theta[q]==2 Pi,{q,T1[[126,1]]}]
  t0=period Input["time since last maximum [1/Q] "]
  P=period Input["expansion time P/Q "]
  m=Input["number of cycles back "]
  scale=Compile[{x},Exp[x/P] (1+eta Cos[theta[Mod[x,period]]])]

  plabel=StringJoin["eta = ",ToString[eta],
                    "  k = ",ToString[k],
                    "  P = ",ToString[P],
                    "  Q = ",ToString[period]
                   ]
  s0=scale[t0]
  imax=Quotient[(t0+m period),deltat]

(* calculation of redshift z *)

  rshift=InputString["redshift y/n "]
  If[rshift=="y",<<redshift.m,
                 {}
    ]

(* calculation of coordinate radius r1*)

  ral=InputString["calculate radius R1 y/n "]
  If[ral=="y",<<radius.m,
              {file=InputString["data file for R1 "],
               instream=OpenRead[file],
               R1=Flatten[ReadList[instream],1],
               Close[instream],
               SetDirectory["~/math/predictions/main"]
              }
    ]

(* flux and source counts *)

  fl=InputString["calculate flux y/n "]
  If[fl=="y",<<flux.m,
             {file=InputString["data file for flux "],
              instream=OpenRead[file],
              F=Flatten[ReadList[instream],1],
              Close[instream],
              SetDirectory["~/math/predictions/main"]
             }
    ]

  nu=InputString["calculate number y/n "]
  If[nu=="y",<<number.m,
             {file=InputString["data file for number "],
              instream=OpenRead[file],
              number=Flatten[ReadList[instream],1],
              Close[instream],
              SetDirectory["~/math/predictions/main"]
             }
    ]

  <<counts.m

(* finito *)
```

```
(* MATHEAMTICA subprogram for theta_t dependence *)
(*          main program version                 *)
(*        Rainer Sachs  05.03.95                 *)

   Clear[Tl,lambda,sbar,p,save,data,outstream]
   Remove[intgr]

(* constants and inputs *)

   k=Input["curvature "]
   eta=Input["amplitude "]
   lambda=10^-56 Input["lambda [10^-56 cm^-2] "]
   sbar=10^28
   p=-1/(lambda sbar^2)
   const=1.83077 10^-27/Sqrt[-lambda]//N


(* integrand *)

   intgr[x_]:=(1+eta Cos[x])/Sqrt[eta^2 (Cos[x]^2+1)+4 eta Cos[x]+6+3 p k];

(* theta_t calculation *)

   Tl=Table[{const NIntegrate[intgr[x],{x,0,t}],t},{t,0,6.30,.05}]


(* save result *)

   save=InputString["save result ot theta_t calculation y/n "]
   If[save=="y",{data=InputString["save as "],
                 outstream=OpenWrite[data],
                 Write[outstream,Tl],Close[outstream]
                },
                {}
     ]


   Clear[save,data,outstream]
```

```
(* MATHEMATICA subprogram for the redshift *)
(*            Rainer Sachs  05.03.95         *)


   Clear[graphz,print,save1,save2,stable,sgraph,outstream,Z]

(* calculation of redshift *)

   Z=Table[{t0-(i-1) deltat,s0/scale[t0-(i-1) deltat]-1},
           {i,1,imax}
          ]

(* graphic output *)

   graphz=Show[ListPlot[Z,PlotJoined->True,
                        PlotRange->{-1,10}
                       ],
               Frame->True,
               Axes->False,
               FrameLabel->{"t/Ga","redshift z"},
               PlotLabel->plabel
              ]

(* print graphics *)

   print=InputString["print redshift y/n "]
   If[print=="y",Display["!psfix | lpr -Plj",graphz],
                 {}
     ]

(* save graphics *)

   save1=InputString["save redshift y/n "]
   If[save1=="y",{sgraph=InputString["save as "],
                  outstream=StringJoin["!psfix>",sgraph],
                  Display[outstream,graphz]
                 },
                 {}
     ]

(* save Z table *)

   save2=InputString["save redshift table y/n "]
   If[save2=="y",{stable=InputString["save as "],
                  outstream=OpenWrite[stable],
                  Write[outstream,Z],
                  Close[outstream]
                 },
                 {}
     ]

   Clear[sgraph,print,save1,save2,outstream]
```

```
(* MATHEMATICA subprogram for coordiante radius r1 *)
(*          Rainer Sachs      05.03.95                *)


   Clear[save2,stable,outstream,R1]
   Remove[rad]

(* functions *)

   If[k==0,rad[x_]:=x,
          {If[k==1,rad[x_]:=Abs[Sin[x]],
                   rad[x_]:=Sinh[x]
             ]
          }
     ]

(* calculation *)

   R1=Table[{0,0},{i,1,imax}]
   R1[[1,1]]=t0
   For[i=2,i<imax+1,i++,
       {R1[[i,2]]=R1[[i-1,2]]+rad[c NIntegrate[1/scale[t],
                                               {t,t0-(i-1) deltat,t0-(i-2) de

ltat}                                          ]
                                  ],
        R1[[i,1]]=t0-(i-1)deltat
       }
      ]

(* save R1 table *)

    save2=InputString["save R1 table y/n "]
    If[save2=="y",{stable=InputString["save as "],
                   outstream=OpenWrite[stable],
                   Write[outstream,R1],
                   Close[outstream]
                  },
                  {}
     ]


    Clear[save2,stable,outstream]
```

```
(* MATHEMATICA subprogram for the flux *)
(*          Rainer Sachs  20.03.95      *)


   Clear[save2,outstream,stable,F,fconst]


(* constants *)

(* unit of flux Jansky for luminosity 3 10^28 W/Hz *)
(* flux = 3 10^28 W / Mpc^2 / Hz = 3 10^9 Jy *)

   fconst= 3 10^9/(4 Pi s0^4)

(* calculation of flux for luminosity 3 10^28 W/Hz *)

   F=Table[fconst scale[R1[[i,1]]]^2/R1[[i,2]]^2,
           {i,2,imax}
          ]//N


(* save Ftable *)

    save2=InputString["save flux table y/n "]
    If[save2=="y",{stable=InputString["save as "],
                   outstream=OpenWrite[stable],
                   Write[outstream,F],
                   Close[outstream]
                  },
                  {}
     ]

    Clear[save2,stable,outstream]
```

```
(* MATHEMATICA subprogram for number *)
(*       Rainer Sachs  26.03.95       *)


   Clear[save,outstream,number,stable,nconst]

(* constants *)
(* n = .1 /Mpc^3 *)

   nconst=N[4 Pi .1 s0^3 c]

(* number of sources upto radius R *)

   number=Table[0,{i,1,imax}]
   For[i=2,i<imax+1,i++,
       {t=0.5 (R1[[i,1]]+R1[[i-1,1]]),
        r=0.5 (R1[[i,2]]+R1[[i-1,2]]),
        number[[i]]=number[[i-1]]+nconst/scale[t] r^2 Exp[3 (t-t0)/P] deltat
       }
      ]
   number=Drop[number,1]
   number=Log[10,number]

(* save number table *)

   save=InputString["save number table y/n "]
   If[save=="y",{stable=InputString["save as "],
                 outstream=OpenWrite[stable],
                 Write[outstream,number],
                 Close[outstream]
                },
                {}
     ]
```

```
(* MATHEMATICA subprogram for counts *)
(*    Rainer Sachs  26.03.95         *)


   Clear[graphc,print,save,outstream,sgraph,stable,
         so,sol,sum,fmax,fmin,smax,lf]
   Remove[nc]

(* constants *)

   fmax=2
   fmin=-2
   smax=5 (fmax-fmin)+1
   lf=Input["exp. of luminosity function "]

(* interpolation of number table *)

   nc=Compile[{x},Interpolation[number, InterpolationOrder->3][x]]

(* summation of sources from different cycles with equal or *)
(* smaller flux than fscan                                  *)
(* nc is multiplied by L^lf                                 *)
(* flux is scanned by s, luminosity by l in equidistant     *)
(* steps on a log-scale                                     *)

   so=Table[{0,0},{i,1,smax}]
   sum=1
   nlow=0
   For[s=1,s<smax+1,s++,
       {f=fmax-.2(s-1),
        For[l=1,l<12,l++,
            {fscan=10^f,
             For[i=1,i<imax,i++,
                 If[F[[i]]>fscan,{},
                    {p=Log[10,(i-1)/i]/Log[10,Abs[F[[i-1]]/F[[i]]]],
                     x=Abs[fscan/F[[i]]]^p i,
                     If[F[[i]]<0,
                        {nlow=10^nc[x]},
                        {nhigh=10^nc[x],
                         sum += 10^(lf (l-1)/10) (nhigh-nlow)
                        }
                       ],
                     For[j=i-1,j<imax,j++,F[[j]]=-F[[j]]],
                     fscan=-fscan
                    }
                 ]
                ],
             F=10^.1 Abs[F],
             nlow=0
            }
           ],
        so[[s,1]]=Abs[fscan],
        so[[s,2]]=sum,
        F=10^-1.1 F,
        sum=1,
       }
      ]

(* differential number in flux-interval *)
```

```
   sol=Table[{Log[10,so[[i,1]]],
              Log[10,Abs[(so[[i,2]]-so[[i+1,2]])/(so[[i,1]]-so[[i+1,1]])]]+2.
5 Log[10,so[[i,1]]]
             },
             {i,1,smax-1}
            ]//N


(* graphic output *)

   graphc=Show[ListPlot[sol],
               Frame->True,
               Axes->False,
               FrameLabel->{"log F","log dN F^2.5"},
               AspectRatio->Automatic,
               PlotLabel->plabel
              ]


(* save graphics *)

   save=InputString["save sourcecounts y/n "]
   If[save=="y",{sgraph=InputString["save as "],
                 outstream=StringJoin["!psfix>",sgraph],
                 Display[outstream,graphc]
                },
                {}
     ]

(* save source table *)

   save=InputString["save sourcecount table y/n "]
   If[save=="y",{stable=InputString["save as "],
                 outstream=OpenWrite[stable],
                 Write[outstream,sol],
                 Close[outstream]
                },
                {}
     ]

   Clear[save1,save2,print,sgraph,stable]
```

```
(* MATHEMATICA program for integral source counts       *)
(* for 3 populations, logarithmic interpolation,        *)

(*          Rainer Sachs  02.08.95                      *)
(*   All the input from previous calculations is used   *)


   Clear[F,R1,c,imax,period,eta,t0,P,s0,nlow,nhigh,sum,
         number1,number2,number3,nconst1,nconst2,nconst3,
         F1,F2,F3,so,sol,s1,s2,s3,fmax,fmin,smax]
   Remove[nc1,nc2,nc3,scale,theta]

(* read input and constants *)

   c=306.61;
   imax=1927;
   period=43.8102;
   eta=0.8;
   t0=0.7 period;
   P=20 period;
   s0=1.25664;
   R1=<<data/radius/17;
   T1=<<data/theta/08008;

(* n = .1 /Mpc^3 *)

   nconst1=N[4 Pi .1 s0^3 c];
   nconst2=0.2 nconst1;
   nconst3=0.0002 nconst1;

(* interpolation of R1, T1 and scale factor *)

   theta=Compile[{x},Interpolation[T1][x]]
   scale=Compile[{x},Exp[x/P] (1+eta Cos[theta[Mod[x,period]]])]

(* number of sources upto radius R, the numbers are logarithms *)

   number1=Table[0,{i,1,imax}];
   For[i=2,i<imax+1,i++,
       {t=0.5 (R1[[i,1]]+R1[[i-1,1]]),
        r=0.5 (R1[[i,2]]+R1[[i-1,2]]),
        number1[[i]]=number1[[i-1]]+nconst1 r^2/scale[t] Exp[3 (t-t0)/P] (R1[
[i-1,1]]-R1[[i,1]])
       }
      ]
   number1=Drop[number1,1];
   number1=Log[10,number1];

   number2=Table[0,{i,1,imax}];
   For[i=2,i<imax+1,i++,
       If[Mod[R1[[i,1]],period]>0.32 period,
          If[Mod[R1[[i,1]],period]<0.68 period,
             {t=0.5 (R1[[i,1]]+R1[[i-1,1]]),
              r=0.5 (R1[[i,2]]+R1[[i-1,2]]),
              number2[[i]]=number2[[i-1]]+nconst2 r^2/scale[t] Exp[3 (t-t0)/P
] (R1[[i-1,1]]-R1[[i,1]])
             },
            number2[[i]]=number2[[i-1]]
          ],
         number2[[i]]=number2[[i-1]]
        ]
       ]
   number2=Drop[number2,1];

   For[i=1,i<imax,i++,If[number2[[i]]==0,number2[[i]]=-3,number2[[i]]=Log[10,n
umber2[[i]]]]];

   number3=Table[0,{i,1,imax}];
   For[i=2,i<imax+1,i++,
       If[Mod[R1[[i,1]],period]>0.4 period,
          If[Mod[R1[[i,1]],period]<0.6 period,
             {t=0.5 (R1[[i,1]]+R1[[i-1,1]]),
              r=0.5 (R1[[i,2]]+R1[[i-1,2]]),
              number3[[i]]=number3[[i-1]]+nconst3 r^2/scale[t] Exp[3 (t-t0)/P]
 (R1[[i-1,1]]-R1[[i,1]])
             },
            number3[[i]]=number3[[i-1]]
           ],
          number3[[i]]=number3[[i-1]]
         ]
        ]
   number3=Drop[number3,1];

   For[i=1,i<imax,i++,If[number3[[i]]==0,number3[[i]]=-3,number3[[i]]=Log[10,n
umber3[[i]]]]];

(* save number table *)

   number1>>data/number/21.1;
   number2>>data/number/21.2;
   number3>>data/number/21.3;

(* interpolation of number table *)

   nc1=Compile[{x},Interpolation[number1, InterpolationOrder->3][x]];
   nc2=Compile[{x},Interpolation[number2, InterpolationOrder->3][x]];
   nc3=Compile[{x},Interpolation[number3, InterpolationOrder->3][x]];

(* the flux 3 10^28 *)

   F=<<data/flux/17;

(* constants *)

   fmax=1.22;
   fmin=-3.18;
   smax=5 Abs[fmax-fmin]+1;

(* summation of sources from different cycles with equal or
   smaller flux than fscan, flux is scanned by s            *)

(* population III  L= 5 10^27 W  rel occurance  1/5000 *)

   s3=Table[0,{j,1,smax}];
   sum=1;
   nlow=0;
   F3=F/6;
   For[s=1,s<smax+1,s++,
       {f=fmax-.2 (s-1),
        fscan=10^f,
```

```
        For[i=1,i<imax,i++,
            If[F3[[i]]>fscan,{},
               {x=i-(fscan-F3[[i]])/(F3[[i-1]]-F3[[i]]),
                If[F3[[i]]<0,
                   {nlow=10^nc3[x]},
                   {nhigh=10^nc3[x],
                    sum += nhigh-nlow
                   }
                  ],
                For[j=i-1,j<imax,j++,F3[[j]]=-F3[[j]]],
                fscan=-fscan
               }
              ]
           ],
        nlow=0,
        F3=F,
        s3[[s]]=sum,
        sum=1,
       }
      ]

(* population II   L= 5 10^25 W   rel occ  1/5  *)

   s2=Table[0,{j,1,smax}];
   sum=1;
   nlow=0;
   F2=F/600;
   For[s=1,s<smax+1,s++,
       {f=fmax-.2 (s-1),
        fscan=10^f,
        For[i=1,i<imax,i++,
            If[F2[[i]]>fscan,{},
               {x=i-(fscan-F2[[i]])/(F2[[i-1]]-F2[[i]]),
                If[F2[[i]]<0,
                   {nlow=10^nc2[x]},
                   {nhigh=10^nc2[x],
                    sum += nhigh-nlow
                   }
                  ],
                For[j=i-1,j<imax,j++,F2[[j]]=-F2[[j]]],
                fscan=-fscan
               }
              ]
           ],
        nlow=0,
        F2=F/100,
        s2[[s]]=sum,
        sum=1,
       }
      ]

(* population I  L= 5 10^24 W  rel occ 1 *)

   s1=Table[{0,0},{i,1,smax}];
   sum=1;
   nlow=0;
   F1=F/6000;
   For[s=1,s<smax+1,s++,
       {f=fmax-.2 (s-1),
        fscan=10^f,
        For[i=1,i<imax,i++,
            If[F1[[i]]>fscan,{},
               {x=i-(fscan-F1[[i]])/(F1[[i-1]]-F1[[i]]),
                If[F1[[i]]<0,
                   {nlow=10^nc1[x]},
                   {nhigh=10^nc1[x],
                    sum += nhigh-nlow
                   }
                  ],
                For[j=i-1,j<imax,j++,F1[[j]]=-F1[[j]]],
                fscan=-fscan
               }
              ]
           ],
        nlow=0,
        F1=F/1000,
        s1[[s,1]]=Abs[fscan],
        s1[[s,2]]=sum,
        sum=1,
       }
      ]

(* summation of all three populations *)

   so=Table[{s1[[j,1]],s1[[j,2]]+s2[[j]]+s3[[j]]},{j,1,smax}]//N;

(* number in flux-interval, integral counts *)

   so1=Table[{Log[10,so[[i,1]]],
              Log[10,so[[i,2]]]+1.5 Log[10,so[[i,1]]]
             },
             {i,1,smax}
            ]//N;

   so>>data/socounts/so.22;
   s1>>data/socounts/s1.22;
   s2>>data/socounts/s2.22;
   s3>>data/socounts/s3.22;
   so1>>data/socounts/22;


   Quit[]
```

```
(* source counts for einstein de sitter model (q=0.5) with h=0.75 and populat
ions like in mainhoyle.m *)

(*Population    luminsosity    rel.occ.   z_min      log f_max  *)

(*    1         5 10^24 W/Hz      1         0          infty   *)
(*    2         5 10^25 W/Hz      1/5       0.0728     0.6778  *)
(*    3         5 10^27 W/Hz      1/5000    0.630      0.7188  *)

       Clear[constn,c1,c2,c3,counts]
       Remove[zf]

(* constn= 32 pi n (c/H)^3 with n=0.1 1/Mpc^3          *)
(* constf= (4 pi (2c/H)^2 )^-1 10^-26  L_1 = 0.000653   *)


       constn=6.434 10^11;
       c1=0.000653;
       c2=0.00635;
       c3=0.653;

(* define function zf : redshift as a function of Log[10,flux density]  *)

       zf[x_,y_]:=0.5 (2 Sqrt[y/10^x]-1+Sqrt[4 Sqrt[y/10^x]+1])

(* and num1,2,3 : number as a function of redshift      *)

       num1[z_]:=constn (1/(z+1)-1/Sqrt[z+1]-1/(3 (z+1)^1.5)+1/3)
       num2[z_]:=constn/5 (1/(z+1)-1/Sqrt[z+1]-1/(3 (z+1)^1.5)+1/3.00012)
       num3[z_]:=constn/5000 (1/(z+1)-1/Sqrt[z+1]-1/(3 (z+1)^1.5)+1/3.031)


(* scanning the desired flux range, from 0.5 mJy to 16.67 Jy    *)
(* first calculate the corresponding redshift and then the      *)
(* number of each population for this z                         *)

       counts=Table[{0,0},{i,45}];
       For[i=1,i<46,i++,
           {flux=0.1 i-3.278,
            counts[[i,1]]=flux,
            If[flux>0.7188,counts[[i,2]]=Log[10,num1[zf[flux,c1]]]+1.5 flux,
               If[flux>0.6778,counts[[i,2]]=Log[10,num1[zf[flux,c1]]+num3[zf
[flux,c2]]]+1.5 flux,
                  counts[[i,2]]=Log[10,num1[zf[flux,c1]]+num2[zf[flux,c2]]+n
um3[zf[flux,c3]]]+1.5 flux
                ]
            ]
           ]
          ]

       counts>>data/socounts/bb5;


       Quit[]
```

Bibliography

[1] Abbott, L. (1988), Sci. Am., **258** (5), 82

[2] Allington-Smith, J. R. (1982), MNRAS, **199**, 611

[3] Allington-Smith, J. R., Spinrad, H., Djorgovski, S. & Liebert, J. (1988), MNRAS, **234**, 1091

[4] Alpher, R. A. & Herman, R. C. (1948), Nature, **162**, 774

[5] Andreani, P., LaFranca, F. & Cristiani, S. (1993), MNRAS, **261**, L35

[6] Arp, H. C., Burbidge, G., Hoyle, F., Narlikar, J. V. & Wickramasinghe, N. C. (1990), Nature, **346**, 807

[7] Bondi, H. & Gold, T. (1948), MNRAS, **108**, 252

[8] Broadhurst, T. & Lehár, J. (1995), astro-ph/9505013, submitted to ApJL

[9] Carroll, S. M., Press, W. H. & Turner, E. L. (1992), ARA & A, **30**, 499

[10] Casimir, H. B. G. (1948), Proc. Kon. Ned. Akad. Wet., **52**, 625

[11] Coleman, S. & Weinberg, E. (1973), Phys. Rev. **D7**, 1888

[12] de Sitter, W. (1917), Proc. Kon. Ned. Akad. Wet., **20**, 229

[13] Downes, D. et al. (1992), ApJ, **398**, L25

[14] Eddington, A. S. (1930), MNRAS, **90**, 668

[15] Einstein, A. (1915), Preuss. Akad. Wiss. Berlin, Sitz. Ber., **844**

[16] Einstein, A. (1917), Preuss. Akad. Wiss. Berlin, Sitz. Ber., **142**

[17] Freedman, W. L. et al. (1994), Nature, **371**, 757

[18] Fukugita, M., Hogan, C. J. & Peebles, P. J. E. (1993), Nature, **366**, 309

[19] Gamow, G. (1946), Phys. Rev., **70**, 572

[43] Peebles, P. J. E., Schramm, N. D., Turner, E. L. & Kron, R. G. (1991), Nature, **352**, 769

[44] Penzias, A. A. & Wilson, R. W. (1965), ApJ, **142**, 419

[45] Robertson, H. P. (1935), ApJ, **82**, 248

[46] Rowan-Robinson, M. et al. (1991), Nature, **351**, 719

[47] Rowan-Robinson, M. et al. (1993), MNRAS, **261**, 513

[48] Sachs, R., Narlikar, J. V. & Hoyle, F. (1995), preprint, submitted to A & A

[49] Schramm, D. N. (1990), in *Astroph. Ages and Dating Methods*, Eds. Vangioni-Flam, E. et al., 365

[50] Serjeant, S. et al. (1995), astro-ph/9506089, submitted to MNRAS

[51] Smoot, G. F. et al. (1992), ApJ, **396**, L1

[52] Solomon, P. M., Downes, D. & Radford, S. J. E. (1992), ApJ, **398**, L29

[53] Spaarnay, M. J. (1957), Nature, **180**, 334

[54] Trentham, N. (1995), astro-ph/9506073, submitted to MNRAS

[55] Walker, A. G. (1936), Proc. Lond. Math. Soc. (2), **42**, 90

[56] Weinberg, S. (1989), Rev. Mod. Phys., **61** (1), 1

[57] Weyl, H. (1923), Z. Phys., **24**, 230

[58] Wickramasinghe, N. C. & Hoyle, F. (1994), APSS, **213**, 143

[59] Wolfram, S. (1991), *Mathematica*, Addison-Wesley, Redwood City

[60] Wright, E. L. (1994), astro-ph/9412045